Effects of Mixed Layer Depth on Productive Marine Ecosystems

-

from seasonality to climate change

Dissertation

zur Erlangung des Doktorgrades

der Mathematisch-Naturwissenschaftlichen Fakultät

der Christian-Albrechts-Universität zu Kiel

vorgelegt von

Tianfei Xue

Kiel, July 2022

Erster Gutachter und Betreuer: Professor Andreas Oschlies

Zweiter Gutachter: Professor Arne Körtzinger

Tag der Disputation: 05.09.2022

. . . . . .

gez. Prof. Dr. Frank Kempken, Dekan

Summary

Marine ecosystems, particularly productive marine ecosystems, substantially impact global fisheries and are considerably influenced by climate change as an integral component of the earth system. Modelling is an essential tool to understand marine ecosystems and project their possible response to climate change. However, current ecosystem modelling projections have significant uncertainties, which are partially caused by a lack of overall understanding of the underlying physical-biological interactions. This thesis seeks to identify the driving mechanisms of the trophodynamics in productive marine ecosystems in the contemporary climate, which is key to improve future ecosystem projections under climate change.

The first part of the thesis investigates the driving mechanisms of phytoplankton seasonality in the contemporary climate, taking the Humboldt Upwelling system as an example of a productive ecosystem. This study is based on a climatological simulation from a regional physical-biogeochemical model (CROCO-BioEBUS). The model results indicate that mixed layer depth surpasses the upwelling process and governs the seasonality of the phytoplankton primarily via dilution and light-limitation. Upwelling, on the other hand, acts as a secondary contributor and influences the seasonality mostly via temperature limitation and advection. Interestingly, phytoplankton seasonality propagates up the food chain and influences trophodynamics and ecosystem functioning (e.g. export efficiency). This study demonstrates the driving role of the mixed layer depth in phytoplankton seasonality and reveals the potential impacts further up the food web.

The second part of the thesis further looks into how the phytoplankton seasonality is transferred up the food web to the zooplankton in the Humboldt and other productive ecosystems. Model results exhibit the feature of "seasonal trophic amplification", with zooplankton revealing more prominent seasonal variation than phytoplankton. The mixed layer depth alters the vertical distribution of phytoplankton and, subsequently, the zooplankton-phytoplankton encounters in the Humboldt system. When the mixed layer is relatively deep, phytoplankton are diluted with a lower concentration, and thereby less zooplankton-phytoplankton encounters. We coin this "seasonal trophic amplification" in other productive regions using two global models (GFDL and UVic model). This study suggests that the mixed layer depth influences trophic transfer from phytoplankton to zooplankton via

dilution. Therefore, the mixed layer plays an important role for trophodynamics in the Humboldt and other productive systems.

The third part of the thesis further explores if and how changes in the planktonic community affect higher trophic levels. Here, we used a one-way coupled physical-biogeochemical-fish model (CROCO-BioEBUS-OSMOSE). The results indicate that the strong variations in observed fish biomass cannot be simulated with the one-way coupled model. Therefore, we conclude that plankton food is not the main driver of the observed interannual fluctuations in higher trophic levels but possibly other biological processes in our model.

The fourth part of the thesis implements the findings from the productive ecosystems under the current climate from the first two parts of the thesis to understand and constrain ecosystem projections under climate change. We based our findings regarding the impact of mixed layer depth on phytoplankton under contemporary seasonality and used observations to constrain the phytoplankton projection under climate change with a method known as "Emergent Constraints". This has significantly reduced the uncertainty of future chlorophyll projections under climate change. The study further applies the observation of seasonal trophic amplification to better understand the trophic amplification along with a changing climate as widely known from climate model projections. The shoaling of the mixed layer as a result of ocean warming would enhance the grazing efficiency and, thereby, more prominent zooplankton biomass increase. Given the impact of changing mixed layer depth on "bottom-up" and "top-down" processes, this study further emphasizes the potential increasing importance of "top-down" control under climate change.

Overall, this thesis emphasizes the critical role of mixed layer depth in productive ecosystems under the current climate, which has significant potential in promoting projections of productive ecosystems under climate change.

Zusammenfassung

Meeresökosysteme, insbesondere produktive, sind fundamental für die weltweite Fischerei und werden als integraler Bestandteil des Erdsystems vom Klimawandel beeinflusst. Die Modellierung ist ein wichtiges Instrument zum Verständnis der Meeresökosysteme und zur Prognose ihrer möglichen Veränderungen im Zuge des Klimawandels. Die Prognosen der Ökosystemmodelle sind derzeit mit erheblichen Unsicherheiten behaftet, was zum Teil auf ein mangelndes Verständnis der diesen zugrunde liegenden physikalisch-biologischen Wechselwirkungen zurückzuführen ist. Ziel dieser Arbeit ist es, Mechanismen in produktiven Meeresökosystemen unter den gegenwärtigen klimatischen Bedingungen zu ermitteln, die für Projektionen der zukünftigen Entwicklung von Ökosystemen in einem sich ändernden Klima wichtig sind.

Im ersten Teil der Arbeit werden Mechanismen der saisonalen Phytoplankton-Aktivität im heutigen Klima untersucht, wobei das Humboldt-Auftriebssystem als Beispiel für ein produktives Ökosystem dient. Diese Studie basiert auf einer klimatologischen Simulation mit einem regionalen physikalisch-biogeochemischen Modell (CROCO-BioEBUS). Die Modellergebnisse zeigen, dass Variationen der Tiefe der gemischten Schicht den Auftriebsprozess überlagern und die Saisonalität der Phytoplankton-Konzentration in erster Linie durch Verdünnung und Lichtlimitierung bestimmen. Der Auftrieb hingegen spielt eine untergeordnete Rolle für die Saisonalität und beeinflusst Phytoplankton hauptsächlich durch Temperatur und Advektion. Interessanterweise pflanzt sich die Saisonalität des Phytoplanktons in der Nahrungskette nach oben fort und wirkt sich auf die Trophodynamik und die Funktionsweise des Ökosystems aus (z. B. auf die Export-Produktion). Diese Studie zeigt die bedeutende Rolle der Tiefe der gemischten Schicht für die Saisonalität des Phytoplanktons und offenbart die potenziellen Auswirkungen in der Nahrungskette.

Im zweiten Teil der Arbeit wird untersucht, wie sich die Saisonalität des Phytoplanktons in der Humboldt-Region und anderen produktiven Ökosystemen auf das Nahrungsnetz, insbesondere Zooplankton, auswirkt. Ergebnisse der derselben Modellsimulationen wie im ersten Teil der Arbeit zeigen im Humboldt-System eine ”saisonale trophische Verstärkung”, wobei das Zooplankton saisonal stärkeren relativen Schwankungen unterliegt als das Phytoplankton. Der Grund hierfür ist, dass die Tiefe der gemischten Schicht die vertikale

Verteilung des Phytoplanktons beeinflusst und damit auch die Frequenz von Begegnungen zwischen Zooplankton und Phytoplankton: In einer tieferen gemischten Schicht wird das Phytoplankton verdünnt, so dass es zu weniger Begegnungen zwischen Zooplankton und Phytoplankton kommt. Zwei globale Modelle (GFDL- und UVic-Modell) zeigen diese "saisonale trophische Verstärkung" auch in anderen produktiven Regionen. Diese Studie legt nahe, dass die Tiefe der gemischten Schicht den trophischen Transfer von Phytoplankton zu Zooplankton über die Verdünnung beeinflusst und daher sowohl im Humboldt-System also auch anderen produktiven Systemen wichtig für das Funktionieren der Ökosysteme ist.

Im dritten Teil der Arbeit wird untersucht, ob und wie sich Veränderungen in der Planktongemeinschaft auf höhere trophische Ebenen auswirken. Hierfür haben wir ein einseitig gekoppeltes physikalisch-biogeochemisches Fischmodell (CROCO-BioEBUS-OSMOSE) verwendet. Die Ergebnisse zeigen, dass starke Variationen der beobachteten Fischbiomasse nicht mit Variationen der Planktonbiomasse (Nahrung der Fische) erklärt werden können. Daraus lässt sich schließen, dass Variationen der Planktonbiomasse wohl nicht die Hauptursache für die interannuellen Schwankungen der höheren trophischen Ebenen ist, sondern eher andere biologische Prozesse.

Der vierte Kapitel der Arbeit verwendet die Ergebnisse hinsichtlich produktiver Ökosysteme im derzeitigen Klima aus den ersten beiden Teilen der Arbeit, um die Projektionen der Ökosysteme unter Bedingungen des Klimawandels zu analysieren und deren Unsicherheiten zu reduzieren. Dabei werden Modellergebnisse über Auswirkungen der Tiefe der gemischten Schicht auf das Phytoplankton unter gegenwärtigen Bedingungen mit Beobachtungen kombiniert, um mittels einer als "Emergent Constraints" bekannten Methode die Unsicherheit von Projektionen von Phytoplankton im Klimawandel in globalen Klimamodellen zu reduzieren. Die Unsicherheit von Chlorophyll-Projektionen konnte erheblich verringert werden. Auch die Analyse der saisonalen trophischen Verstärkung aus Teil zwei kann helfen, deren Effekte unter einem sich ändernden Klima in globalen Klimamodellen besser zu verstehen. Die Verflachung der gemischten Schicht infolge der Erwärmung des Ozeans steht im Einklang mit einer erhöhten Fraßeffizienz von Zooplankton und damit einer Erhöhung von dessen Biomasse. Angesichts der Auswirkungen der sich ändernden Tiefe der gemischten Schicht auf die Fraßeffizienz unterstreicht diese Studie die potenziell zunehmende Bedeutung der "Top-down"-Kontrolle von Phytoplankton im Zuge des Klimawandels.

Insgesamt unterstreicht diese Arbeit die kritische Rolle der Tiefe der gemischten Schicht in produktiven Ökosystemen im gegenwärtigen Klima und bietet daher ein erhebliches Potenzial für die Verbesserung von Projektionen produktiver Ökosysteme im Klimawandel.

Contents

Chapter 1

Introduction

The marine ecosystem is an important component in the earth system and plays a key role in global fisheries and climate change. The use of models is a constructive method for studying marine ecosystems and projecting their potential changes with climate change. However, current ecosystem model projections are highly uncertain and there is an overall lack of knowledge about the underlying mechanisms controlling the structure and dynamics of marine ecosystems. The aim of this study is to identify the underlying mechanisms controlling marine ecosystems in contemporary climates, which are essential for future projections. This chapter will provide an introduction to the study by first discussing the background and current research gap, followed by the research aim, the significance and research areas of the study and finally the outline of the thesis along with the author contribution.

1.1 Marine ecosystem: from phytoplankton to export

Marine ecosystems, consisting of phytoplankton, zooplankton, fish, and eventually organic carbon being exported into the deep ocean (Fig. 1.1), are essential in the context of climate change and provide humans with valuable goods and services. However, how the ecosystem will shift under climate change remains a major uncertainty in projections.

1.1.1 Phytoplankton: the starting point

Phytoplankton, as the base of the marine ecosystem, plays a key role in climate change, accounting for almost 50% of global primary production (Field et al., 1998; Behrenfeld et al., 2006). Each year, roughly 50 billion tons of carbon are transferred into the marine ecosystem via photosynthesis in the upper ocean by phytoplankton (Field et al., 1998), some eventually being fished out (Pauly and Christensen, 1995; Stock et al., 2017) and some sinking into the deep ocean (Legendre and Rassoulzadegan, 1996; Henson et al., 2012). Because of its farreaching importance, it has been long studied using observations (e.g., in situ, satellite; Behrenfeld and Falkowski, 1997; Boyce et al., 2010), lab experiments (Shifrin and Chisholm, 1981) and numerical modelling (Taucher and Oschlies, 2011) which is also the

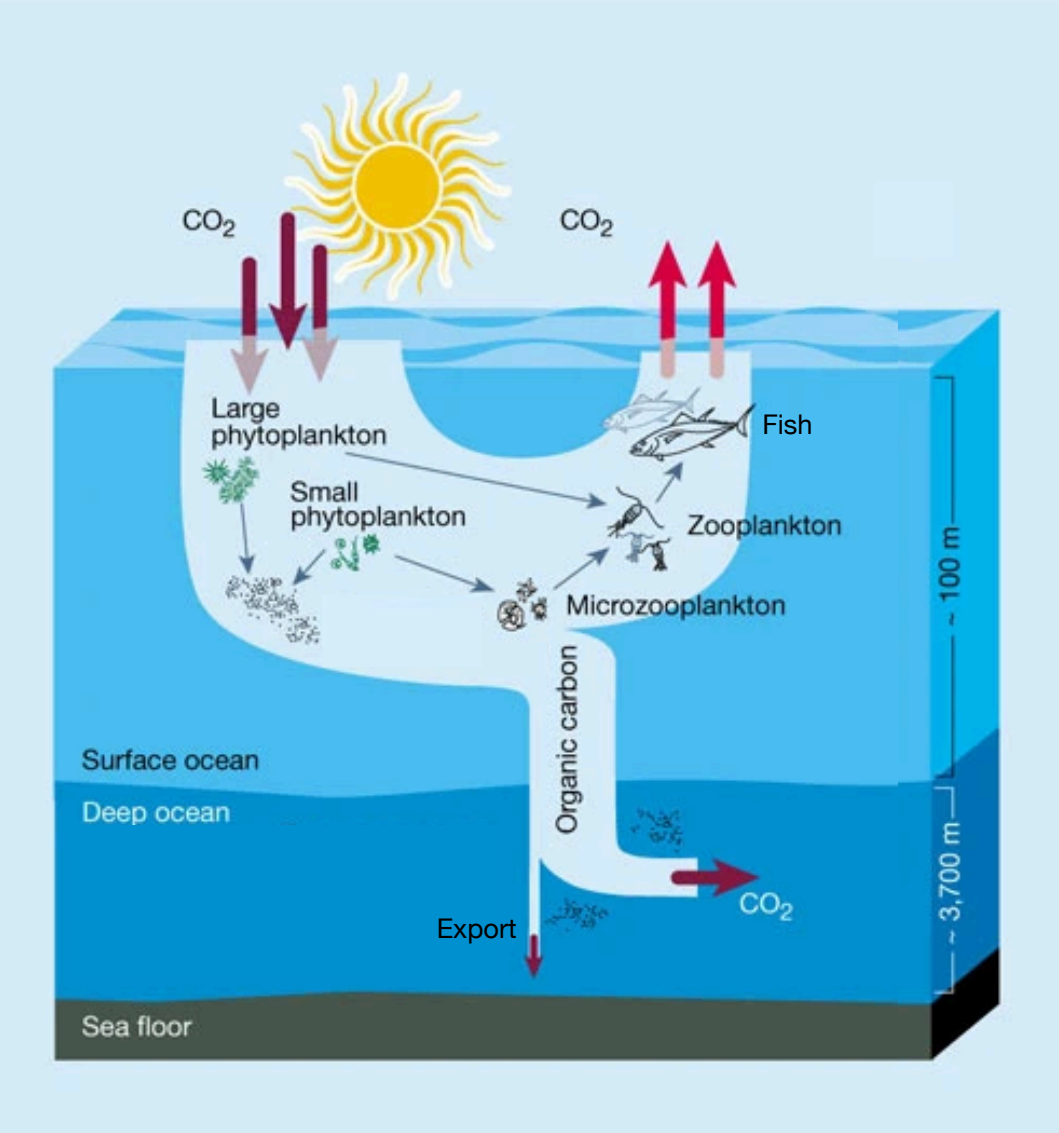

Figure 1.1: **Illustration of the marine ecosystem: from phytoplankton to export.** Phytoplankton fix atmospheric CO_2 into organic carbon via photosynthesis at the surface ocean. The organic carbon subsequently passes through the food web to zooplankton and further to fish. Part of the organic carbon from the food web is exported to the deep ocean. Modified from Chisholm (2000)

main tool used for this study. Phytoplankton growth is commonly believed to be determined by environmental conditions (nutrients, temperature, and light; Eppley et al., 1969; Eppley, 1972). Phytoplankton of different sizes cope with environmental conditions differently. Hence, phytoplankton within commonly employed large-scale ocean ecosystem models tend to be grouped together based on size, such as nanophytoplankton and microphytoplankton. Nanophytoplankton, despite their small size, are very abundant. Benefiting from the high surface to volume ratio, it can efficiently utilize the nutrients and thrive in low-nutrient systems, like oligotrophic regions (Eppley et al., 1969; Pasciak and Gavis, 1974; Reynolds, 2006). Microphytoplankton, with diatoms as a representative group, tend to dominate in nutrient-rich environments such as upwelling regions (Reynolds, 2006).

Despite models capturing phytoplankton ecology in increasing detail (D'Alelio et al., 2016), simulations of phytoplankton and its growth are still susceptible to significant uncertainties (Laufkötter et al., 2015). In addition to the underlying physical forcing, there are also great uncertainties arising from the biogeochemical and biological processes (Laufkötter et al., 2015). Considering the biological processes, changes in phytoplankton are determined by both "bottom-up" and "top-down" controls that both appear to be poorly constrained among model simulations. For the responses of "bottom-up" processes to climate change, nutrient limitation tends to be more severe in most regions, particularly at low-latitude regions (Doney, 2006; Behrenfeld, 2010). However, growth conditions for phytoplankton at high-latitude regions are predicted to improve as a result of warming and light conditions under climate change (Sarmiento et al., 2004).

1.1.2 Zooplankton: a vital link

Zooplankton is a vital link in the marine ecosystem. It is the primary consumer of phytoplankton (Reynolds, 2006; Prowe et al., 2012) and a major food source for fish (Espinoza and Bertrand, 2008; Bakun and Weeks, 2008). The marine zooplankton community includes many different groups, ranging in size from microzooplankton and mesozooplankton that are commonly included in biogeochemical models. Microzooplankton is an essential component of the food web. It is accounting for 60-75% of primary production consumption (Calbet and Landry, 2004), particularly in oligotrophic regions (Azam et al., 1983). Mesozooplankton dominates more in the productive systems like upwelling regions. It provides a direct link between phytoplankton and fish, which enables a short and efficient food chain that allows a high fish yield (Schukat et al., 2021).

Despite the fact that zooplankton often represents the highest trophic level in most ocean ecosystem models, which greatly influences the ecosystem dynamics, it is often poorly simulated (Le Quéré et al., 2016; Lotze et al., 2019). In addition to the uncertainties that are introduced from phytoplankton simulation, a simplified depiction of food web mechanisms

is unable to capture the complex trophic interactions necessary to adequately simulate zooplankton (Le Quéré et al., 2016; Lotze et al., 2019). Furthermore, most global biogeochemical models haven't been calibrated thoroughly, especially when it comes to variables like zooplankton (Stock et al., 2014b).

1.1.3 Fish: of great social & economic interests

Fish is of great social and economic interest to our daily lives. About 20% of the animal protein consumed by humans is provided by fish, which supports a multibillion-dollar industry (Lalli and Parsons, 1997). Increasing evidence highlights that past fishing management was not able to maintain fish yields and stocks. For example, it has been reported that global fish landings have been continuously declining ever since the collapse of the Peruvian anchoveta fishery in 1972-1973 (Pauly et al., 1998). Moreover, existing studies recognize the simultaneous or even amplified impacts from climate change and overfishing (Cury et al., 2008; Link et al., 2010). Therefore, there is an urgent need to address the drivers behind fish production and the trophodynamics from phytoplankton to zooplankton, and eventually fish.

While plenty of studies have been done to study the plankton community, few studies have investigated the trophodynamics including fish in any systematic way. Previously published studies on fishery estimation merely rely on the measurement of phytoplankton (Pauly and Christensen, 1995; Stock et al., 2017). Phytoplankton has later been found out to be an unreliable indicator of fishery, due to unable to include the variations from phytoplankton to fish (Friedland et al., 2012). Recent developments in the End-to-End model with the aim of representing the whole ecosystem within the models have led to a renewed interest in the linkage between plankton and fish and what the future fishery may look like. End-to-End models should be able to provide new insights into the "whole picture" (Moloney et al., 2011; Heath, 2012; Travers-Trolet et al., 2014b). However, they are still at a pioneering stage, and can only include limited processes linking the physical and biogeochemical model to the higher trophic level model (e.g., fish feeding on plankton; Travers-Trolet et al., 2014b).

1.1.4 Export: flux to the deep ocean

Export, also known as the biological pump, is a crucial link in the global carbon cycle (Buesseler et al., 2020). It is a combined process of phytoplankton fixing atmospheric CO_2 via photosynthesis and the subsequent sinking of the fixed organic carbon into the deep ocean. Consequently, the export is regulated by phytoplankton production and export efficiency (Henson et al., 2012).

Apart from the above discussed phytoplankton production, export efficiency (the ratio of

primary production over export; Murray et al., 1996) has been previously suggested to be affected by phytoplankton community structure (Buesseler, 1998; Boyd and Newton, 1999) due to the formation of aggregates. Recent extensive studies have shown that the export efficiency is not merely controlled by the phytoplankton community structure but more strongly by the ecosystem structure (Henson et al., 2019; Boyd et al., 2019). Numerous studies have demonstrated the importance of zooplankton to carbon export in consideration of its fast sinking fecal pellets and vertical migration (Cavan et al., 2015, 2017). This means that zooplankton can export organic carbon more efficiently than phytoplankton, and the ratio of zooplankton to phytoplankton biomass would thereby influence the export efficiency and thus export.

1.2 Underlying mechanisms: physical conditions shape marine ecosystem

Physical environments influence biological processes in a variety of ways, not only by providing a background for biological processes to occur, but also by indirectly influencing biological processes (Mann and Lazier, 2013). Marine ecosystems can differ dramatically and are determined largely by different scales of physical processes like mixed layer dynamics and oceanic upwelling (Doney, 2006). Therefore, it is crucial to investigate the underlying mechanisms that shape the ecosystem and aim to better understand and project the potential changes in the future.

1.2.1 Mixed Layer: regulates surface ocean

The mixed layer at the ocean surface acts as an interface, isolating the deep ocean from the atmosphere and influencing global climate by regulating heat, carbon and oxygen exchange between the atmosphere and the oceanic interior (Bopp et al., 2015; Bindoff et al., 2019; Sallée et al., 2021). Moreover, it also hosts most of the ocean primary production and indirectly regulates the ecosystem (Sverdrup, 1953). Aside from retaining phytoplankton at the ocean surface layer, the depth of the mixed layer determines available light and temperature, which directly influence phytoplankton growth (Reynolds, 2006). Furthermore, the mixed layer also governs nutrient flux into and out of the euphotic zone and thereby the accessibility of nutrients for phytoplankton growth (Chen et al., 1994).

A comprehensive observational system is crucial to better assess the surface layers of global climate models and investigate the impact of the mixed layer depth on the ecosystem (Belcher et al., 2012). Fortunately, several mixed layer products are already available: (1) Argo Mixed Layers (http://mixedlayer.ucsd.edu/; Holte et al., 2017); (2) de Boyer Montégut climatology data (https://cerweb.ifremer.fr/deboyer/mld/home.php; de Boyer Montégut et al., 2004); (3) the World Ocean Atlas mixed layer climatology (https://www.ncei.noaa.gov/

products/world-ocean-atlas; Locarnini et al., 2018). Additionally, there is a growing body of literature that looks into the role of mixed layer depth in biological processes using observational data (Behrenfeld, 2010; Messié and Chavez, 2015; Arteaga et al., 2020) and model simulations (Evans and Parslow, 1985; Echevin et al., 2008).

1.2.2 Upwelling: fuels the mixed layer in some regions

Ocean upwelling is a process that brings cold, nutrient-rich water from the deep ocean up to the surface mixed layer in some regions and thereby fuels the ecosystem (Chavez et al., 2008; Messié et al., 2009). As for the mechanisms that produce upwelling systems, the wind-driven upwelling creates the largest and most persistent upwelling systems (Kämpf and Chapman, 2016). Numerous studies have been conducted about the physical process of wind-driven upwelling (Sverdrup et al., 1942; Bakun, 1990, 1997; Messié et al., 2009). Among the wind-driven upwelling systems, there are four major upwelling systems, also known as the Eastern Boundary Upwelling Systems (EBUSs), consisting of: the Humboldt, Benguela, California, and Canary Systems. The impacts of climate change on EBUSs will have disproportionately large consequences for humans, despite their small surface area compared to other pelagic ecosystems (Bindoff et al., 2019).

Benefiting from the upwelled nutrients, EBUSs sustain disproportionally productive ecosystems, contributing approximately 20% of the global fishing yield while covering less than 1% of the global ocean (Chavez and Messié, 2009). The main fish catch in the four EBUSs is from small pelagic fish, accounting for approximately 12 out of a total of 17 million metric tons of fishing yield between 2000 and 2007 (FAO, http://www.fao.org/fishery/statistics/global-capture-production/query/en). Considering the important role of EBUSs in global fisheries and their great social and economic interests for the public, they have been intensively studied with respect to their high primary production (Carr and Kearns, 2003; Messié and Chavez, 2015), high fish yields (Bakun and Weeks, 2008; Chavez et al., 2008; Espinoza and Bertrand, 2008) and intense oxygen minimum zones (Stramma et al., 2008, 2010).

1.3 Perspectives: for better climate change projection

Although major advances in climate science have been made with collaborative international efforts, future climate change projections are still rather uncertain, especially for future ecosystem projections (Fig. 1.2; Laufkötter et al., 2015; Lotze et al., 2019). Employing the well-founded, verified mechanisms of how physical processes shape marine ecosystem on different timescales, such as seasonal (e.g., Hall and Qu, 2006) and inter-annual scales (e.g., Kwiatkowski et al., 2017), can unravel the linkages between physical variability and marine ecosystems. Furthermore, this can provide insights that will ultimately improve ecosystem projections under climate change (Hall et al., 2019; Williamson et al., 2021).

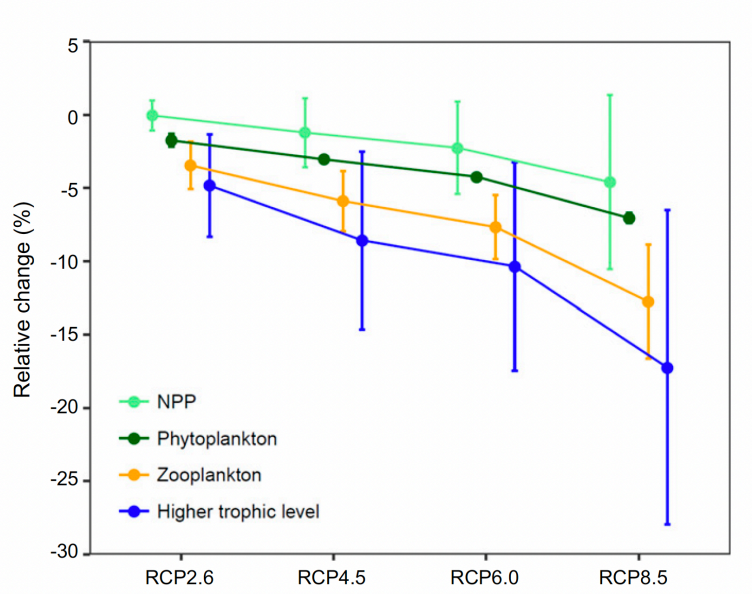

Figure 1.2: **Future climate change projections of the ecosystem are highly uncertain.** The magnitude of projected mean changes in 2090-2099 relative to 1990-1999 (percent, ±SD) for NPP, phytoplankton, zooplankton biomass and higher trophic levels under four Representative Concentration Pathways (RCP2.6, RCP4.5, RCP6.0 and RCP8.5). Figure from Lotze et al. (2019)

1.3.1 Contemporary Seasonality

Plankton populations are heavily driven by the seasonal cycle of physical conditions. Previous studies have identified the mixed layer depth as a critical factor in the seasonal dynamics of plankton (Sverdrup, 1953; Behrenfeld, 2010). The physical-biological interaction behind the seasonal cycle of the plankton dynamics has long been studied (Banse, 1992). In 1953, Sverdrup proposed the Critical Depth Hypothesis as "the phytoplankton bloom occurs when the mixed layer shoals to a depth less than the constant critical depth (the depth where phytoplankton growth matches the losses within this depth interval), allowing the phytoplankton biomass to accumulate". Thereby, the critical role of mixed layer depth in regulating the phytoplankton growth condition was recognized. Behrenfeld (2010) later proposed a Dilution-Recoupling Hypothesis based on the initial Critical Depth Hypothesis, which focuses on the balance between phytoplankton growth and zooplankton grazing, both of which are influenced by the seasonally varying mixed layer. The Dilution-Recoupling Hypothesis highlights the role of "top-down" control and does not simply consider the loss processes as a constant term in contrast to the Critical Depth Hypothesis. In general, the vertical structure of the water column is determined by buoyancy from surface heating and freshwater flux, together with stirring due to wind stress (Simpson and Sharples, 2012). When the mixed layer shoals with both phytoplankton and zooplankton concentrated within the narrow surface, it simultaneously improves the phytoplankton growth (Reynolds, 2006)

while increases the grazing pressure (Evans and Parslow, 1985).

1.3.2 Interannual to Multidecadal variability

In response to underlying physical environment fluctuations, fish production usually exhibits interannual to multidecadal variations, unlike the seasonal variations shown in the plankton community. A prominent example is El Niño, which is characterized by an exceptional warming and has great impact on the Humboldt ecosystem, especially in fish (Bakun and Broad, 2003; Alheit and Niquen, 2004; Bakun and Weeks, 2008). It causes ecosystems to shift between anchovy and sardine regimes, reshaping the ecosystem from phytoplankton to fish population (Alheit and Niquen, 2004). Moreover, Chavez et al. (2003) demonstrate that multidecadal environmental fluctuations also drive similar fish regime shifts but on longer time scales. It has been observed that the Pacific system shifted from an "anchovy regime" to a "sardine regime" and back to an "anchovy regime" from the mid 1970s to the late 1990s (Kawasaki, 1983; Chavez et al., 2003; Alheit and Niquen, 2004). The sardine and anchovy regime shifts are found to be strongly associated with the ocean temperature. The regime shifted from anchovy to sardine dominance during the warm phase and vice versa (Chavez et al., 2003; Alheit and Niquen, 2004). How the regime shifts relate to variations of plankton as food is still unclear.

1.3.3 Climate Change

Phytoplankton biomass and primary production have been observed to decline over the past decade (Behrenfeld et al., 2006; Boyce et al., 2010), and the decreasing trend is projected to continue on a global scale with significant spatial differences under global warming (Doney, 2006; Sarmiento et al., 2004; McQuatters-Gollop et al., 2011). The general decline of phytoplankton is mainly occurring in the low-latitude regions due to the changes in the mixed layer depth and, subsequently, the availability of nutrients for phytoplankton growth (Behrenfeld et al., 2006; Doney, 2006). In contrast, phytoplankton commonly shows a rising trend in the high-latitude region as a result of improved light conditions (e.g., lengthening the growing season; Bopp et al., 2001; Sarmiento et al., 2004; Doney, 2006), which coincides with the mechanism on a seasonal scale (Echevin et al., 2008; Messié and Chavez, 2015).

Global warming effects on phytoplankton are expected to have a nonlinear impact on higher trophic levels, causing zooplankton and fish to change even more than phytoplankton, a phenomenon known as "trophic amplification" (Chust et al., 2014; Stock et al., 2014a; Kwiatkowski et al., 2019; Lotze et al., 2019). Similar to phytoplankton, climate models predict different zooplankton responses to global warming in different regions. Negative trophic amplification is expected in low-latitude regions, with zooplankton biomass decreasing more prominently than phytoplankton. This could possibly be explained by zooplankton starvation as a result of phytoplankton decline (Stock et al., 2014a; Kwiatkowski et al., 2019).

Contrastingly, high-latitude regions show evidence of positive trophic amplification, with zooplankton biomass increasing more prominently than phytoplankton. This may be due to the better feeding condition of zooplankton caused by the increasing stratification (Chust et al., 2014; Stock et al., 2014a; Kwiatkowski et al., 2019). In temperate regions, zooplankton biomass is expected to decrease but less than phytoplankton (known as "trophic attenuation"; Chust et al., 2014; Kwiatkowski et al., 2019). However, the underlying mechanisms of how the ocean warming signal propagates through the food web and leads to different responses at higher trophic levels are still unclear.

The impacts of climate change on the ocean ecosystems are not limited to ocean warming but can also be caused via ocean acidification (decreasing ocean pH; Riebesell et al., 2000; Raven et al., 2005) and ocean deoxygenation (ocean oxygen loss; Keeling et al., 2010; Oschlies et al., 2018). The increase in surface ocean CO_2 has relatively little effect on phytoplankton growth (Gervais and Riebesell, 2001) while the corresponding decrease in pH strongly reduces the calcification of marine plankton (Riebesell et al., 2000). Ocean deoxygenation is closely linked to the warming-induced solubility decline (Oschlies et al., 2018) and has an important influence on fisheries (Rose et al., 2019). However, the processes of ocean acidification and deoxygenation will not be addressed in further detail in this thesis.

1.4 Focus on: only productive systems

The responses of different marine ecosystems to ocean warming mainly follow two schemes (Fig. 1.3; Doney, 2006; Sarmiento et al., 2004; Bopp et al., 2001; Behrenfeld et al., 2006): (1) in nutrient-limited systems, ocean warming primarily affects the system by causing shoaling of mixed layers, which results in a decrease in surface nutrient supply and more severe nutrient limitation for phytoplankton growth; (2) in productive (non-nutrient-limited) systems, ocean warming-induced shoaling mixed layer can improve light and temperature conditions, thereby promoting phytoplankton growth. Since phytoplankton is the base of the food web, any changes there would propagate up and impact the whole ecosystem. Here, in this thesis, I only focus on productive systems that are not nutrient-limited, such as the Humboldt Upwelling System and the Southern Ocean.

1.4.1 The Humboldt Upwelling System

Among the productive EBUSs, the Humboldt Upwelling System (HUS) produces more fish per unit area than any other EBUSs and also any other ocean in the world. The HUS covers less than 0.1% of the world ocean yet produces approximately 10% of global fishing yields (Chavez et al., 2008). Surprisingly, despite being driven by the same physical mechanism and hosting similar primary production, the HUS supports over one order of magnitude higher fish catch than the other three EBUSs (known as the "anchoveta paradox"). This

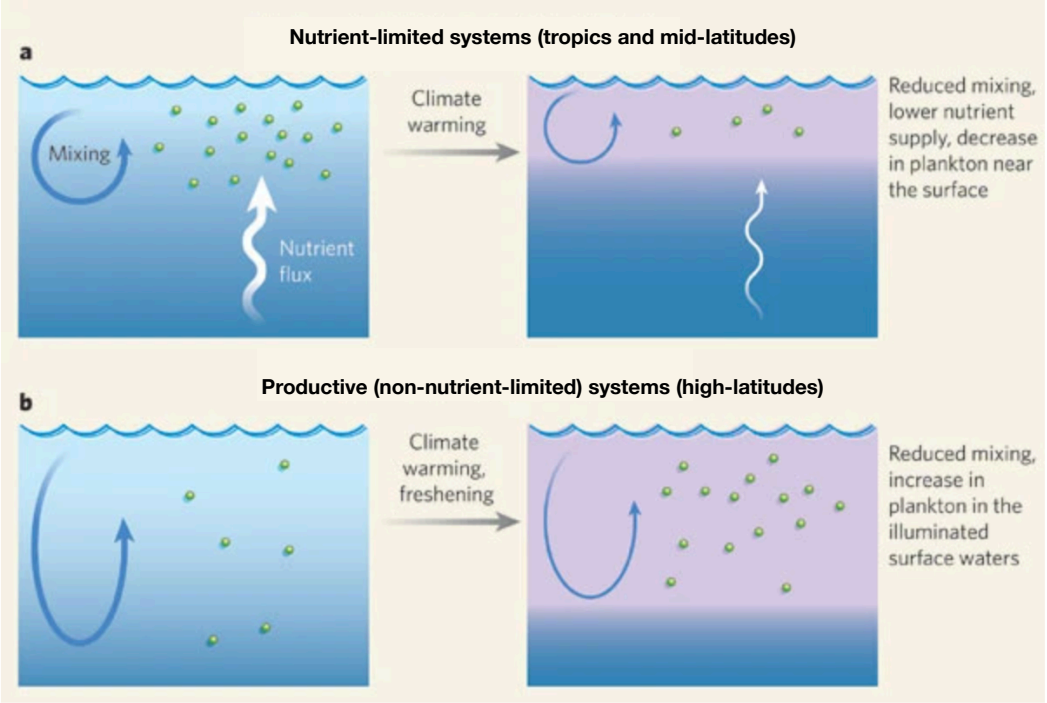

Figure 1.3: **The responses of different marine ecosystems to ocean warming mainly follow two schemes:** (a) nutrient-limited systems (mostly in the tropics and at mid-latitudes), decrease in plankton to upper-ocean warming as a result of reduced nutrient supply; (b) productive (non-nutrient-limited) systems (mostly at higher latitudes), climate change-induced shoaling mixed layer can improve light and temperature, thereby promoting phytoplankton growth. Figure modified from Doney (2006)

suggests strikingly higher trophic transfer efficiencies from phytoplankton to fish in the HUS (Ryther, 1969; Pauly and Christensen, 1995; Chavez et al., 2008). Nevertheless, the HUS and its fishery are strongly influenced by environmental fluctuations on an interannual to multidecadal scale (Chavez et al., 2003). It has been reported that the anchovy fisheries collapsed following a strong El Niño in 1972 and again in 1997-1998 (Bakun and Broad, 2003; Alheit and Niquen, 2004). A marked change in ecosystem structure has been paralleled by changes in the abundance of small pelagic fishes (Cury et al., 2000).

The HUS is used as a case study not only because of its importance to the global fishery, but also because it is one of the most productive systems in the world. The opposite trends are observed between the upwelling intensity, which reflects the nutrient condition, and the phytoplankton concentration on a seasonal scale known as the "seasonal paradox" (Carr and Kearns, 2003). This suggests that the seasonality of ecosystem functioning in the Humboldt Upwelling System is not regulated by the upwelled nutrients. The "seasonal paradox" exhibits the unique feature of high chlorophyll concentration in austral winter when upwelling is strong and low chlorophyll concentration in austral summer when upwelling is weak, which is only observed in HUS but not other EBUSs (Chavez and Messié, 2009; Messié and Chavez, 2015). A few studies (Echevin et al., 2008; Messié and Chavez, 2015) have investigated the driving mechanism behind the "seasonal paradox", yet it has not been fully resolved. Given that the signal of phytoplankton would obviously propagate up the food web and alter the ecosystem, it is crucial to have a deeper understanding of the underlying mechanisms.

1.4.2 The Southern Ocean

The Southern Ocean has a pivotal role in the global carbon cycle and climate, accounting for approximately 40% of global ocean anthropogenic carbon uptake (Caldeira and Duffy, 2000; Gruber et al., 2019; Terhaar et al., 2021) and controlling the global surface nutrient distribution and ocean productivity (Sarmiento et al., 2004; Gruber et al., 2019; Nissen et al., 2021). Even though the Southern Ocean plays an important role, observations of it have been insufficient (Majkut et al., 2014), and simulations are highly uncertain (Laufkötter et al., 2015).

The Southern Ocean is selected as a case study not just for its crucial role in the global carbon cycle but also for its surplus macronutrients, alongside the absence of nutrient-limited signals in both contemporary climate studies (Arteaga et al., 2020; Le Quéré et al., 2003; Boyce et al., 2010) and global warming projections (Doney, 2006; Sarmiento et al., 2004). The phytoplankton biomass in the Southern Ocean is found to be governed by the mixed layer depth-driven light conditions on a seasonal scale (Arteaga et al., 2020). As a characteristic nutrient-rich high latitude region, the Southern Ocean prolonged growing season and

improved mixed-layer light conditions enhance the environment for phytoplankton growth due to the ocean warming (Doney, 2006; Sarmiento et al., 2004). In addition to the phytoplankton increase, zooplankton is also projected to increase, with even an amplified signal under climate change (Chust et al., 2014; Kwiatkowski et al., 2019).

1.5 Chapter synopsis and author contribution

The aims of this thesis are fourfold:

1. To investigate the driving mechanisms of phytoplankton seasonality.
2. To understand how the phytoplankton seasonality transfer up to the zooplankton.
3. To test how changes in the planktonic community affect higher trophic levels.
4. To use current climate to understand and constrain ecosystem simulations under climate change.

To serve these aims, my thesis is composed of four themed chapters. It has been organized as follows:

Chapter 2
Chapter 2 presents the results of climatological simulations of the Humboldt upwelling system to investigate the underlying mechanisms of the primary producer on a seasonal scale under the present climate. While the ecosystem is fueled by the wind-driven upwelling of nutrient-rich waters, surface phytoplankton biomass reveals an opposite pattern to that of upwelling intensity through the course of the year (the "seasonal paradox"). To address the mystery of the "seasonal paradox" and its potential impact, we used a coupled regional physical-biogeochemical model (CROCO-BioEBUS) to simulate the "seasonal paradox" and how it propagates through the ecosystem in the coastal upwelling zone. Our results show that, despite the strong influence of upwelling variation, mixed layer depth (MLD) change still dominates the seasonality of phytoplankton growth and concentration within the water column via dilution and MLD-driven light limitation. This is a first-step signal that propagates up the food web and results in MLD-driven modulation of export efficiency. This study emphasizes the key role of MLD in regulating phytoplankton seasonality in a productive ecosystem that is not nutrient limited, like the Humboldt upwelling system.

This chapter is based on the paper: Xue, T., Frenger, I., Prowe, A. E., José, Y. S., & Oschlies, A. (2022). Mixed layer depth dominates over upwelling in regulating the seasonality of ecosystem functioning in the Peruvian upwelling system. *Biogeosciences*, 19(2), 455-475. https://doi.org/10.5194/bg-19-455-2022. IF and AO conceived and designed the experiments. TX implemented and performed the experiments with support from YSJ. TX

analysed the data with support from IF and FP. TX wrote the manuscript with contributions from IF, FP, AO and YSJ.

Chapter 3

Chapter 3 investigates the response to MLD change further up the food web and discovers the feature of trophic amplification on a seasonal scale. This study uses the same model set-up as in Chapter 2 (CROCO-BioEBUS). We find the seasonal signal of phytoplankton is not proportionally transferred to zooplankton but amplified in the Humboldt upwelling system. This means the consequences for higher trophic levels (e.g., fish) from environmental change would be potentially more severe than our estimation simply based on phytoplankton. Following the notion from Ulanowicz (1995), we have been able to disentangle the disproportional energy transfer to the variation of trophic transfer efficiency (TTE) and the variation of food chain length (FCL). We find the mechanism behind the seasonal trophic amplification comes mainly from the MLD-driven TTE variation. More importantly, we notice the finding also applies to other oceanic regions that are characterized by elevated surface chlorophyll. This study stresses the crucial role of MLD in trophodynamics in productive ecosystems on a seasonal scale.

This chapter is based on the paper: Xue, T., Frenger, I., Oschlies, A., Stock, C. A., Koeve, W., John, J. G., & Prowe, A. E. (2022). Mixed layer depth promotes trophic amplification on a seasonal scale. *Geophysical Research Letter*, 49(12), e2022GL098720. https://doi.org/10.1029/2022GL098720. TX conceived and designed the experiments. TX implemented and performed the experiments and analyzed the data with support from FP and IF. TX wrote the manuscript with contributions from FP, IF, AO, CS, WK, and JJ.

Chapter 4

Chapter 4 is a first attempt to see the bottom-up control, how the lower trophic level (plankton) changes propagate up to the higher trophic level (fish). In this study, a regional physical-biogeochemical model (CROCO-BioEBUS) coupled one-way with an individual-based fish model (OSMOSE) is used to explore the effects of bottom-up forcing on simulated fish community variability and further understand the drivers of fish interannual variability in the Humboldt upwelling system. The results suggest that interannual variation in the plankton community has a minor influence on fish production as the one-way coupled model is not able to simulate the strong interannual variation as observed. Interestingly, our results indicate that changes in fish larval mortality can greatly alter fish production, which highlights the potential impact induced by other physical-biological interactions (e.g., fish larval mortality, habitat distribution), rather than prey (plankton) availability.

This chapter is based on the paper 'Understanding the drivers of fish variability in an end-to-end model of the Northern Humboldt Current System'. The paper is under review

in *Ecological Modelling* by Cruz M., Frenger I., Getzlaff J., Kriest I., Xue T., and Shin Y. (2022). MC, IK, JG conceived and designed the experiments. TX implemented model coupling and calibration of the physical-biogeochemical model. MC further performed the experiments and analyzed the data. MC wrote the manuscript with contributions from IF, JG, IK, TX, and YS.

Chapter 5

Chapter 5 uses previous findings of the impact of mixed layer depth on phytoplankton in a productive ecosystem from contemporary seasonality (Chapter 2) to better constrain simulations within the context of global warming in another productive ecosystem, the Southern Ocean. Current climate change projections towards phytoplankton (chlorophyll) differ dramatically across different model estimations. Therefore, we implement a recently established method, known as "Emergent Constraints," to reduce the climate change model estimation uncertainties based on the observed seasonal correlation between mixed layer depth and surface chlorophyll concentration in the Southern Ocean. The observational constraint implies a 10-16% increase in surface chlorophyll throughout the 21st century under high emissions scenarios, with the uncertainty significantly reduced from 15 to 6%.

Moreover, we associate our findings of the impact of mixed layer depth on trophic transfer from contemporary seasonality (Chapter 3) to better understand the projected trophic amplification under climate change in the Southern Ocean. While total phytoplankton biomass within the water column is projected to increase by 4%, zooplankton reveals a more prominent increase of 12%. A significant part of this is attributable to improved trophic transfer efficiency as a result of shoaling mixed layers, which is similar to our findings on the seasonal scale. With improved phytoplankton growth conditions and the stronger grazing pressure, this study emphasizes the potential increasing importance of "top-down" control under climate change.

This chapter is a manuscript in preparation by Xue T., Frenger I., Koeve, W., and Oschlies A. (2022). TX, IF, and WK conceived the experiment. TX analyzed the data and wrote the manuscript with contributions from IF, WK, and AO.

Chapter 2

Mixed layer depth dominates over upwelling in regulating the seasonality of ecosystem functioning in the Peruvian Upwelling System

This chapter is based on the paper 'Mixed layer depth dominates over upwelling in regulating the seasonality of ecosystem functioning in the Peruvian Upwelling System' published in the Biogeosciences.

Citation: Xue, T., Frenger, I., Prowe, A. E., José, Y. S., & Oschlies, A. (2022). Mixed layer depth dominates over upwelling in regulating the seasonality of ecosystem functioning in the Peruvian upwelling system. Biogeosciences, 19(2), 455-475. https://doi.org/10.5194/bg-19-455-2022

Abstract

The Peruvian Upwelling System hosts a marine ecosystem with extremely high productivity. Observations show that the Peruvian Upwelling System is the only Eastern Boundary Upwelling System (EBUS) with an out-of-phase relationship between seasonal surface chlorophyll concentrations and upwelling intensity. This "seasonal paradox" triggers the following questions: (1) What are the unique characteristics of the Peruvian Upwelling System, compared with other EBUS, that lead to the out-of-phase relationship; and (2) How does the seasonal paradox influence ecosystem functioning? Using observational climatologies for four EBUS, we diagnose that the Peruvian Upwelling System is the only one to reveal that intense upwelling coincides with deep mixed layers. We then apply a coupled regional ocean circulation-biogeochemical model (CROCO-BioEBUS) to assess how the interplay between mixed layers and upwelling regulates the seasonality of surface chlorophyll in the Peruvian Upwelling System. Our model reproduces the "seasonal paradox" within 200 km off the Peruvian coast. We confirm previous findings regarding the main contribution of mixed layer depth to the seasonality of chlorophyll, relative to upwelling. Deep mixed layers in austral winter cause vertical dilution of phytoplankton and strong light limitation, impacting growth. The effect of advection, though second-order, is consistent with previous findings for the Peruvian system and other EBUS, with enhanced offshore export opposing the coastal buildup of biomass. In addition, we find that the relatively colder temperatures of upwelled waters slightly dampen phytoplankton productivity and further slow the buildup of phytoplankton biomass. This impact from the combination of deep mixed layers and upwelling propagates through the ecosystem, from primary production to export and export efficiency. Our findings emphasise the crucial role of the interplay between mixed layer depth and upwelling and suggest that surface chlorophyll may increase, along with a weakened seasonal paradox, in response to shoaling mixed layers under climate change.

2.1 Introduction

The Peruvian Upwelling System (PUS) hosts a disproportionally productive ecosystem, supporting 10% of the world's fishing yield while covering only 0.1% of the ocean area (Chavez et al., 2008). As one of the Eastern Boundary Upwelling Systems (EBUS), winds favouring upwelling raise cool, nutrient-rich waters to the surface, supporting high primary production and fish yield. Simultaneously, high primary production, together with subsequent export and remineralisation contributes to the formation of a sub-surface oxygen-deficient zone which is particularly shallow and intense in the PUS (Fuenzalida et al., 2009; Stramma et al., 2010; Getzlaff et al., 2016). Particularly due to its high productivity, the response of the PUS to climate change is of great social and economic interest (Pauly et al., 1998; Bakun, 1990; Bakun et al., 2010), and a variety of studies have investigated how physical and biogeochemical processes influence the production of phytoplankton as well as its po-

tential links to ecosystem functioning in the PUS.

While the PUS has been frequently compared to other EBUS (e.g., the Benguela, California, and Canary Systems), it is set apart by how surface chlorophyll responds to the variation of upwelling on a seasonal scale. The high productivity of EBUS primarily benefits from the upwelling of nutrient-rich waters, driven by alongshore equatorward winds. Hence, it is commonly assumed that the magnitude of phytoplankton biomass in EBUS is directly correlated with the wind-driven upwelling intensity (Bakun, 1973). However, in the PUS, upwelling intensity and surface chlorophyll are not correlated on a seasonal scale (hereafter referred to as "seasonal paradox"; Chavez, 1995; Thomas et al., 2001; Echevin et al., 2008; Chavez and Messié, 2009). Instead, they are out of phase, with the lowest surface chlorophyll concentration in austral winter corresponding to maximum upwelling intensity (Calienes et al., 1985). Echevin et al. (2008) used a regional coupled physical-biogeochemical model to simulate the "seasonal paradox" and found that deep mixed layers caused dilution of surface phytoplankton, reduced growth due to limited light, and subsequently reduced iron levels (as phytoplankton require more iron under low-light conditions). This ultimately leads to low chlorophyll under strong upwelling conditions. Results from Messié and Chavez (2015) corroborated iron and light limitations found in Echevin et al. (2008), showing additionally that relatively strong offshore advection in austral winter regulated the buildup of phytoplankton and thus also contributed to the seasonal paradox. Guillen and Calienes (1981) suggested that lower surface irradiation in winter might amplify light limitation and further limit phytoplankton growth, while insolation was found not to play a major role in Echevin et al. (2008). Additionally, Echevin et al. (2008) concluded that temperature played no role in regulating phytoplankton growth. Despite previous research on surface chlorophyll seasonality, uncertainty still remains regarding why the seasonal paradox occurs only in the PUS and not in the other EBUS, and it is unexplored how the seasonal paradox affects ecosystem functioning.

This study addresses the following key questions: (1) what are the unique characteristics of the PUS, compared to other EBUS, that lead to this seasonal paradox; (2) what are the mechanisms that cause low surface phytoplankton in winter; and (3) how do these mechanisms affect ecosystem functioning.

2.2 Data and Methods

2.2.1 Regional ocean circulation-biogeochemical model: setup and simulation

We use a climatological simulation of the three-dimensional regional ocean circulation model CROCO (Coastal and Regional Ocean COmmunity model; Debreu et al., 2012) coupled with

the biogeochemical model BioEBUS (Biogeochemical model for the Eastern Boundary Upwelling Systems; Gutknecht et al., 2013) for this study.

The same technical setup, including the model grid, is used as in José et al. (2017), along with an updated version of the ocean circulation model CROCO. CROCO is the next generation of the ROMS AGRIF model (Tedesco et al., 2019), and is a free-surface and split-explicit regional ocean model system (ROMS; Shchepetkin and McWilliams, 2005). We employ a two-way nesting approach, with the larger coarser-resolution domain covering the Southeast Pacific and the smaller higher-resolution domain focusing on the PUS. The larger domain has a 1/4° resolution, spanning from 69°W to 120°W and from 18°N to 40°S. The embedded "child" domain has a resolution of 1/12° and extends from 5°N to 31°S and from 69°W to 102°W (Fig. 2.1a-b & A.1) and is used in this study. Both the coarse- and fine-resolution domains use 32 sigma levels in the vertical direction, with finer resolution towards the surface and shallower regions. The surface layer thickness ranges from 0.5 m in the coastal region (water depth around 50 m) to around 3 m in the offshore region (water depth of more than 4000 m). Initial and boundary conditions are provided by the monthly climatological SODA reanalysis (Simple Ocean Data Assimilation; Carton and Giese, 2008) from 1990−2010. Surface forcing is based on the monthly climatological heat and freshwater fluxes from COADS (Comprehensive Ocean-Atmosphere Data Set; Worley et al., 2005), along with wind data from QuikSCAT (Quick Scatterometer; Liu et al., 1998). The physical setup is the same as in José et al. (2017) and has been evaluated therein, showing that the model reproduces the circulation of the region reasonably well.

The biogeochemical BioEBUS model used in this study was developed explicitly for applications to EBUS and oxygen minimum zones (Gutknecht et al., 2013). BioEBUS is a nitrogen-based model, originating from the $N_2P_2Z_2D_2$ model by Koné et al. (2005). It simulates two phytoplankton and two zooplankton groups: small and large phytoplankton, along with micro- and mesozooplankton. Furthermore, there are two detritus pools, categorised by size. BioEBUS resolves the N species (nitrate, nitrite and ammonium) and simulates processes under oxic, hypoxic and suboxic conditions (e.g., remineralisation, nitrification, denitrification and anammox). The BioEBUS model was first used to study the Peruvian marine biogeochemistry by Montes et al. (2014), and is capable of producing a realistic simulation of the oxygen distribution. Initial and boundary conditions for nitrate and oxygen are taken from CARS (CSIRO (Commonwealth Scientific and Industrial Research Organisation) Atlas of Regional Seas; Ridgway et al., 2002), and initial conditions for phytoplankton are based on monthly climatological SeaWiFS (Sea-viewing Wide Field-of-view Sensor; O'Reilly et al., 1998) estimates. A detailed description of these biogeochemical processes can be found in Gutknecht et al. (2013). The parameter settings are the same as in José et al. (2017), except for a few adjustments of biological parameters (Table. A.1) to improve the fit between the simulated ecology, in particular phytoplankton and zooplank-

ton, and the observations.

CROCO-BioEBUS is run in coupled mode from the beginning of the simulation. The time-stepping of the physical model is the same as the coupling time step, with a duration of 1200 seconds. The time-stepping of the biogeochemical model has a duration of 400 seconds. The coupled model is run for a 25-year spin-up period. Physical and biogeochemical fields are spun up after one year for the upper 10 m, while waters in the depth range of upwelling (100 m) require 3–10 years longer to reach a statistical quasi-equilibrium (Fig. A.8). We run the model for a total of 30 climatologically-forced years, using the last five years for the analyses. As we observe from the surface ecology, our results are not sensitive to deep ocean spin-up. This study focuses on the 200 km band off the Peruvian coast (white line region in Fig. 2.1a-b), which shows clear seasonal variation as well as strong upwelling.

2.2.2 Analysis approaches

To assess the seasonal variance of phytoplankton biomass concentration in each grid box (C), we analysed the budget of the phytoplankton biomass and how its tendency is driven by physical versus biological processes:

$$\frac{\partial C}{\partial t} = PHY(C) + BIO(C) \tag{2.1}$$

$$\text{with } [BIO = PP - GRAZ - MORT - EXU - SINK;\ PHY = MIX + ADV] \tag{2.2}$$

PHY represents the physical processes, including advection ADV and mixing MIX, whereas BIO represents the biological processes, namely primary production PP, consumptive mortality $GRAZ$, natural mortality $MORT$, exudation EXU and sinking $SINK$. All biological and physical fluxes were saved monthly from the simulation, with units of mmol N m^{-3} s^{-1}, and we integrated the terms offline over the mixed layer depth (MLD) using the croco-tools provided for post-processing (https://www.croco-ocean.org/download/croco-project/). The mixing term also includes entrainment from varying MLD as a minor contribution.

We analysed in detail the drivers of PP, which was calculated online by multiplying phytoplankton concentration (C) and the growth factors ($L_{(PAR)}, L_{(T)}, L_{(N)}$)

$$PP = C \cdot L_{(PAR)} \cdot L_{(T)} \cdot L_{(N)} \tag{2.3}$$

where $L_{(PAR)}, L_{(T)}, L_{(N)}$ represent the light-, temperature- or nitrogen-related growth factors, respectively. Here, the phytoplankton growth rate was defined as a multiplicative function of the light-, temperature- or nitrogen-related growth factors. The limitation experienced by phytoplankton within the mixed layer L_{mld} is calculated offline from each growth factor ($L_{(\text{PAR})}$, $L_{(\text{T})}$ and $L_{(\text{N})}$), using phytoplankton concentration (C) within the mixed layer as a weight (Eq. 2.4). Light-, temperature- and nitrogen-related growth factors

that each phytoplankton cell experienced were computed online.

$$L_{\mathrm{mld}} = \frac{\sum_0^{\mathrm{mld}} L_{(\mathrm{PAR})} \cdot L_{(\mathrm{T})} \cdot L_{(\mathrm{N})} \cdot C}{\sum_0^{\mathrm{mld}} C} \tag{2.4}$$

For the analysis, we attributed the seasonal change of the average phytoplankton biomass concentration (ΔC_{mld}) within the mixed layer to the change in the integrated phytoplankton content within the mixed layer (ΔB_{mld}), as well as the change in volume of the mixed layer (ΔV_{mld}). Using the chain rule and the condition that $V^2 >> V\Delta V$, we approximated a discrete change in the mixed layer tracer concentration (ΔC_{mld}) as follows:

$$\Delta C_{\mathrm{mld}} = \frac{1}{V_{\mathrm{mld}}}\Delta B_{\mathrm{mld}} - B_{\mathrm{mld}}\frac{\Delta V_{\mathrm{mld}}}{V_{\mathrm{mld}}^2} = \frac{B_{\mathrm{mld}}}{V_{\mathrm{mld}}}\frac{\Delta B_{\mathrm{mld}}}{B_{\mathrm{mld}}} - \frac{B_{\mathrm{mld}}}{V_{\mathrm{mld}}}\frac{\Delta V_{\mathrm{mld}}}{V_{\mathrm{mld}}} \tag{2.5}$$

To assess the relative contributions, we then divided by $C_{\mathrm{mld}} = B_{\mathrm{mld}} \cdot V_{\mathrm{mld}}^{-1}$ to obtain

$$\frac{\Delta C_{\mathrm{mld}}}{C_{\mathrm{mld}}} = \frac{\Delta B_{\mathrm{mld}}}{B_{\mathrm{mld}}} - \frac{\Delta V_{\mathrm{mld}}}{V_{\mathrm{mld}}} \tag{2.6}$$

which allowed us to attribute decreased concentration of phytoplankton in the mixed layer C_{mld} to a decrease in the phytoplankton biomass B_{mld} or an increase in the mixed-layer volume V_{mld}, and vice versa.

2.2.3 Observational data and model assessment

For EBUS comparisons, we digitised SeaWIFS climatological surface chlorophyll and upwelling (a combination of Ekman transport and Ekman pumping; Messié et al., 2009), estimated based on winds from QuikSCAT, from Chavez and Messié (2009). Additionally, we used surface nitrate data from the World Ocean Atlas (WOA; Garcia et al., 2019), the gridded ARGO mixed layer dataset (http://mixedlayer.ucsd.edu/; Holte et al., 2017), monthly climatologies of MODIS sea surface temperature (SST) and chlorophyll data (https://oceancolor. gsfc.nasa.gov/data/aqua/) to analyse and evaluate the model results.

The model was evaluated based on averages over the focus region, with monthly observational data. The correlation coefficient between the model simulation and observations, the root mean square error (RMSE) and the normalised standard deviation (SD) of the observations relative to the model results are shown in a Taylor diagram as a summary of the evaluation (Fig. 2.1c; Taylor et al., 1991, a comparison of the spatial pattern and the seasonal cycles of variables is provided in the appendix, see Figs. A.3-A.6). Model results fit the observational data reasonably well. The model effectively simulated SST with R>0.95, 1<σ^*<1.2 and $RMSE^*$<0.4 (R: correlation coefficient, σ^*: normalised SD, and RMSE*: normalised RMSE). It also captured the observed seasonal cycle well, though it produced slightly stronger seasonal variations compared to those from the observational data. Although the seasonal variation was somewhat overestimated, the simulated MLD

(defined based on a 0.2 ^oC temperature difference criterion) remained largely within the observed range of ARGO-based MLD (Fig. A.5). As for biogeochemical variables, the model effectively simulated surface nitrate, with R>0.95, 0.6<σ^*<1 and $RMSE^*$<0.4, but overestimated the nitrate compared to WOA. However, cruise data (Fig. A.4c-d) show that the overestimation could have arisen from WOA failing to capture the high-surface nitrate concentration in the coastal region under strong upwelling. A comparison of the simulated and observed seasonal cycle of surface chlorophyll in the focus region (Fig. 2.1d) revealed that modelled chlorophyll generally followed the seasonal trend of satellite and *in situ* data, with the amplitude of the seasonal cycle in between amplitudes from satellite and *in situ* data. Overall, the model showed reasonably good agreement with observational data on a seasonal scale, sufficiently supporting an investigation of the seasonal paradox with CROCO-BioEBUS.

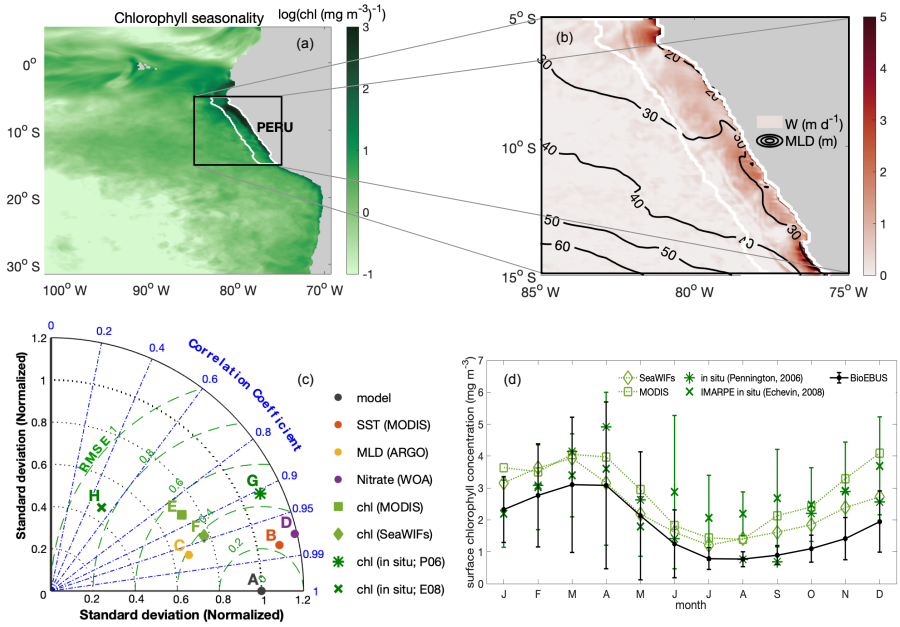

Figure 2.1: (a) Spatial distribution of the amplitude of the annual cycle of surface chlorophyll in log scale ($log(chl\,(mg\,m^{-3})^{-1})$); (b) Map of annual mean upwelling velocity w ($m\,d^{-1}$) at the bottom of the mixed layer, with contour lines indicating MLD (m). White lines highlight the focus area; (c) Taylor diagram for seasonal SST (red), MLD (yellow), surface nitrate (purple) and chlorophyll (green) concentrations. The black dot indicates the model simulation as a reference. The radial distance from the origin is proportional to the standard deviation, normalised by the standard deviation of the data. The green dashed lines show the RMSE. The correlations between model and observations are given by the azimuthal position; (d) Seasonal cycles of surface chlorophyll concentration from model simulation (black solid line), satellite data (dotted line; SeaWIFS (diamond) and MODIS (square)) and in-situ data (digitised from Pennington et al. (2006, star, 250 km band off the coast) and Echevin et al. (2008, cross)). Error bars indicate the standard deviation.

2.3 Results

2.3.1 Anticorrelation of chlorophyll and upwelling: The seasonal paradox only appears in the Peruvian upwelling system

Compared with other EBUS (spatial extent of EBUS regions indicated in Fig. A.2), the Peruvian system is unique in that it shows a clear anticorrelation between surface chlorophyll concentration and upwelling intensity on a seasonal scale, with lowest chlorophyll concentrations when upwelling is most intense (Fig. 2.2a, $R^2 = 0.71$; Chavez and Messié, 2009). While the surface chlorophyll in the Benguela system does not feature a strong seasonality, surface chlorophyll closely follows upwelling intensity in the California ($R^2 = 0.92$) and Canary ($R^2 = 0.88$) systems, suggesting that upwelling of nutrient-rich waters fuels the increase in chlorophyll. Indeed, comparatively low surface nitrate concentrations indicate that nitrate is depleted, potentially limiting phytoplankton growth throughout the year in the California system and for approximately half the year in the Canary system (Fig. 2.2b). In contrast, the Benguela ($R^2 = 0.63$) and Peruvian systems ($R^2 = 0.90$) feature replete surface nitrate over most of the year. Because higher nitrate concentrations correlate with lower chlorophyll in these cases, nitrate is not observed to be a limiting factor.

In the Peruvian system, a strong relationship exists between deepening mixed layers and decreasing chlorophyll (Fig. 2.2c, $R^2 = 0.91$), which supports the notion that dilution of phytoplankton over a deeper mixed layer and/or light limitation plays a role, as found by Echevin et al. (2008). The California system shows a similar response to mixed layer variations ($R^2 = 0.62$), suggesting that the same process may play a role there as well. Additionally, surface chlorophyll shows significant correlation with SST in the Peruvian (Fig. 2.2d, $R^2 = 0.73$) and California systems ($R^2 = 0.65$), suggesting that increasing temperatures stimulate phytoplankton growth.

Strikingly, the Peruvian system is the only one of the four EBUS where strong upwelling coincides with deep MLD (Fig. 2.2e, $R^2 = 0.79$). The Canary and Benguela systems exhibit pronounced seasonality either in upwelling or in mixed layer depth, respectively. In the California system, the relationship of upwelling and mixed layer depth is opposite to that of the Peruvian system, with the strongest upwelling occurring in the shallowest mixed layers. Given the paradox that strong upwelling in the Peruvian system occurs at the time of the yearly chlorophyll minimum, it is intuitive that the concurrent deep mixed layers offset the positive impact of upwelled nutrients. Nutrient enrichment would only stimulate higher productivity if the region was nutrient limited. If concentrations are already elevated, adding more nutrients would have a weak impact. We will further investigate the interplay of the seasonality of mixed layers and upwelling in the Peruvian system in the following sections.

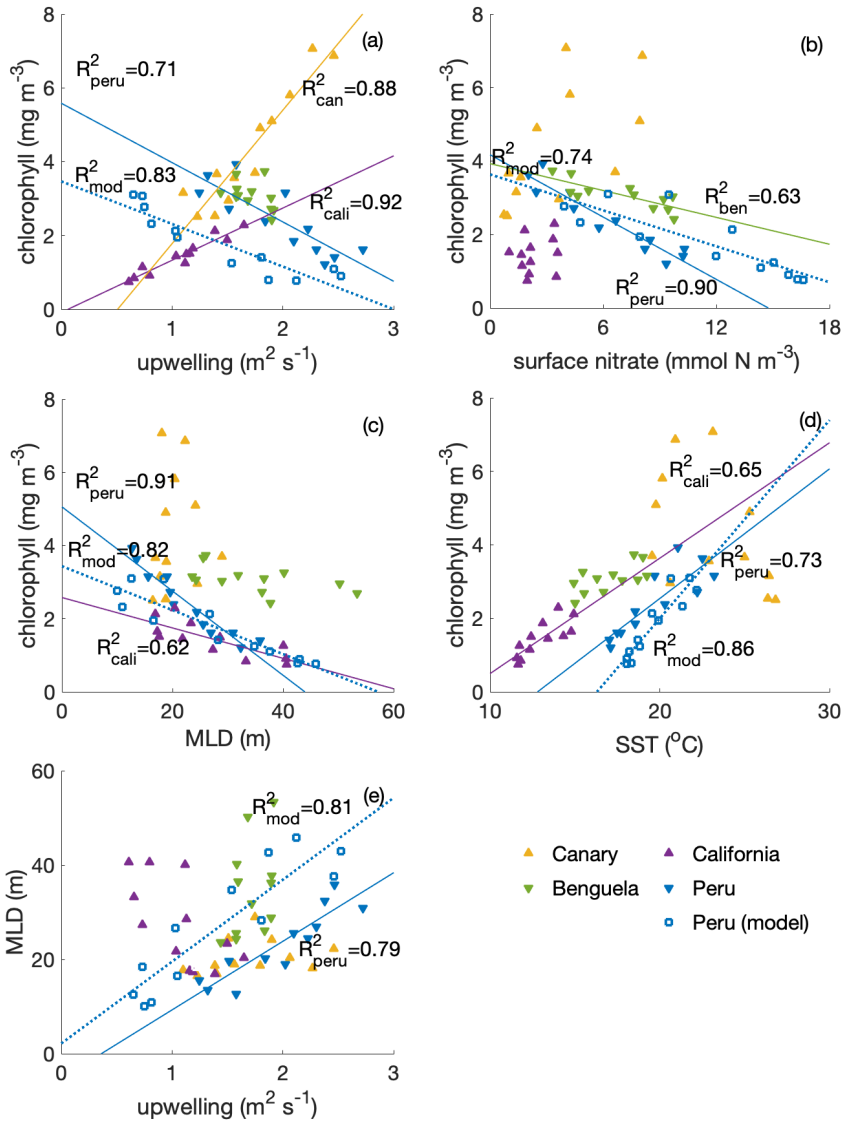

Figure 2.2: Correlations of surface chlorophyll (SeaWIFS climatology, in $mg\,m^{-3}$) with (a) upwelling (a combination of Ekman transport and Ekman pumping, estimated based on winds from QuikSCAT, in Sv, digitised from Chavez and Messié (2009), for calculations see Messié et al. (2009)); (b) surface nitrate concentration (WOA, in $mmol\,N\,m^{-3}$); (c) MLD (ARGO, in m); (d) SST (MODIS, in ^oC) and (e) correlation of MLD and upwelling transport among four eastern boundary upwelling systems (EBUS). For the Peruvian system, we also show the model (CROCO-BioEBUS) results. Lines and R^2 values are displayed for correlations with $R^2 > 0.5$.

2.3.2 Modelled phytoplankton biomass, dissolved inorganic nitrogen, upwelling and the MLD in the Peruvian system

We used a regional ocean circulation model, coupled to a marine biogeochemical model (CROCO-BioEBUS), to further analyse the Peruvian system (see the "Data and Methods" section). The model effectively reproduced the observed estimate of the seasonal out-of-phase relationship between surface phytoplankton biomass and upwelling intensity as well as nitrate concentrations (Fig. 2.2, open squares). Over the course of the year, surface chlorophyll, surface nitrogen concentrations, upwelling intensity and MLD varied by 40 - 60% relative to their annual mean values. Surface phytoplankton biomass concentration reached its maximum from late austral summer to early autumn (March to April), when upwelling was relatively weak (Fig. 2.3a-b). During this time window, less nitrogen is available within a shallow MLD compared with the rest of the year. In austral winter (July to September), when upwelling introduces ample nitrogen into the deep mixed layer, surface phytoplankton concentration reaches a minimum.

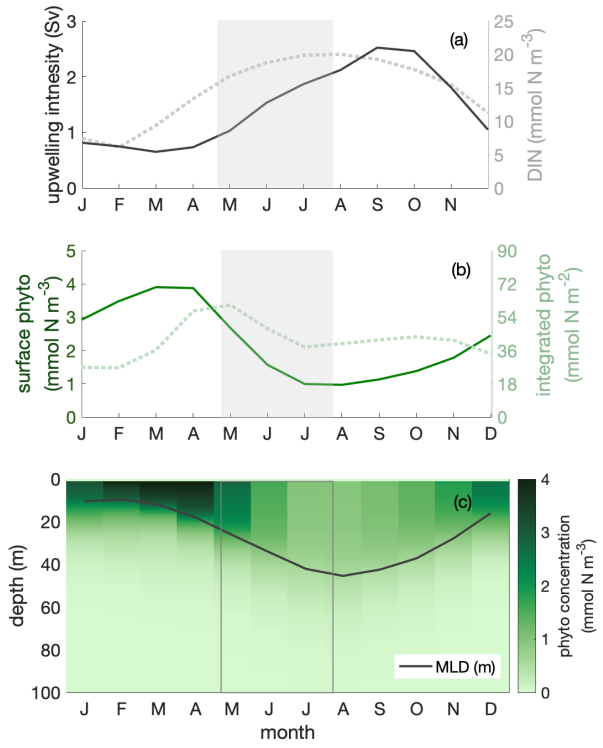

Figure 2.3: Seasonal cycles of (a) upwelling intensity (in Sv, solid line) and surface dissolved inorganic nitrogen (DIN) concentration (in $mmol\,N\,m^{-3}$, dotted line); (b) surface (in $mmol\,N\,m^{-3}$, solid line) and mixed layer depth (MLD)-integrated phytoplankton biomass (in $mmol\,N\,m^{-2}$, dotted line); (c) phytoplankton depth-month distribution, showing the seasonal cycle of MLD (in m, solid line) within the focus region. The shaded area indicates the decline phase of MLD-integrated phytoplankton biomass.

2.3.3 Biomass dilution by the deepening mixed layer

Dilution of phytoplankton in deepening winter mixed layers is a key driver behind the seasonality of surface phytoplankton concentration. Within the research area, the MLD showed a seasonal variation with the shallowest mixed layer in austral summer, around 10 m, and the deepest mixed layer in austral winter, around 45 m. Phytoplankton were vertically well mixed within the mixed layer throughout the year (Fig. 2.3c). In austral winter, within the 'deep-mixing' regime, phytoplankton were evenly distributed over a relatively deep mixed layer, diluting phytoplankton biomass. Accordingly, phytoplankton biomass concentrations in the mixed layer as well as at the surface decreased. Hence, we infer that seasonal mixed layer deepening and shoaling alone is an important factor in driving phytoplankton concentrations at the ocean surface, as observed for instance from satellite images.

While dilution caused a decrease in winter surface phytoplankton biomass, it explained only part of the observed biomass decrease. The decline persisted, even though attenuated, when integrating phytoplankton over the mixed layer (Fig. 2.3b). The phytoplankton concentration at the surface and within the mixed layer declined by around 70%, while it declined by around 30% for MLD-integrated biomass between late April and late July (shaded area in Fig. 2.3 2.6, hereafter referred to as the decline phase). The decline of surface phytoplankton concentrations can be attributed to the decline due to the increase in mixed layer volume ΔV (dilution effect, see Eq. 2.6) and the decrease in biomass ΔB within the mixed layer through local biological and physical processes (see Eq. 2.6). During the decline phase, ΔV contributed by slightly more than half to the concentration change, while ΔB contributed slightly less than half. That is, the dilution effect due to the deepening mixed layer in the decline phase amplified the decline of surface biomass concentrations by approximately a factor of two. However, dilution could not fully explain the low phytoplankton biomass in conditions where the supply of nitrogen is ample; in such conditions, MLD-integrated biomass still declined by around 30%.

2.3.4 Biological and physical processes change the total biomass within the mixed layer

Disentangling physical and biological processes

In addition to causing dilution due to the deepening mixed layer, the imbalance of a series of biological and physical processes during the decline phase diminished phytoplankton concentrations. To disentangle their contributions to the decline of phytoplankton concentration without the complicating factor of the dilution effect, we next analysed the change of phytoplankton biomass integrated over the mixed layer (Fig. 2.4a) and its drivers; that is, the mixed layer budget of phytoplankton biomass (Eq. 2.1). We separated biological processes (primary production, grazing from zooplankton, natural mortality, exudation and

sinking) and physical processes (mixing and advection) that affect the integrated biomass. Throughout the year, the net biological flux (the sum of all biological fluxes) was positive ("biological gain", Fig. 2.4b), thus supporting an increase in biomass. In contrast, the net physical flux, the sum of all physical fluxes, was negative ("physical loss"), therefore supporting a decrease in biomass. The time point t1 marks the seasonal maximum of the MLD-integrated phytoplankton biomass, and t2 marks the minimum at the end of the decline phase. At t1 and t2, the net biological and physical fluxes balanced (Fig. 2.4b-c) and the tendency of the mixed layer phytoplankton biomass was zero (Fig. 2.4a). Between t1 and t2 (Fig. 2.4b), the net biomass supply due to biological fluxes decreased more quickly than the net biomass removal due to physical fluxes, resulting in an imbalance of the fluxes and the decrease in biomass between t1 and t2.

To determine which terms from Eq. 2.1 mostly drove the decrease of the biomass between t1 and t2 (Fig. 2.5a), we integrated the change of each term over time (that is, the derivatives) between t1 and t2. Therefore, in Fig. 2.5b and c, if a bar was positive, the change of the term during the decline phase (t1 - t2) promoted an increase of the phytoplankton biomass, mostly as a result of reduced grazing pressure and reduced downward mixing. If the bar was negative, the change of the term during the decline phase (t1 - t2) opposed an increase in phytoplankton biomass. The "opposing terms" that acted to reduce phytoplankton biomass were the ones that contributed to the seasonal paradox; that is, decline in biomass despite increased supply of nutrients due to upwelling. These terms mostly referred to the reduced primary production, with a secondary contribution from the increased divergence due to advection. Details regarding the two major contributors, primary production and advection, are presented in the following sections.

Factors limiting primary production

Primary production changed due to variations in both the growth factor and the biomass (Eq. 2.3). The growth factor (calculated as in Eq. 2.4, Fig. 2.6a) combined the effects of light, temperature and nitrogen on phytoplankton growth. It showed a clear decrease of around 30% during the decline phase. Optimal phytoplankton growth conditions were reached in March, despite the low dissolved inorganic nitrogen (DIN) conditions, within the warmest and brightest environment. The lowest growth rate occurred just after the decline phase, despite relatively high nitrogen concentrations, due to limiting light and temperature conditions.

Strong light limitation experienced by phytoplankton, in combination with low temperatures, slowed growth during the decline phase. Light conditions for phytoplankton growth were optimal in March when the water was rather stratified and worsened over the decline phase to a minimum in August when the water column was most deeply mixed (Fig. 2.6a).

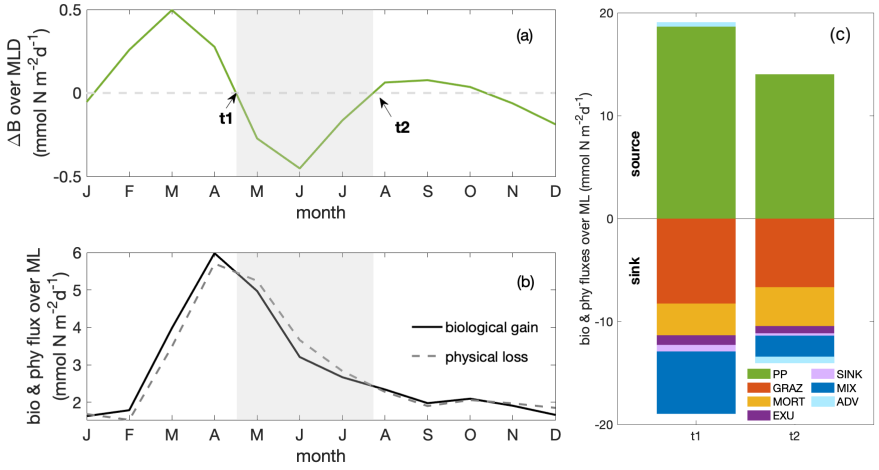

Figure 2.4: Seasonal cycles of (a) total phytoplankton biomass change (ΔB; in mmol N m^{-2} d^{-1}). Grey shading indicates the decline phase, with t1 and t2 marking the beginning and end of the decline phase; (b) phytoplankton fluxes resulting from net biological gain (bio) and net physical loss (phy, in mmol N m^{-2} d^{-1}, as shown in Eq. 1); (c) Balancing budgets of phytoplankton fluxes at t1 and t2 (PP: primary production; GRAZ: consumptive mortality; MORT: natural mortality; EXU: exudation; SINK: sinking; MIX: mixing; ADV: advection). Fluxes are distinguished as sources (positive values) and sinks (negative values) of phytoplankton biomass, with the sum of all source and sink terms balancing at times t1 and t2. All fluxes are integrated over the MLD.

The light-related growth factor declined by 17% during the decline phase and would decrease the growth factor by approximately 60% in the absence of other limiting factors (estimated from the product rule for differentiation and the multiplicative relation of growth factors shown in Eq. 2.3 & 2.4). Decreasing temperature was the second most important contributor in slowing the growth rate during the decline phase. The temperature-related growth factor reached its maximum by March, similar to the light-related growth factor, and reached its minimum by October. The temperature-related growth factor declined by 12% and would decrease the growth factor by around 40% during the decline phase, in the absence of other limiting factors. In contrast, the seasonality of the growth factor due to nitrogen showed the opposite seasonality compared to the total growth factor. Clearly, light and temperature regulated primary production and overrode the effect of enhanced nitrogen supply during the decline phase. Therefore, while light was the dominant mechanism that reduced productivity towards winter, we found that temperature played a relevant secondary role.

Stronger light and temperature limitation during the decline phase were due to deeper mixing and stronger upwelling of cold waters, respectively (Fig. 2.6b-c). While upwelling intensity was approximately correlated with MLD, the maximum upwelling occurred just after the deepest mixed layers. The variation of MLD-averaged light limitation was correlated (R^2 = 0.92) with the change of MLD. As phytoplankton were evenly distributed

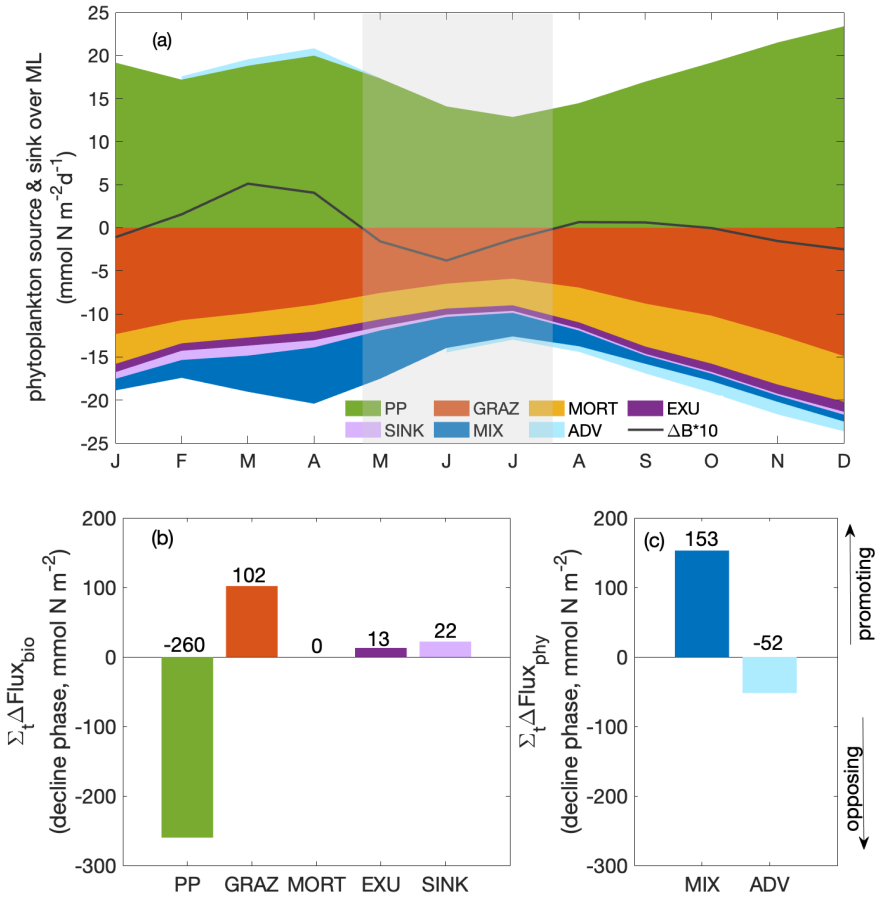

Figure 2.5: (a) Seasonal cycle of phytoplankton source and sink processes, as well as phytoplankton biomass change (ΔB multiplied by a factor of 10; solid line); bar plots of the integrated change over the decline phase due to (b) biological fluxes and (c) physical fluxes averaged over the focus region (PP: primary production; GRAZ: consumptive mortality; MORT: natural mortality; EXU: exudation; SINK: sinking; MIX: mixing; ADV: advection). A positive or negative sign of the bars here designates fluxes promoting and opposing an increase in MLD-integrated phytoplankton biomass, respectively. The magnitude (including the sign) of the integrated change is given as numbers above and below the bars.

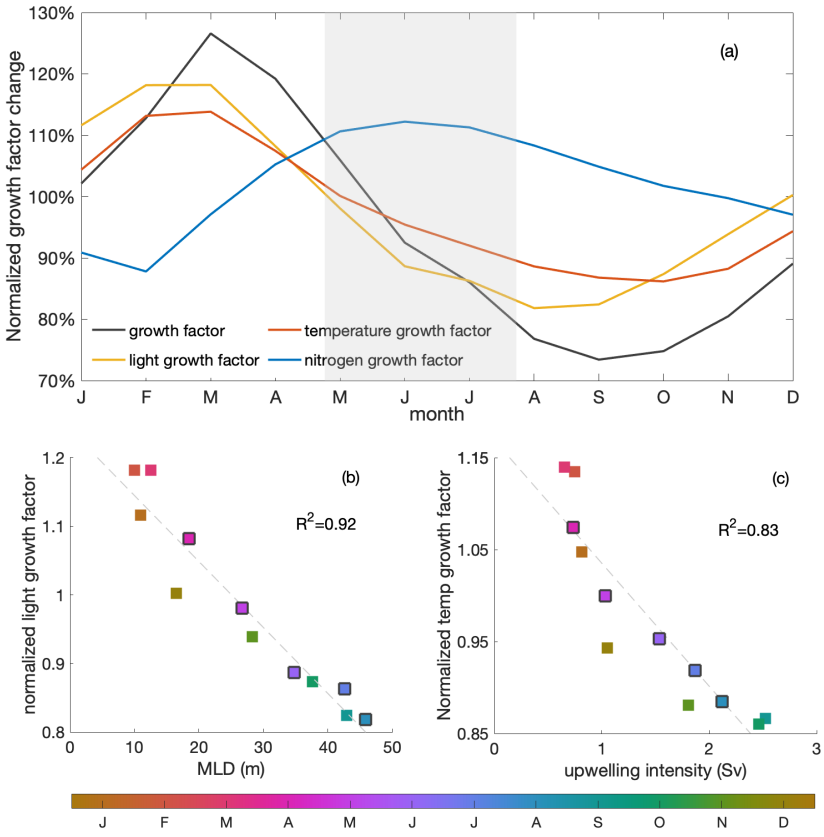

Figure 2.6: (a) Seasonal cycles of the normalised total (black) growth factor and light (yellow)-, temperature (red)- and nitrogen (blue)-related growth factors for phytoplankton over the mixed layer. The grey shading indicates the decline phase. (b) Seasonal correlation of MLD and mixed layer-averaged light-related growth factor; (c) correlation of upwelling intensity and mixed layer-averaged temperature-related growth factor. Colours indicate the time of the year (months), with black edges indicating the months of the decline phase. The R^2 values of the correlations are shown in the right-hand sides within the panels.

within the mixed layer, deeper MLD indicated that, on average, more phytoplankton were exposed to lower light conditions during the decline phase, with a minimum in August when mixed layers were deepest. The change of the temperature-related growth factor within the mixed layer was closely related with the seasonal variation of upwelling intensity ($R^2 = 0.83$), with the lowest values occurring in September and October when upwelling intensity reached its maximum. During the decline phase, cold waters were upwelled into the mixed layer at a higher rate, further damping phytoplankton growth in addition to the effects of limiting light conditions. Reduced winter surface solar radiation and heat loss to the atmosphere also played a role in the seasonality of the light and temperature growth factors, respectively (Fig. A.9), though to a much smaller extent (not shown) which agrees with findings in Echevin et al. (2008).

Enhanced upwelling and offshore transport of phytoplankton

An enhanced advective loss of mixed layer phytoplankton is a second-order process, promoting the decrease of MLD-integrated phytoplankton biomass during the decline phase (Fig. 2.5c). Similar to the effects of nutrients, phytoplankton biomass is affected by the seasonality of upwelling and offshore export of waters. Relatively dilute concentrations of phytoplankton growing below the base of the mixed layer are upwelled into the mixed layer, while waters with mixed-layer-averaged phytoplankton concentrations are pushed offshore. During the decline phase, the upwelling and offshore transport of water increased and a greater volume of what was produced in coastal waters was exported offshore: 4% of primary production was lost via advection by the end of the decline phase compared to 2% gained at the beginning. This greater loss of biomass due to divergent lateral advection was mainly caused by stronger upwelling during the decline phase (Fig. A.10).

2.3.5 Seasonal Paradox: from phytoplankton to export

Small and large zooplankton exhibit the same "seasonal paradox" pattern as phytoplankton, and so does the export of organic material to the deeper ocean. Similar to phytoplankton, both small and large zooplankton are vertically well mixed within the mixed layer throughout the year (contours and colours in Fig. 2.7a, respectively). Biomass concentrations are high in austral summer and low in austral winter, in opposition to the upwelling trend. Additionally, the particulate organic matter, the sum of plankton biomass and other organic particles, follows the same pattern, with large amounts of particulate organic matter concentrated in a shallow mixed layer during the productive summer (Fig. 2.7b). The pattern of organic matter in the water column is then reflected in the export pattern of sinking organic material, composed of large phytoplankton as well as small and large detritus (Fig. 2.7c). Export below 100 m depth is high during the productive summer, when the mixed layer is shallow and particulate organic matter is large, and low in winter (Fig. 2.7b, black line). That is, the model's ecosystem is affected by the seasonal variation of the MLD.

Finally, export efficiency also follows the seasonal cycle of the MLD. Export efficiency is defined as the export of sinking organic material through the 100 m depth level, relative to primary production in the upper 100 m. It reaches a maximum in austral summer, when MLD is shallow, and a minimum in austral winter, when MLD is deep (Fig. 2.7d). As both export and primary production show the same seasonal trend as phytoplankton biomass, export must overcompensate the change in primary production and vary even more, in order to allow export efficiency to reveal the same seasonal trend. Export largely consists of large detritus originating from large zooplankton faecal pellets and mortality (Fig. 2.7c). Since large detritus possesses the fastest sinking speed compared to other components, it sinks the most efficiently. The relative contribution of fast-sinking large detritus to total export is largest in summer, close to 100 %, which may partially explain the higher export efficiency. In addition to changes in composition of the sinking organic material, other processes may cause export to be amplified relative to phytoplankton production. These include: (1) changes in structure and trophic transfer efficiency of the plankton food web, and (2) a varying degradation of sinking organic matter in the upper 100 m, that is, differences in the remineralisation. The detailed mechanisms behind the seasonality of export efficiency are beyond the focus of this paper and will be investigated in a separate study.

2.4 Discussion

2.4.1 Mixed layer depth drives surface phytoplankton biomass seasonality in the Peruvian upwelling system

The regional ocean circulation-biogeochemical model that we used successfully reproduced the "seasonal paradox", defined as the seasonal out-of-phase surface chlorophyll concentration and upwelling intensity, as derived from observations. As shown in the results, the low surface chlorophyll concentration in strong upwelling conditions during austral winter was constrained by a combined effect of MLD-driven and upwelling-driven processes. Under strong upwelling conditions during austral winter, phytoplankton was diluted over a deeper mixed layer, leading to a decrease within the mixed layer. Likewise, surface phytoplankton concentrations decreased by over 50%. Also, phytoplankton growth was slowed due to deteriorating light and temperature conditions, as well as strong upwelling pushing phytoplankton offshore.

Several previous studies have also focused on the possible reasons behind the seasonal paradox in the PUS. Echevin et al. (2008) also used a regional ocean circulation-biogeochemical model to examine the reasons for the relatively low surface chlorophyll concentration off the Peruvian coast in austral winter. Based on a series of model sensitivity experiments regarding vertical mixing, surface temperature, iron limitation and insolation cycle, Echevin et al.

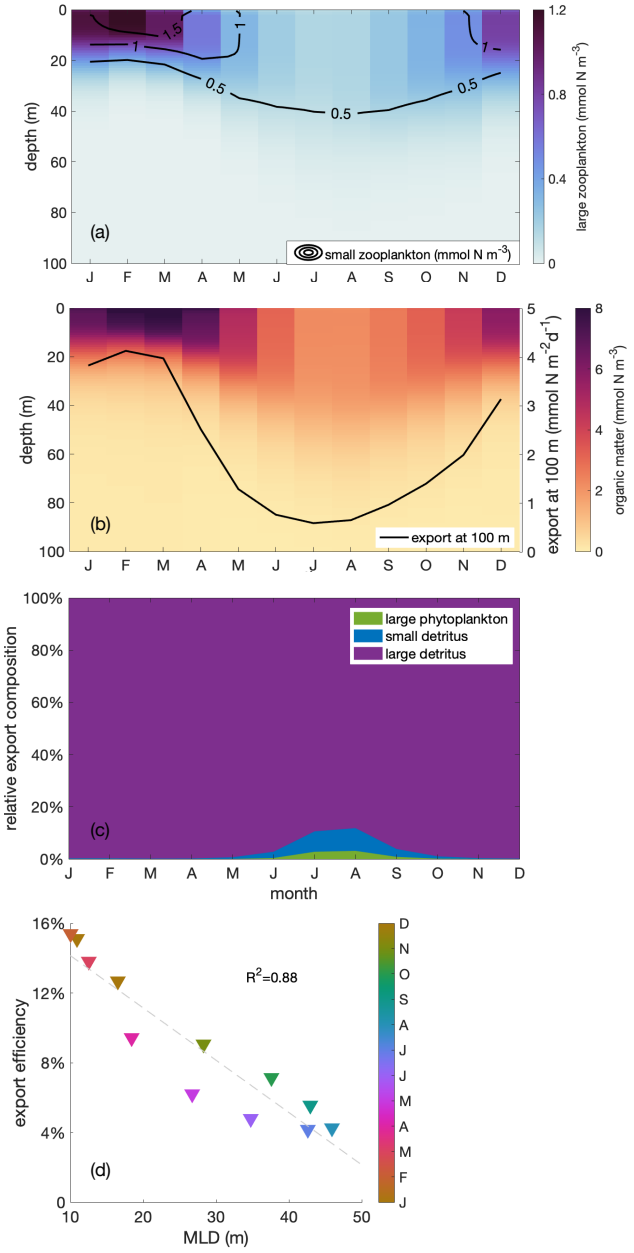

Figure 2.7: Monthly depth distribution of (a) large and small zooplankton (in colours and contour lines, respectively) and (b) organic matter with the seasonal cycle of vertical export through the 100 m depth horizon (black line); (c) Seasonal cycle of the relative contributions to sinking organic matter from large phytoplankton (green) and small (blue) and large (purple) detritus; (d) correlation of export efficiency with mixed layer depth (MLD) within the focus region. The export efficiency is defined as the ratio of export through the 100 m depth level to primary production in the upper 100 m. Colours indicate the month of the year.

(2008) concluded that the low surface chlorophyll in austral winter is mainly generated by the combined effect of dilution and deteriorating light with deepening mixed layers. Additionally, the iron sensitivity experiment confirmed the existence of iron limitation in austral winter, which corroborated the findings in Messié and Chavez (2015). Messié and Chavez (2015) pointed out that more severe iron limitation under low light could also be one of the reasons behind low primary production under strong upwelling conditions. According to results from culture experiments, phytoplankton iron demand would increase under light limitation (Sunda and Huntsman, 1997). Based on observations, Friederich et al. (2008) suggested that winds in the strong-upwelling winter conditions favour curl-driven offshore upwelling, which would draw more offshore iron-deficient waters to the surface. On the contrary, a model study (Albert et al., 2010) found that stronger wind-curl-driven upwelling actually recruits more nutrient-rich water from a shoaling coastal undercurrent, thus enhancing surface chlorophyll concentrations. We could not assess the role of iron in regulating the seasonality of phytoplankton biomass because our biogeochemical model did not simulate iron. Nevertheless, our study confirmed the importance of vertical redistribution of biomass and light limitation due to vertical mixing.

2.4.2 Upwelling into deep mixed layers: A unique feature of the Peruvian upwelling system and its implications

As stated in the previous paragraphs, based on the differences in the seasonalities of MLD and upwelling in the Peruvian system, upwelling of nutrient-rich waters occurs when growth conditions are least optimal, in particular when light availability is lowest due to deep mixed layers. In contrast, within the California system, nutrients are upwelled into the shallowest mixed layers. While this nutrient supply coincides with shoaling mixed layers, associated with improved light conditions and reduced dilution, it does not result in as high a level of phytoplankton concentrations as for the Peruvian system. This supports that nutrient limitation contributes substantially to processes in the California system, as the supply of nutrients to shallow mixed layers through upwelling appears to be insufficient to relieve nutrient limitation. Additionally, if nutrients are upwelled into deep mixed layers as in the Peruvian system and allow the onset of a bloom, zooplankton standing stocks might be low and require more time to catch up, eventually reducing phytoplankton biomass. On the contrary, if nutrients are upwelled into shallow mixed layers, zooplankton standing stocks are likely already elevated, allowing zooplankton to immediately limit any increase in phytoplankton biomass.

While the Canary and Benguela systems lack a pronounced seasonality in MLD and phytoplankton, respectively, we point out a few aspects that may elucidate the role of MLD in these systems. Given that the Canary system does not feature a substantial seasonal MLD variability, it is intuitive that phytoplankton follows the seasonality of upwelling in-

tensity more strongly compared to the other EBUS. While mixed layer conditions do not modulate the seasonality of phytoplankton, they may contribute to high phytoplankton concentrations in the Canary system insofar as mixed layers are shallow throughout the year, creating favourable light conditions. Finally, the Benguela system features a rather constant upwelling throughout the year into varying mixed layers. The unresponsiveness of phytoplankton to the varying MLD could hypothetically be due to compensating effects of deepening mixed layers that dilute phytoplankton and deteriorate light conditions, but are simultaneously accompanied by an enhanced supply of nutrients that are mixed up from below.

Other factors may also contribute to regulating phytoplankton in the EBUS aside from nutrients, dilution and light associated with upwelling and MLD, including the advection of biomass and regulation by temperature that varies with upwelling (also see the Results section; Messié and Chavez, 2015). Eddies have been found to favour offshore export and subduction of phytoplankton and nutrients (Lathuilière et al., 2010; Gruber et al., 2011; Messié and Chavez, 2015). In addition, Lachkar and Gruber (2011) suggest that a longer residence time because of a wide shelf and weak mesoscale activity may promote phytoplankton growth in the Canary system. Next to iron supply from the shelves and upwelling of source waters, Fung et al. (2000) also found that atmospheric deposition of iron varies between EBUS.

2.4.3 Seasonal paradox and ecosystem functioning

The interplay of mixed layer depth and upwelling that leads to the seasonal paradox in the PUS propagates further up the food chain, modulating the trophodynamics. In austral summer, the shallow mixed layer along with the add-on effect from upwelling supports the highest phytoplankton biomass and primary production, providing an ideal feeding place for zooplankton. In contrast, during the winter zooplankton face a food shortage, less efficient grazing due to dilution, and transport offshore due to enhanced upwelling. Similar to the spatial match-mismatch observed for phytoplankton and top predators in the Benguela system (Grémillet et al., 2008), mesozooplankton with its slower growth rate may also be negatively affected by enhanced upwelling.

In our model, mesozooplankton is responsible for the major part of the export in the coastal upwelling region. During the productive season, the faecal material of mesozooplankton accounts for close to 100% of the sinking matter, which is in good agreement with what Stukel et al. (2013) observed for the California system. We found that both primary production and export can be determined from the mixed layer dynamics and food web structures (consistent with Ducklow et al., 2001; Turner, 2015; Steinberg and Landry, 2017). The efficiency of the export, defined as the ratio of export to primary production, is also related to tropho-

dynamics. We find that export efficiency is positively correlated with MLD on a seasonal scale. As mentioned in the "Results" section, it partially depends on the composition of the exported material. Mesozooplankton produce fast-sinking large detritus, which enhances the export efficiency during the productive season. Kelly et al. (2018) observed that export efficiency is negatively correlated with net primary productivity in the California system. They suggested that the negative correlation in the California system arises from a seasonal decoupling of export and particle production through long-lived particles that introduce a temporal lag of mesozooplankton production and export to depth. Henson et al. (2019) also identify a negative correlation between export efficiency and primary productivity on a global scale. They imply in their study that not just the phytoplankton community, but also the food web structure, is important to export efficiency. Currently, it is not entirely clear why the PUS export efficiency behaves differently in our model. We suggest that the interplay of the mixed layer and upwelling in EBUS and ecosystem functioning are closely linked, warranting further examination.

2.5 Conclusions and potential implications

In summary, CROCO-BioEBUS performs well with respect to observational data and successfully reproduces the "seasonal paradox" with an out-of-phase relationship between surface chlorophyll and upwelling intensity in the Peruvian coastal waters. In agreement with an earlier model study (Echevin et al., 2008), the seasonal cycle of surface chlorophyll concentration in our simulations is driven mostly by MLD-related processes, specifically dilution and light limitation. Furthermore, our model results provide evidence for secondary contributions from upwelling-related processes such as temperature limitation and advection. This is consistent with Lachkar and Gruber (2011) and Messié and Chavez (2015), who suggested that advection is relevant to the seasonal cycle, but in contrast to Echevin et al. (2008), who found that temperature was not important. Differences in results from Echevin et al. and our results likely originate in the different biogeochemical model components (e.g., different parameterisations of temperature dependencies of phytoplankton growth). Given the disparity of the models, the role of temperature limitation in the PUS warrants further investigations in order to better constrain second-order drivers of the seasonal paradox. The sensitivity of the different processes within the plankton ecosystem to temperature, as well as their interplay, are topics of active research (e.g. Thomas et al., 2017; Chen and Laws, 2017; Morán et al., 2018; Marañón et al., 2018; Barton and Yvon-Durocher, 2019) and relevant particularly in light of global warming.

We find that the seasonal variability of phytoplankton propagates up the food chain and is reflected in trophodynamics and ecosystem functioning. In particular, zooplankton and organic matter within the water column mirror the seasonal cycle of phytoplankton. Finally, export and export efficiency are well-correlated with the MLD over the course of the annual

cycle. Given that changes in MLD are correlated to many ecosystem components related to plankton ecosystem functioning, we argue for a more thorough understanding of the impact of the seasonal paradox on the ecosystem. In particular effects on the trophic transfer of energy through the plankton food web to higher trophic levels such as fish will determine ecosystem functions like trophic transfer efficiency, fish production, and ultimately potentially fisheries yields. Thus, a better understanding of how the interplay of MLD and upwelling impacts the ecosystem in the contemporary PUS will ultimately help to better project how coastal upwelling ecosystems, and in particular the Peruvian system, may vary under climate change.

Phytoplankton will inevitably be influenced by climate change, responding to changes in the biotic and abiotic environment. Impacts in a changing climate will arise from changes in stratification and upwelling, that further lead to shifting growth conditions due to changes of light, temperature and nutrients (Behrenfeld, 2014). A recent regional modelling study (Echevin et al., 2020) projects a weak decrease in upwelling along with increasing stratification in the PUS due to climate change. Our results suggest that the decreasing upwelling and increasing stratification will both contribute to an increase in surface phytoplankton, in agreement with the findings of Echevin et al. (2020). While a reduction of upwelling might lead to a reduced supply of nutrients, the region is far from being nutrient limited. Therefore, a reduction in upwelling could rather have an effect via temperature, reducing the cooling effect of upwelled waters. We hypothesise that the coastal region would experience more phytoplankton growth and biomass buildup with a reduction of upwelling, due to warmer surface waters and weaker offshore advection compared to the current environmental situation. Moreover, according to our results, shoaling of the mixed layer will be more relevant than a decrease in upwelling intensity, reducing the dilution of phytoplankton and the light limitation in austral winter. This could possibly lead to an attenuation of the seasonal paradox in the future. As export and export efficiency are also regulated by MLD dynamics, we expect not only enhanced export but also an increase in the fraction of primary production that is transported to the deep ocean under global warming.

Chapter 3

Mixed layer depth promotes trophic amplification on a seasonal scale

This chapter is based on the paper 'Mixed layer depth promotes trophic amplification on a seasonal scale' published in Geophysical Research Letter

Citation: Xue, T., Frenger, I., Oschlies, A., Stock, C. A., Koeve, W., John, J. G., & Prowe, A. E. (2022). Mixed layer depth promotes trophic amplification on a seasonal scale. Geophysical Research Letters, e2022GL098720. https://doi.org/10.1029/2022GL098720

Abstract

The Humboldt Upwelling System is of global interest due to its importance to fisheries, though the origin of its high productivity remains elusive. In regional physical-biogeochemical model simulations, the seasonal amplitude of mesozooplankton net production exceeds that of phytoplankton, indicating "seasonal trophic amplification". An analytical approach identifies amplification to be driven by a seasonally varying trophic transfer efficiency due to mixed layer variations. It alters the vertical distribution of phytoplankton and thus the zooplankton and phytoplankton encounters, with lower encounters occurring in a deeper mixed layer where phytoplankton are diluted. In global model simulations, mixed layer depth appears to affect trophic transfer similarly in other productive regions. Our results highlight the importance of mixed layer depth for trophodynamics on a seasonal scale which has significant implications, given mixed layer depth changes projected under climate change.

Plain Language Summary

The Humboldt Upwelling System is a fishery-important region. A common assumption is that a certain amount of phytoplankton supports a proportional amount of fish. However, we find that a small seasonal change in phytoplankton can trigger a larger variation in zooplankton. This implies that one may underestimate changes in fish solely based on phytoplankton. Using ecosystem model simulations, we investigate why changes of phytoplankton are not proportionally reflected in zooplankton. The portion of phytoplankton that ends up in zooplankton is controlled by the changing depth of the surface ocean "mixed layer". The "mixed layer" traps both the phytoplankton and zooplankton in a limited amount of space. When the "mixed layer" is shallow, zooplankton can feed more efficiently on phytoplankton as both are compressed in a comparatively smaller space. We conclude that in the Humboldt System, and other "food-rich" regions, feeding efficiently, determined by the "mixed layer", is more important than how much food is available.

3.1 Introduction

The Humboldt Upwelling System is one of the most important regions contributing to global fisheries, though the origin of the high fish production relative to phytoplankton production remains unclear. Benefiting from constantly upwelled nutrients, the Humboldt system is highly productive throughout the year, supporting a productive zooplankton community and further nourishing a rich small pelagic fish stock (e.g., anchovies and sardines; Bakun and Weeks, 2008). While Pauly and Christensen (1995) suggest that 25% of phytoplankton production is required to sustain fish catch in upwelling regions, Friedland et al. (2012) found phytoplankton production to be a poor predictor for fishing yield. Phytoplankton and fish production are related by trophodynamics which may boost or buffer responses

of different trophic levels to changes in environmental conditions. The terms ”trophic amplification” and ”trophic attenuation”, therefore, were introduced to describe a change in higher trophic level is more or less prominent than lower trophic level, respectively (Kirby and Beaugrand, 2009).

Traditional theory Lindeman (1942) assumes that the portion of phytoplankton production transferred to fish (food chain efficiency) depends on the efficiency of energy transfer across trophic levels (trophic transfer efficiency) and the length of the food chain (food chain length). Different biomes strongly differ in their trophic transfer efficiencies and food chain lengths (Ryther, 1969; Pauly and Christensen, 1995). For these differences, multiple factors play a role, such as physical-biogeochemical conditions (e.g., temperature, light and nutrients; Du Pontavice et al., 2020; Dickman et al., 2008) and multiple ecological processes (e.g., zooplankton feeding strategy; Mitra et al., 2014; Heneghan et al., 2016; Prowe et al., 2019). Previous model studies resolving ecology up to mesozooplankton suggest that trophic transfer efficiency is affected by hydrodynamically driven predator-prey encounter (Legendre and Rassoulzadegan, 1996) and growth efficiencies of each trophic level, while food chain length is determined, amongst others, by phytoplankton composition (Stock et al., 2014b).

The Humboldt system is characterized by a strikingly high food chain efficiency, even compared to other eastern boundary upwelling systems (Chavez et al., 2008). The lower trophic ecosystem is highly seasonal with plankton, and export efficiency, oddly opposing the seasonality of upwelling of nutrient-rich waters (Echevin et al., 2008; Xue et al., 2022b). The pelagic ecosystem structure reacts strongly to environmental change (Ruiz-Cooley et al., 2017). Therefore the seasonality of lower trophic levels due to environmental conditions is expected to affect higher trophic levels in the Humboldt system. To better understand the Humboldt system trophodynamics, we derive equations for trophic transfer efficiency and food chain length based on Ulanowicz (1995). It allows us to disentangle their roles in variations of the food chain efficiency and identify a dominant contribution of trophic transfer efficiency. The mechanism is regulation of predator-prey encounters due to compression and dilution of prey with varying mixed layer depths. We then extrapolate our findings to the global scale by using the seasonal cycle of observational estimates and simulations from two global models to investigate how the governing mechanism may act in other biomes that are similarly productive as the Humboldt system.

3.2 Methods

3.2.1 Regional physical - biogeochemical model: CROCO-BioEBUS

We use a three-dimensional regional physical model CROCO (Coastal and Regional Ocean COmmunity model; Shchepetkin and McWilliams, 2005) coupled with the biogeochemical model BioEBUS (Biogeochemical model for the Eastern Boundary Upwelling Systems; Gutknecht et al., 2013) for analyses of the seasonality of trophodynamics. A detailed description of the model set-up and evaluation can be found in Xue et al. (2022b). We focus on the 200 km wide band off the Peruvian coast (Fig. B1b) characterized by high phytoplankton production that overlaps with the coastal habitat of anchovy (Bertrand et al., 2004).

CROCO is a free-surface, split-explicit regional ocean circulation model. We employ a two-way nesting approach and use the embedded "small" domain for analyses. It has a resolution of 1/12° extending from 5°N to 31°S and 69°W to 102°W, and 32 vertical sigma levels, with a finer resolution towards the surface of 0.5 - 2 m in shallow waters. Initial and boundary conditions and surface forcing are provided by monthly climatological SODA reanalysis from 1990 - 2010 (Carton and Giese, 2008) and COADS heat and freshwater flux data (Worley et al., 2005). BioEBUS is a nitrogen-based model with four plankton groups representing small and large phytoplankton along with microzooplankton and mesozooplankton (Gutknecht et al., 2013). Microzooplankton graze on both phytoplankton with a preference for small phytoplankton, while mesozooplankton graze on the other three groups, favoring microzooplankton the most and small phytoplankton the least. Initial and boundary conditions for phytoplankton are based on monthly climatological SeaWiFS (O'Reilly et al., 1998), nitrate and oxygen concentrations are taken from CARS (Ridgway et al., 2002). The model is climatologically forced for 30 years and the last five years are used for analyses.

3.2.2 Analytical derivation of trophic transfer efficiency and food chain length

Following the original concept in Kirby and Beaugrand (2009), we define "seasonal trophic amplification" as a more prominent relative seasonal amplitude of higher trophic level (mesozooplankton) net production compared to that of a lower trophic level (phytoplankton). To investigate the disproportionate energy transfer, we attribute variations of food chain efficiency (FCE) to variations of trophic transfer efficiency (TTE) and food chain length (FCL). We calculate TTE and FCL based on the amount of energy transferred between trophic levels (TL), applying the analytical formulations in Ulanowicz (1995). This approach accounts for the fact that food webs typically represent "webs" where predators graze on multiple prey types and converts them into "chains". In our derivations below we

calculate net production (NP, in $mmol\ N\ m^{-3}$) of each plankton group as the part that is potentially available for the next trophic level: net phytoplankton production ($\mathrm{NP_{sphy}}$ and $\mathrm{NP_{lphy}}$ of small and large phytoplankton, respectively) is computed as the nitrogen uptake subtracting exudation; net zooplankton production ($\mathrm{NP_{szoo}}$ and $\mathrm{NP_{lzoo}}$ of micro- and mesozooplankton, respectively) is the assimilated fraction of grazing (grazing minus fecal pellets) minus respiration.

Food chain length (FCL)

We define FCL as the highest trophic position, mesozooplankton in our model. Following Ulanowicz (1995), we define a trophic transformation matrix **T** (Equ. 3.1) that allows the mapping of net production of the plankton compartments of the model food web to a chain. The rows of **T** represent trophic levels, and the columns are different plankton groups, i.e. small and large phytoplankton and then small and large zooplankton.

$$\mathbf{T} = \begin{pmatrix} 1 & 1 & 0 & 0 \\ 0 & 0 & 1 & D_{\mathrm{pz}} \\ 0 & 0 & 0 & D_{\mathrm{zz}} \\ 0 & 0 & 0 & 0 \end{pmatrix} \tag{3.1}$$

$$\text{with } D_{\mathrm{pz}} = \frac{G^{\mathrm{sphy}}_{\mathrm{lzoo}} + G^{\mathrm{lphy}}_{\mathrm{lzoo}}}{G_{\mathrm{lzoo}}}, \text{ and } D_{\mathrm{zz}} = \frac{G^{\mathrm{szoo}}_{\mathrm{lzoo}}}{G_{\mathrm{lzoo}}},$$

$G_{\mathrm{lzoo}} = G^{\mathrm{sphy}}_{\mathrm{lzoo}} + G^{\mathrm{lphy}}_{\mathrm{lzoo}} + G^{\mathrm{szoo}}_{\mathrm{lzoo}}$ represents total mesozooplankton grazing. D_{pz} and D_{zz} are the fractions of phyto- and microzooplankton in the mesozooplankton diet. By definition, the sums of the columns add up to 1, that is $D_{\mathrm{pz}} + D_{\mathrm{zz}} = 1$. Mesozooplankton (column 4) can be considered partially trophic level 2 ($\mathrm{TL_2}$, row 2) and 3 ($\mathrm{TL_3}$, row 3) as it grazes on both phytoplankton ($\mathrm{TL_1}$, row 1) and microzooplankton ($\mathrm{TL_2}$, row 2). The trophic level of mesozooplankton, that is FCL, can then be calculated as:

$$\mathrm{FCL} = \mathrm{TL_{lzoo}} = 2 * D_{\mathrm{pz}} + 3 * D_{\mathrm{zz}} = 2 * (D_{\mathrm{pz}} + D_{\mathrm{zz}}) + D_{\mathrm{zz}} = 2 + D_{\mathrm{zz}} \tag{3.2}$$

Hence, a value of 2 indicates complete herbivory, 2.5 50% herbivory, 50% carnivory, and 3 complete carnivory.

Trophic transfer efficiency (TTE)

We calculate TTE based on the net production of the plankton compartments combined with the trophic transformation matrix. First, we get the net production for each trophic level ($\mathrm{NP_{TL}}$) by multiplying the trophic transformation matrix **T** with the vector composed of the net production values of each plankton compartment:

$$\begin{pmatrix} \mathrm{NP}_{\mathrm{TL}_1} \\ \mathrm{NP}_{\mathrm{TL}_2} \\ \mathrm{NP}_{\mathrm{TL}_3} \\ \mathrm{NP}_{\mathrm{TL}_4} \end{pmatrix} = \mathbf{T} * \begin{pmatrix} \mathrm{NP}_{\mathrm{sphy}} \\ \mathrm{NP}_{\mathrm{lphy}} \\ \mathrm{NP}_{\mathrm{szoo}} \\ \mathrm{NP}_{\mathrm{lzoo}} \end{pmatrix} \tag{3.3}$$

Thus, net production of TL_3 refers to the part of mesozooplankton that is grazing on microzooplankton.

$$\mathrm{NP}_{\mathrm{TL}_3} = D_{\mathrm{zz}} * \mathrm{NP}_{\mathrm{lzoo}} \tag{3.4}$$

Then, we define TTE as the ratio of net production between trophic levels (TL):

$$\mathrm{TTE}_n = \frac{\mathrm{NP}_{\mathrm{TL}_{n+1}}}{\mathrm{NP}_{\mathrm{TL}_n}} \tag{3.5}$$

Food chain efficiency (FCE)

Based on the FCL (Section 3.2.2) and the TTE (Section 3.2.2), we obtain an equation for the FCE. Equ. 3.5 allows us to express $\mathrm{NP}_{\mathrm{TL}_3}$ in terms of the production of lowest trophic level and the subsequent energy transfers to TL_3:

$$\mathrm{NP}_{\mathrm{TL}_3} = \mathrm{NP}_{\mathrm{TL}_2} * \mathrm{TTE}_2 = (\mathrm{NP}_{\mathrm{TL}_1} * \mathrm{TTE}_1) * \mathrm{TTE}_2 \tag{3.6}$$

Equating Eqs. 3.4 and 3.6 and considering Equ. 3.2 leads to an equation relating mesozooplankton net production ($\mathrm{NP}_{\mathrm{lzoo}}$) with net phytoplankton production ($\mathrm{NP}_{\mathrm{phy}}$), TTE and FCL:

$$\mathrm{NP}_{\mathrm{lzoo}} = \mathrm{NP}_{\mathrm{phy}} \frac{\mathrm{TTE}_1 \cdot \mathrm{TTE}_2}{\mathrm{FCL} - 2} \tag{3.7}$$

From this follows that FCE, here representing the ratio of net mesozooplankton production to phytoplankton production, is directly linked with TTE and anti-correlated with FCL:

$$\mathrm{FCE} = \frac{\mathrm{NP}_{\mathrm{lzoo}}}{\mathrm{NP}_{\mathrm{phy}}} = \frac{\mathrm{TTE}_1 \cdot \mathrm{TTE}_2}{\mathrm{FCL} - 2} \tag{3.8}$$

Predator-prey encounter efficiency (EE)

To assess the importance of predator-prey vertical encounter efficiency for TTE, we define EE within the water column as:

$$\mathrm{EE} = \frac{\sum_{i=1}^{n} (\mathrm{prey}_i \cdot \mathrm{pred}_i)}{\sum_{i=1}^{n} \mathrm{prey}_i \cdot \sum_{i=1}^{n} \mathrm{pred}_i} \tag{3.9}$$

n stands for the number of vertical grid boxes. prey_i and pred_i represent the biomass concentrations of predator and prey within the grid box i. EE is calculated by weighting the thicknesses of the grid boxes. It is affected by both vertical distributions and biomass concentration of predator and prey, with the value ranging from 0 to 1. An EE of 0

means no overlap between predator and prey. A value of 1 means both predator and prey are concentrated in the same single grid box, reaching the full potential of predator-prey trophic transfer (every predator can eat all prey).

3.2.3 Global models and observation

To test the global applicability of our findings in the Humboldt system, we use two contrasting global models: (1) the University of Victoria Earth System Climate Model version 2.9 (UVic-model; Weaver et al., 2001; Keller et al., 2012) with relatively coarse resolution and simple food web structure; (2) the Geophysical Fluid Dynamics Laboratory Earth System Model 2.6 (GFDL-model; Stock et al., 2017) with relatively fine resolution and complex food web structure.

The UVic-model uses a horizontal resolution of 1.8° (latitude) × 3.6° (longitude) and 19 vertical levels, with 50 m vertical resolution near the surface. The marine ecosystem component has two phytoplankton (nitrogen fixers, regular phytoplankton) and one zooplankton groups. Detailed model set-up description and evaluation are in (without iron configuration; Yao et al., 2019). Model results after a 3000-year spin up are used in this study.

The GFDL-model combines the global climate model GFDL CM2.6 (Delworth et al., 2012) with the planktonic ecosystem model COBALT (Stock et al., 2014b). Its ocean component has an approximate spatial resolution of 10 km and 50 vertical layers, with 10 m vertical resolution over the top 200 m. COBALT contains three phytoplankton (small, large, diazotrophs) and three zooplankton groups (micro-, meso-, macrozooplankton). Trophic interactions are size-based and designed to represent plankton physiology and predator-prey interactions (see Stock et al., 2017, for details). Model results after a 50-year simulation with fully coupled configuration, forced by year 1990 conditions, are used in this study.

The observationally-based FCE is calculated following Stock and Dunne (2010) using satellite-based phytoplankton production estimates (VGPM; Behrenfeld and Falkowski, 1997). Mesozooplankton production is calculated using mesozooplankton biomass from the COPEPOD Database (O'Brien, 2007) and growth rate estimated following Hirst and Bunker (2003) based on temperature and chlorophyll from MODIS (https://oceancolor.gsfc.nasa.gov/data/aqua/). The seasonal pattern of the FCE is first normalized at each station and then averaged over a biome to avoid weighting large absolute values of the FCE higher. The seasonal cycles for specific locations with data coverage throughout the year yield similar results (Fig. B5). The observed mixed layer depth (MLD) is taken from the ARGO mixed layer database (http://mixedlayer.ucsd.edu/) using the temperature threshold mean MLD (Holte et al., 2017), which was also used to infer the simulated MLD with a starting depth of 0.5–2 m. For detailed model MLD evaluations, please see Xue et al. (2022b).

3.2.4 Biome definition

The relation of MLD and FCE is analyzed globally, subdivided by productive and oligotrophic regions. Productive and oligotrophic regions are categorized by the annual mean surface chlorophyll above and below 0.1 $mg\,Chl\,m^{-3}$ for observational data and 0.15 $mg\,Chl\,m^{-3}$ for model results, respectively. A higher threshold for model simulations is used to account for the relatively high bias (Fig. B2) and achieve similar biome distribution in comparison with observational estimates. Productive regions reflect the high-latitude, tropical and coastal regions with high macronutrient and pronounced phytoplankton concentrations. The oligotrophic regions generally correspond to the subtropical gyres.

3.3 Results and Discussion

3.3.1 Trophic transfer efficiency drives trophic amplification

The amplitude of seasonal variations in mesozooplankton production is more prominent than that of phytoplankton, revealing the feature of trophic amplification on a seasonal scale (hereafter referred to as "seasonal trophic amplification", Fig. 3.1a). Phytoplankton and mesozooplankton production vary seasonally in phase, with high production in austral summer and low production in winter. On average, the fraction of phytoplankton production resulting in mesozooplankton production, that is FCE, is 9.5% with a maximum of 17% in austral summer and a minimum of 3% in winter. The seasonal variation of the FCE is reflected in an amplified seasonal variation of mesozooplankton production (83% relative to its annual mean) compared to that of phytoplankton (35%).

Seasonal trophic amplification in our model is mainly introduced by variations in TTE, while FCL plays a negligible role (Fig. 3.1b). As evident from Equ. 3.8, variations of the FCE can be decomposed into effects from TTE and FCL. TTE varies seasonally in phase with net phytoplankton and mesozooplankton production, contributing most to the seasonal variation of the FCE and thus trophic amplification (Fig. 3.1b). The seasonal variation of FCL is small by comparison. We, therefore, focus on TTE of seasonal trophic amplification in the following sections.

3.3.2 Taking a mixed layer depth perspective to grazing

TTE, as the dominant driver of seasonal trophic amplification, is mainly affected by variations of predator grazing. The fate of phytoplankton production is either grazing by zooplankton, which is then used for respiration, egested as fecal pellets, or passed on to the next trophic level, or not to be consumed by grazers (Fig. 3.2a-b). In austral winter, a relatively smaller fraction of phytoplankton production is being grazed (57%) than in summer (65%). The fraction of production that is passed on to the next trophic level (TTE) is also lower

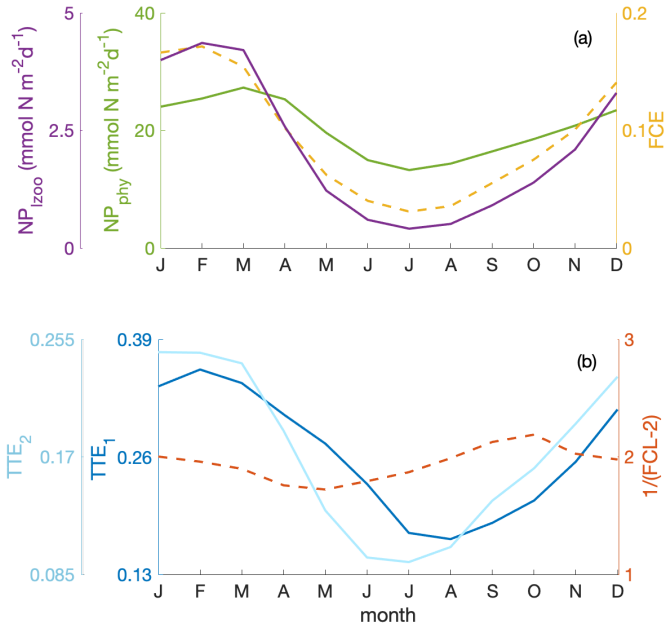

Figure 3.1: Trophic amplification due to seasonally varying trophic transfer efficiency (TTE): (a) Seasonal cycles of net phytoplankton (NP_{phy}, green), mesozooplankton production (NP_{lzoo}, purple) and FCE (NP_{lzoo}/NP_{phy}, yellow). The y axis range spans 100% of change relative to the annual mean for each variable; (b) seasonal cycles of the terms in Equ. 3.8 to assess the relative contributions from trophic transfer efficiency between trophic levels 1 and 2 (TTE_1, light blue) and trophic levels 2 and 3 (TTE_2, dark blue), and food chain length (FCL; as $1/(FCL-2)$, red) over the water column within the focus region. The y axis range spans 50% of change relative to the annual mean for each variable.

in winter (17%) than in summer (33%). The production of fecal pellets relative to phytoplankton production stays approximately the same in winter and summer (Fig. 3.2a-b), while biomass-specific production of fecal pellets is substantially smaller in winter. While a larger share of phytoplankton production is used for zooplankton respiration in austral winter, this is due to reduced biomass-specific zooplankton grazing combined with a roughly constant biomass specific respiration rate (Fig. 3.2c). Therefore, with reduced losses to fecal pellets in winter, and an approximately constant biomass-specific respiration, the dominant process determining how much production is available to the next trophic level, thus TTE, is predator grazing.

For predator grazing, predator-prey encounter efficiency, which is driven by the MLD, is more important than total (vertically integrated) prey biomass (Fig. 3.3). If predator and prey are diluted over a deeper mixed layer, the potential for predator-prey encounters is smaller. Comparing conditions in February and June as examples (Fig. 3.3a) reveals that both months host roughly the same amount of total prey biomass within the water column (60 $mmol\ N\ m^{-2}$) at different MLD (February: 10 m; June: 35 m). Predator and prey are more concentrated in a shallower mixed layer in February while they are more diluted in June. The high predator and prey concentration in a thinner layer allows the predator to graze more efficiently due to a high encounter efficiency, hence supporting a high specific grazing rate for the predator. This mechanism reflects a significant correlation between MLD and the vertical encounter efficiency (Fig. 3.3b). Similar findings have also been proposed in a horizontal perspective that the spatial distribution drives the covariance of predator and prey and dominates over total biomass in regulating the system production and food web structure (e.g., front system; Benoit-Bird and McManus, 2012; Woodson and Litvin, 2015).

3.3.3 A negligible role of food web structure?

Seasonal changes in food web structure, thus food chain length, have a negligible effect on the trophic amplification (Fig. 3.1b). In our model, the food chain length varies very little around 2.5 (thus $1/(FCL-2)$ stays around 2), with mesozooplankton grazing nearly equally on phytoplankton and microzooplankton. The food chain tends to be shorter when the phytoplankton community is more strongly dominated by large phytoplankton, reflecting a more efficient food web structure.

The limited flexibility in our simulated food web structure, e.g., through fixed diet preferences, cannot fully capture the complex trophic interactions of the real ecosystem. The predator diet preference in the model is fixed based on body size (Boyce et al., 2015), allowing only for a limited variation of the food web structure and FCL and their contribution to variations of the FCE. A previous study found that different FCL is the major cause

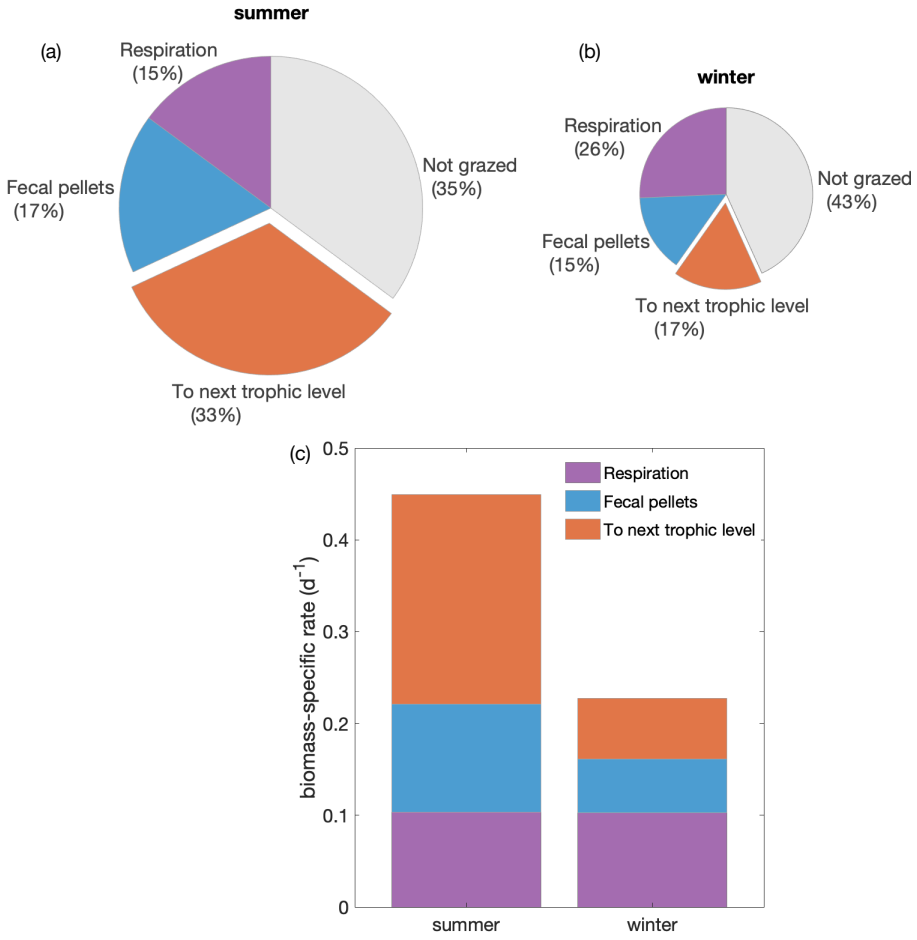

Figure 3.2: Reduced trophic transfer efficiency in winter (TTE) due to reduced efficiency of grazing: Fate of phytoplankton production in austral (a) summer; and (b) winter. The sizes of the pie charts are representative for the magnitude of phytoplankton production. (c) Biomass-specific rate of respiration (purple), fecal pellet production (blue) and production available to the next trophic level (red) in austral summer and winter. The sum of all colored components (respiration, fecal pellets and the production available to the next trophic level) represents zooplankton grazing; only the grazed (colored) parts are being processed by zooplankton.

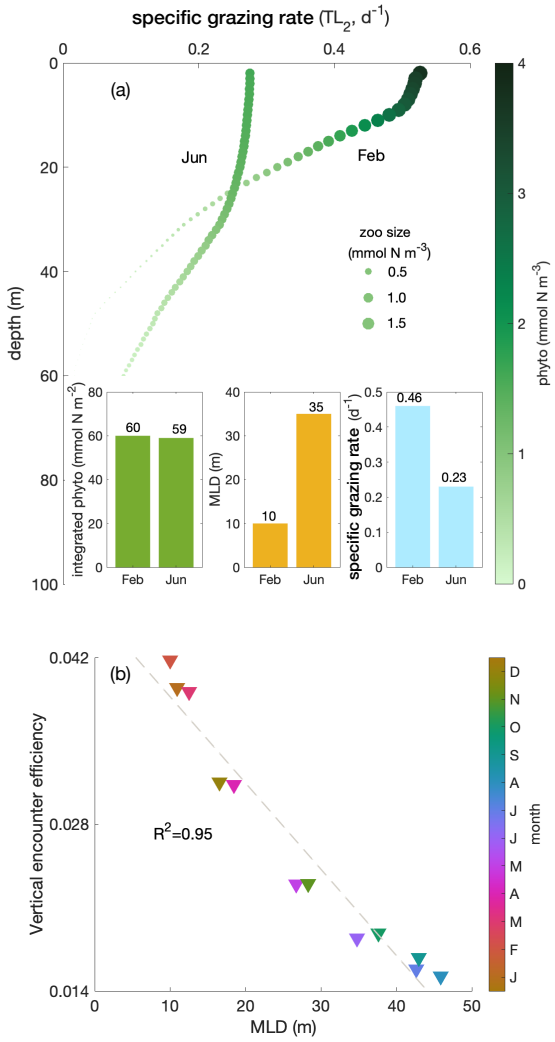

Figure 3.3: Reduced efficiency of grazing (specific grazing rate) due to prey dilution in deep winter mixed layers: (a) Vertical profiles of predator biomass specific grazing rate (d^{-1}) in February and June with color indicating the prey concentration (TL_1, $mmol\,N\,m^{-3}$) and size of the circle indicating the predator concentration (TL_2, $mmol\,N\,m^{-3}$) within the focus region; inserts show prey vertically integrated over the water column (green), the mixed layer depth (yellow), and the average mixed layer biomass specific ingestion rate (light blue); (b) Correlation of mixed layer depth and vertical encounter efficiency (EE, Equ. 3.9) with colors indicating the time of the year (months). R^2 value of the correlation is shown on the left side.

of FCE differences across ocean biomes (Stock and Dunne, 2010). A deliberate change in food web structure (albeit limited to the lower trophic levels that the model resolves) by manipulating the diet of the two zooplankton groups does not have a notable effect in our model (see supporting information for detailed sensitivity studies).

3.3.4 MLD driving trophic transfer: a common feature of productive regions

The negative correlation between MLD and FCE is not only apparent in the Humboldt system but also in other productive regions. To test the importance of the MLD for the FCE, we globally define "productive regions", which include the Humboldt system, versus "oligotrophic regions" that are bottom-up limited and comparatively low in phytoplankton production (see Methods section). The spatial patterns of the simulated productive regions from the UVic-model and the GFDL-model generally match the observational estimates (Fig. 3.4a-c). A clear negative correlation of the FCE and the MLD in the productive regions (Fig. 3.4d-f) is apparent in the observational estimates and the model simulations. A relatively low FCE generally coincides with deep MLD, consistent with the dilution and concentration of prey reducing the predator-prey encounter efficiency, and thereby grazing and the FCE. Worth noticing, while the dominant mesozooplankton group in the Humboldt upwelling system has not been observed to do diel vertical migration (Massing et al., 2022), it has been commonly observed elsewhere. Despite using deep waters as a refuge during the day, diel vertical migration is unlikely to affect MLD and FCE correlations because zooplankton feed primarily near the surface (Hays, 2003), where prey is diluted regardless of zooplankton movement. Stock et al. (2014a) compared annual average FCE across different regions of the globe and similarly found a comparatively prominent role of dilution of prey for the high latitude regions.

The seasonal variation of FCE is governed by different mechanisms in oligotrophic regions, with much lower correlation coefficients compared to productive regions (Fig. 3.4g-i). As oligotrophic regions are nutrient-limited, deepening mixed layers in the models bring up nutrients from below that stimulate phytoplankton growth. Mixing events have been observed in the North Pacific gyre to significantly increase not only phytoplankton production but also zooplankton biomass (McGowan and Hayward, 1978). When food availability for zooplankton is low, as is the case in oligotrophic regions, zooplankton growth efficiency is very sensitive to a given change in food. This is because the limited grazed food is needed to sustain basic functions (e.g., respiration), as zooplankton is "starving". In contrast, zooplankton growth efficiency is much less sensitive to changes in food concentration when food is plentiful (Fig. 2 in Stock et al., 2014a). Thus, in oligotrophic regions, one may expect a positive response of the FCE to deepening mixed layers, as partially indicated in the global models.

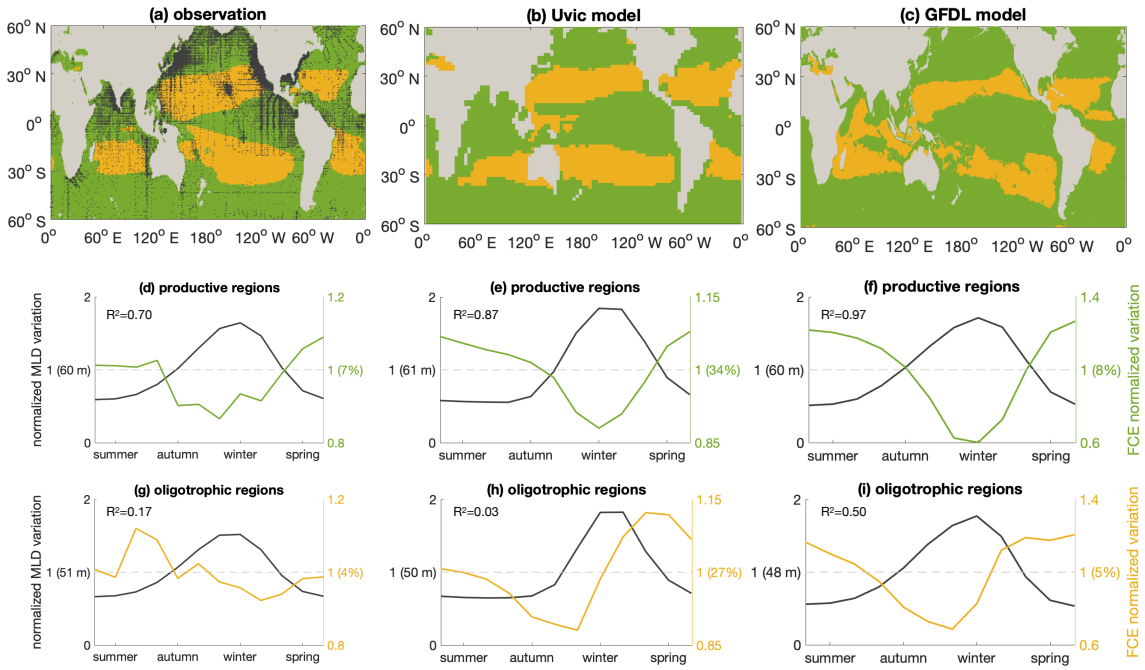

Figure 3.4: Indication for seasonal mixed layer depth (MLD) variations driving food chain efficiency (FCE) beyond the Humboldt system: Ocean biomes calculated from (a) observations, (b) UVic-model and (c) GFDL-model with productive (green, above 0.1 $mg\ Chl\ m^{-3}$ (observations)/0.15 $mg\ Chl\ m^{-3}$ (model)) and oligotrophic (yellow, below 0.1 $mg\ Chl\ m^{-3}$ (observations)/0.15 $mg\ Chl\ m^{-3}$ (model)) regions. Dots in (a) indicate the locations of observations. Average seasonal cycles of MLD (black) and food chain efficiency (FCE, the ratio of net mesozooplankton production to phytoplankton production, Equ. 6, color) for (d,g) observations, (e,h) UVic-model and (f,i) GFDL-model, normalized by the mean MLD and FCE for each biome: productive (green, d-f) and oligotrophic (yellow, g-i) regions. Values in brackets indicate the absolute values of annual means. R^2 values of the correlations between MLD and FCE are shown in the top-left side of each panel.

Both global models tend to capture the correlation between MLD and FCE in productive regions, regardless of different trophic resolutions. While the value of FCE in the GFDL-model roughly matches the observed estimate of 6% in the productive regions, the value of FCE is much higher in the UVic-model, possibly due to resolving only one trophic link. Nevertheless, in agreement with the classic paradigm (Ryther, 1969), the FCE in both models is generally higher in productive than in oligotrophic regions.

3.4 Implications and Conclusions

Our model simulates seasonal trophic amplification driven by mixed layer dynamics in the Humboldt and other productive systems. To pinpoint the origin of the seasonal amplification, we have applied an analytical approach that allowed us to define and disentangle the contributions to the seasonal variation of the food chain efficiency (FCE) of the efficiency of production transfer between trophic levels (TTE), and the length of the food chain up to the top predator (FCL). In our model, the TTE is the main contributor to the seasonal amplification in the Humboldt system, and it is mainly driven by the mixed layer dynamics. The same mechanism also seems to apply to other oceanic biomes characterized by elevated chlorophyll, such as coastal and high latitude oceans. A caveat of our models is that the food web structures do not fully resolve the complexity of the real ecosystem, that is, seasonal variations of the FCL may play a larger role in the real ocean. Our results highlight that the annual values of FCE typically analyzed by previous studies emerge from a dynamic seasonal cycle.

The term trophic amplification was coined in analyses of climate change projections, with ocean warming affecting more strongly the higher than the lower trophic levels (Kirby and Beaugrand, 2009; Chust et al., 2014; Stock et al., 2014a; Kwiatkowski et al., 2019; Lotze et al., 2019). Different responses of phytoplankton biomass are projected by climate models for low versus high latitude regions with global warming. Positive trophic amplification, with increases of biomass in each trophic level, is found more commonly in high latitude regions. Stock et al. (2014a) suggest that shoaling of winter mixed layers and ice melting due to global warming may play a role, leading to productivity increases and tighter coupling between predators and prey. In contrast, increased nutrient limitation arising from enhanced stratification may cause negative trophic amplification in low latitude regions (Chust et al., 2014; Stock et al., 2014a; Kwiatkowski et al., 2019).

We note that next to mixed layer dynamics other mechanisms may affect predator-prey encounters, with the potential to further intensify trophic amplification, such as expanding oxygen minimum zones. Schukat et al. (2021) observed in the Humboldt system that key mesozooplankton species, such as calanoid copepods, almost exclusively restrict themselves

to the surface layer above the oxygen minimum zone, allowing the Peruvian anchovies to forage more easily and efficiently and supporting the high fish yield in the Humboldt system. We hypothesize a potential positive feedback loop where positive amplification triggered by shallowing mixed layers, or a shoaling of the oxycline, increases the export of organic material to the deeper ocean, as a result of both enhanced phytoplankton production and export efficiency (Xue et al., 2022b). The enhanced export then could lead to enhanced oxygen consumption at depth, and to a further expansion of the oxygen minimum zone (Riebesell et al., 2007), resulting in further enhanced prey concentration and trophic amplification, and in turn more export, thereby closing the feedback loop.

Based on our findings of the present-day seasonality of the Humboldt lower trophic ecosystem dynamics, we suggest that positive trophic amplification may promote export of organic material under global warming not only in the Humboldt system but also in the high latitudes as a result of both increasing phytoplankton production (e.g., Sallée et al., 2013, 2021), and higher food chain efficiency (Chust et al., 2014; Stock et al., 2014a; Kwiatkowski et al., 2019) with shallowing mixed layers. Improving understanding of seasonal dynamics may facilitate the interpretation of ecosystem sensitivities in observational data, and help to further improve the simulation of sensitivities in climate models, thereby improving climate projections.

Chapter 4

Understanding the drivers of fish variability in an end-to-end model of the Northern Humboldt Current System

This chapter is based on the paper 'Understanding the drivers of fish variability in an end-to-end model of the Northern Humboldt Current System' currently under review at Ecological Modelling by Cruz M., Frenger I., Getzlaff J., Kriest I., Xue T., and Shin Y. (2022).

Abstract

The Northern Humboldt Current System is the most productive eastern boundary upwelling system, generating about 10 % of the global fish production, mainly coming from small pelagic fish. It is bottom-up and top-down affected by environmental and anthropogenic variability, such as El Niño Southern Oscillation and fishing pressure, respectively. The high variability of small pelagic fish in this system, as well as their economic importance, call for a careful management aided by the use of end-to-end models. This type of models represent the ecosystem as a whole, from the physics, through plankton up to fish dynamics. In this study, we utilised an end-to-end model consisting of a physical-biogeochemical model (CROCO-BioEBUS) coupled one-way with an individual-based fish model (OSMOSE). We investigated how time-variability in plankton food production affects fish populations in OSMOSE and contrasted it against the sensitivity of the model to two parameters with high uncertainty: the plankton accessibility to fish and fish larval mortality. The results show a small impact of interannual variability of plankton on the modelled fish in this productive ecosystem. In contrast, changes in larval mortality have a strong effect on anchovies. In OSMOSE, it is a common practice to scale plankton food for fish, accounting for processes that may make part of the total plankton in the water column unavailable. We suggest that this scaling should be done constant across all plankton groups when previous knowledge on the different availabilities is lacking. In addition, end-to-end modelling systems should consider environmental impacts on larval mortality in order to better capture the interactions between environmental processes, plankton and fish.

4.1 Introduction

The Northern Humboldt Current System (NHCS), located in the eastern-tropical south Pacific (ETSP) ocean, is the most productive eastern boundary upwelling system, generating about up to 10 % of the global fish production (Chavez et al., 2008; FAO, 2020). It hosts the largest single-species fishery of the planet, the Peruvian anchovy (*Engraulis ringens*) (Chavez et al., 2003; Aranda, 2009). Along with the Pacific sardine (*Sardinops sagax*), these small pelagic fish feed on plankton and build up huge biomasses that support a large industry of fish meal production. They are also valued by the local communities culturally (López de la Lama et al., 2021) and economically (Christensen et al., 2014), and are consumed by many marine predators such as seabirds (Muck, 1987; Jahncke et al., 2004), marine mammals (Majluf and Reyes, 1989) and larger predatory fish (Pauly et al., 1987). However, they have shown to be prone to collapses related to environmental variability along with overfishing (Boerema and Gulland, 1973), putting at risk the fishing industry (Paredes and Gutierrez, 2008). The drivers behind the disproportionately large fish production of the NHCS compared to other eastern boundary upwelling systems are not fully understood (Carr, 2002). Possible explanations include the reset of the system succession

to small pelagic fish during the El-Niño periods (Bakun and Broad, 2003), the compression of zooplankton prey for small pelagic fish at the surface by a shallow oxygen minimum zone, and increased trophic transfer efficiency caused by relatively weak winds in combination to high primary production (Chavez and Messié, 2009). The ETSP is affected by strong interannual variability. In addition to El-Niño and La-Niña events, the ETSP is subjected to regimes of cold ocean temperature, named La Vieja, and warm temperature, called El Viejo (Chavez et al., 2003). Anchovies and sardines also fluctuate interannually with regimes of high anchovy abundance alternating with regimes of high sardine abundance (Schwartzlose et al., 1999; Chavez et al., 2003). Causes for these fluctuations are not completely clear and have been related to interannual variability in water temperature (Chavez et al., 2003). Between the 1970s and 1990s, the ecosystem was under a regime of abundant sardines. The regime shifted during the 1990s towards an anchovy-dominated ecosystem. Anchovy collapsed during the El-Niño of 1998 but managed to recover while sardines continued declining to almost no presence by 2000 (Chavez et al., 2003; Alheit and Niquen, 2004). In addition, red squat lobsters (*Pleuroncodes monodon*), a generally benthic species off central Chile but mostly pelagic off Peru (Gutiérrez et al., 2008), became particularly abundant in the pelagic system after this event (Gutiérrez et al., 2008). Finally, the system is both bottom-up and top-down affected by environmental and anthropogenic drivers, such as changes in temperature and productivity due to El-Niño Southern Oscillation, and fishing pressure, respectively (Boerema and Gulland, 1973; Barrett et al., 1985; Barber and Chavez, 1983). The high and poorly understood temporal variability of fishes in the NHCS, as well as their importance for the economy, food security and the rest of the ecosystem, call for a careful and sustainable fisheries management using an ecosystem-based-management approach supported by end-to-end models (Pikitch et al., 2004).

End-to-end models aim at representing the marine ecosystems as a whole by including environmental components as well as lower (plankton) and higher trophic levels (HTL) such as fish and their utilisation by humans. Common ecosystem models represent functional groups or individual species interacting in a trophic web (see Fulton, 2010; Tittensor et al., 2018, for reviews). End-to-end models also include primary producers, such as plankton, which are affected by the environment, either already included in the model (e.g., Atlantis; Fulton et al., 2004) or provided by physical-biogeochemical models (e.g., PISCES-APECOSM; Maury, 2010). Among other types of ecosystem models, the multispecies individual-based models are as detailed as simulating the single individuals or schools of fish (e.g., Rose et al., 2015). Belonging to such type of models, the Object-oriented Simulator of Marine Ecosystems (OSMOSE) simulates the whole life cycle of fish (Shin and Cury, 2001, 2004, `www.osmose-model.org`). It is usually one-way coupled with biogeochemical models which provide lower trophic levels, or plankton, as food for some of the fish in the ecosystem (e.g., Halouani et al., 2016; Moullec et al., 2019b). In this study, we simulated the ETSP ecosystem with a one-way coupled model system including a physical-biogeochemical (Coastal

and Regional Ocean COmmunity model (CROCO) - Biogeochemical model developed for the Eastern Boundary Upwelling Systems (BioEBUS); Shchepetkin and McWilliams, 2005; Gutknecht et al., 2013) model and OSMOSE as HTL model.

To improve the model fit to observations, models have to be calibrated by adjusting model parameters for which no values are available easily or unambiguously from literature. Using optimisation algorithms – here in particular evolutionary algorithms – provides an automated and objective way for calibration, and can converge to solutions that may not be reached manually or analytically when handling complex models (Duboz et al., 2010; Oliveros-Ramos and Shin, 2016). Yet, the strong variability in physical forcing and in fish abundance observed in the NHCS makes the calibration of OSMOSE for this specific ecosystem challenging. OSMOSE has been implemented in several ecosystems using time-constant parameters to represent a steady ecosystem state (Travers et al., 2006; Fu et al., 2012; Grüss et al., 2015; Halouani et al., 2016; Xing et al., 2017; Bănaru et al., 2019; Moullec et al., 2019b), which can serve as a starting point for evaluating the ecosystem response under changing conditions (e.g., Fu et al., 2012; Moullec et al., 2019a; Diaz et al., 2019; Travers-Trolet et al., 2014b). Marzloff et al. (2009) developed a configuration of OSMOSE with time-constant parameters for the pelagic ecosystem off Peru using years 2000 to 2006 as reference for the calibration, just after the regime shift of 1998. On the other hand, Oliveros-Ramos et al. (2017) addressed the interannual variability of the NHCS by calibrating time-varying parameters. The resulting configuration matched the seasonal and interannual fluctuations in observations. This approach implicitly assumes that the observed variability in fish may be caused by processes that need to be accounted for by temporally varying parameter values and it provides an estimation for such parameters. However, it might dampen any variability caused bottom-up by fluctuations in physical forcing and its propagation to plankton biomass. On the other hand, using constant parameters allows to isolate the impact of time-variability in the forcings.

To investigate the potential relevance of bottom-up causes of fluctuations of fish biomass, we decided here to allow for process studies and apply a calibrated configuration of OSMOSE for the ETSP with constant parameters. We then explored whether interannual variability in a physical-biogeochemical model propagates through plankton to OSMOSE. To do so, we first calibrated OSMOSE against biomass and landings data of nine fish and invertebrate species from the post-El-Niño, low-sardine regime between 2000 and 2008, period in which no strong El-Niño event occurred. For calibration, OSMOSE was forced with a plankton climatology that we obtained from the biogeochemical model (CROCO-BioEBUS) hindcast over the time-period from 2000 to 2008. We then forced the calibrated OSMOSE configuration with an interannually varying biogeochemical hindcast from 1992 to 2008 to assess whether or not the plankton forcing alone could generate the regime shift after the El-Niño of 1998 in OSMOSE. To put the effects of interannual forcing into perspective, we also car-

ried out sensitivity experiments varying two different parameters of the OSMOSE model, which are either directly related to the food availability of the biogeochemical model, or address the larval mortality of fish species, which in previous studies has often been adjusted to calibrate OSMOSE. The results of this study provide insight on advisable improvements for the connection of OSMOSE with biogeochemical models for a better representation of the effect of environmental variability in end-to-end models.

4.2 Methods

4.2.1 The lower trophic levels model: CROCO-BioEBUS

We used the Coastal and Regional Ocean COmmunity model (CROCO, Shchepetkin and McWilliams, 2005) coupled online with a Biogeochemical model developed for Eastern Boundary Upwelling Systems (BioEBUS, Gutknecht et al., 2013). The model domain spans from 10°N to 33°S and from 69° to 118°W with a horizontal resolution of $\frac{1}{12}^\circ$ and 32 sigma layers. BioEBUS consists of 12 prognostic variables: oxygen, ammonium, nitrate, nitrite, nitrous oxide, dissolved organic nitrogen, small and large detritus, small and large phytoplankton, and small and large zooplankton. Following a spin-up of 30 years with forcing from 1990, the coupled ocean physical-biogeochemical model was simulated from 1990 to 2010 with interannually-varying forcing. The configuration used in this study is described in detail by José et al. (2019) and a list of the parameters that were adjusted for this configuration is available in Xue et al. (2022b).

For coupling with OSMOSE, small and large phyto- and zooplankton were integrated above the oxygen minimum zone (OMZ; here defined by an oxygen threshold of 90 μmol O_2 kg^{-1}, Karstensen et al., 2008) and integrated concentrations were transformed from nitrogen to wet weight (WW, main currency in OSMOSE) by multiplying them by the conversion factors: 720, 720, 675 and 1000 mg WW mmol N^{-1}, respectively (Travers-Trolet et al., 2014a, their Tab. 4), regridded from $\frac{1}{12}^\circ$ to $\frac{1}{6}^\circ$ resolution, and then provided as food forcing for the fish in OSMOSE (see Section 4.2.2).

4.2.2 The higher trophic levels model: OSMOSE

OSMOSE is an object-oriented individual-based model that simulates the whole-life cycle of fish, from eggs to adults. Individual fish are grouped in schools of the same size and age. These are distributed over a 2-dimensional grid (see Figure 4.1) and within species and life stage specific distribution maps that are produced by statistical climate niche models (Oliveros-Ramos et al., 2017). On every time step, each school moves randomly to one adjacent grid cell within its distribution map. Predation is opportunistic, based on the spatial overlap of predator and prey. Every species or group feeds on prey that falls within certain minimum and maximum predator-prey size ratios. In consequence, predatory

interactions are not set *a priori* by the model user but these emerge from the size structure of the populations. A full description of the model is available in Shin and Cury (2001, 2004) and Travers et al. (2009).

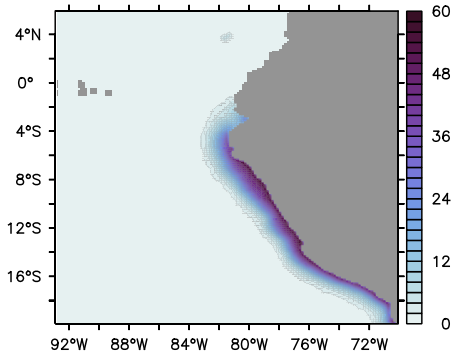

Figure 4.1: Spatial distribution of simulated anchovy in the climatological set-up (see Section 4.2.3). All schools averaged over time, after spin-up, and transformed to concentration (g wet weight m^{-2}).

Configuration overview

The configuration in this project uses OSMOSE version 3.3.3 and was derived from the configuration by Oliveros-Ramos et al. (2017), which covers the same region, from 20°S to 6°N and from 93° to 70°W (see Figure 4.1), spans from 1992 to 2008 and was calibrated against interannually-varying observations. For our configuration, we averaged the observations from 2000 to 2008, to produce a configuration representative of this period of time, after the strong El Niño of 1998. Observations were available for all groups simulated in the model for this period of time. We also averaged the plankton simulated by CROCO-BioEBUS from 2000 to 2008 to produce a plankton climatology as forcing for OSMOSE. This time period is dominated by anchovies while sardines were dominant through the 1980s and decreased during the 1990s until their final collapse after the El-Niño event of 1997–1998 (Chavez et al., 2003). We set up a configuration with constant parameters to generate a mechanistic model that can be used to understand the ecosystem response to certain forcings, such as fishing pressure and environmental changes, in sensitivity studies.

In OSMOSE, fish distribution is constrained by maps defining their habitat. The maps define the probability of a school to occur on each of the grid cells of the domain, with the sum of all wet grid cells equalling 1. In our study, the distribution maps of each species vary for every season. At the beginning of the season, the schools are randomly located over the new map taking into account the provability given by each grid cell. We averaged the distribution maps of the configuration mentioned above, provided by Oliveros-Ramos and Lujan-Paredes (personal communication), from 2000 to 2008, to produce a climatology.

The configuration for the Northern Humboldt Current System (NHCS) consists of Peruvian anchovy (*Engraulis ringens*), Peruvian hake (*Merluccius gayi*), Pacific sardine (*Sardinops sagax*), Chilean jack mackerel (*Trachurus murphyi*), Pacific chub mackerel (*Scomber japonicus*), mesopelagic fish, squat lobster (*Pleurocondes monodon*), Humboldt squid (*Dosidicus gigas*) and euphausiids. Parameters as well as distribution maps for all groups are provided in Appendix C.1 and in the supplement. The parameters in our configuration are the same as in Oliveros-Ramos et al. (2017), with the exceptions mentioned in Sect. 4.2.2. We applied constant annual fishing rates for each species in our climatological set-up. Because anchovies are only fished during certain seasons, their landings show a marked seasonality. Therefore, a seasonality of fishing rate was derived from the anchovy landings observations (see Figure C.1 in the Appendix C.1). The fishing rate of all other species was assumed to be constant over the year. The model is initialised through a seeding process that generates schools of fish at the egg and larval stages during several years at the beginning of the model run. After the initial 12 years of the spin-up, the seeding is stopped and all further eggs are only produced by adult fish.

Model calibration

The model was calibrated using the evolutionary algorithm developed by Oliveros-Ramos et al. (2017). Detailed instructions on the calibration are available in the OSMOSE documentation: `http://documentation.osmose-model.org/index.html`. The calibration ran for 400 hundred generations using a population size of 75 individuals (an individual is a vector of parameter values in this calibration framework) per generation for the evolutionary algorithm. In every iteration, the model was run for 50 years consisting of 25 years of spin-up and evaluating against observations the last 25 years of the simulation. Available observations included biomasses from acoustic surveys integrated over the exclusive economic zone of Peru (EEZ) and averaged from 2000 to 2008, and monthly landings of exploited species (anchovy, hake, sardine, jack mackerel, chub mackerel and Humboldt squid) also averaged from 2000 to 2008. Because the acoustic indices only cover the EEZ of Peru, we scaled the model output by dividing it by a factor q (see Table C.1), which represents the proportion of the averaged distribution map of each group that falls within the Peruvian EEZ.

In their configuration, Oliveros-Ramos et al. (2017) calibrated a time-varying larval mortality (LM), constant natural additional mortality, time- and size-class-varying fishing rate, time-varying plankton accessibility coefficient (AC) and time-varying incoming flux of squat lobster. In our climatology, no incoming flux of squat lobster is included, because the squat lobster is present since the beginning of the simulation, and we only calibrated time-constant LM and plankton AC. Time-constant natural additional mortalities and fishing rates (with a seasonality for anchovies, see Section 4.2.2) were obtained from the literature (see Table

C.1). In addition, we manually adjusted the fishing rate of Humboldt squid before the calibration process since our configuration had a tendency to overestimate the landings of this species.

The AC is the fraction of the total plankton that is provided as food for the fish. It parameterises a range of processes that affect the availability of plankton for the fish such as turbulence, stratification and vertical migrations and distribution (see Travers-Trolet et al., 2014a). Literature values of this parameter for OSMOSE vary strongly, from very low values of 10^{-5} % (Marzloff et al., 2009) up to 69 % (Grüss et al., 2015). Our calibration suggested optimal values AC of 3.0, 5.0, 2.0 and 0.4 % for small and large phytoplankton and zooplankton, respectively. The larval mortality rate (LM; ts^{-1}) is applied to the first stage of fish in OSMOSE (eggs and larvae) during its first time step (ts) of life. This parameter is typically calibrated for OSMOSE (e.g., Travers et al., 2009; Marzloff et al., 2009; Halouani et al., 2016; Bănaru et al., 2019) since field observations are scarce. The optimal parameter values are available in Tab. C.1 in Appendix C.1.

After calibrating the model, we simulated the configuration for 300 years to evaluate its stability. With the calibrated parameters, the sardine population collapses after the initial 50 years of simulation (see Supplement). To avoid this decrease, we adjusted by hand the natural mortality of juvenile and adult sardine, as well as its LM (see Table C.1 in Appendix C.1).

4.2.3 Experimental design

To evaluate the effect of an interannual versus a climatological plankton forcing on the simulated biomass of fish and macroinvertebrates, we carried out six simulations. First, starting from the calibrated climatological set-up as described in Sect. 4.2.2, we changed the plankton forcing as described below, while keeping the same calibrated parameter sets:

1. Climatological: 25 years spin-up with climatological plankton followed by 21 years of simulation using the same plankton climatology.
2. Interannual: The spin-up consisted of 4 years with climatological plankton forcing and then 21 years with interannual forcing. After the spin-up, we simulated an additional 21 years applying the interannual hindcast of plankton from 1990 to 2010.
3. Hybrid: 25 years of spin-up time with climatological plankton followed by 21 years of simulation using the interannual hindcast of plankton from 1990 to 2010.

Because OSMOSE is a stochastic model (random movement of schools and ordering of mortality events in a time-step), the output varies slightly among simulations. Therefore, we

analysed the average of 20 simulations for each scenario. After the 25-year spin-up, the following 21 years of simulation (either interannual or climatological) were used for model analysis.

We contrasted the experiments with time-varying forcing with three further experiments, in which we fixed the plankton forcing to scenario "Hybrid", but changed two parameters of OSMOSE which were calibrated and have a high uncertainty. Firstly, we evaluated the effect of a reduction in the AC by 10% (Hybrid-AC), which translates into less plankton being available as potential food. In reality, this can be interpreted as, for example, zooplankton hiding in a shallower oxygen minimum zone, or a deeper mixed layer that dilutes phytoplankton. However, the specific AC for each plankton group might, to some extent, dampen the effect of the variability of different plankton groups on fish. To investigate this further, in a second parameter experiment, we set the AC to a constant value of 10% for all plankton groups (Hybrid-eqAC). We note that the resulting biomasses of this experiment are not directly comparable to the other scenarios because of the strong increase in AC. In all experiments described so far, we have investigated the effect of changing food, i.e. the gains of fish biomass, either through the forcing, or through the AC. In a sixth experiment (Hybrid-aLM), we finally investigated how these changes on the "gain", or food, side compare to changes in loss terms of fish, by increasing the LM of anchovies by 10%. We only manipulated the LM of anchovy in order to avoid an effect obscured by trophic interactions when manipulating the LMs of the other groups.

4. Hybrid-AC: Hybrid set-up with AC reduced by 10 %.

5. Hybrid-eqAC: Hybrid set-up with AC of all four plankton groups equal to 10 %.

6. Hybrid-aLM: Hybrid set-up with anchovy LM increased by 10 %.

This study explores the effect of plankton variability on OSMOSE. Therefore, we kept climatological distribution maps in all configurations. Appendix C.3 provides the results of an alternative set-up where interannually-varying distribution maps were applied from 1992 to 2008 in the hybrid configuration.

4.3 Results

4.3.1 CROCO-BioEBUS model evaluation

We evaluated the plankton compartments in the physical-biogeochemical model due to their importance as food (forcing) for the higher trophic levels model. Simulated phytoplankton biomass was converted to chlorophyll *a* using function get_chla.m of the croco_tools package (Penven, 2019) and compared against MODIS remotely sensed chlorophyll *a* (NASA,

2018). The model reproduces the temporal variability in chlorophyll *a* observations generally well, replicating the seasonal pattern with higher chlorophyll *a* in austral summer (Figure 4.2). However, from 2006 on-wards it tends to overestimate chlorophyll *a*, especially during the austral summer.

Large zooplankton model concentrations were compared against mesozooplankton observa-

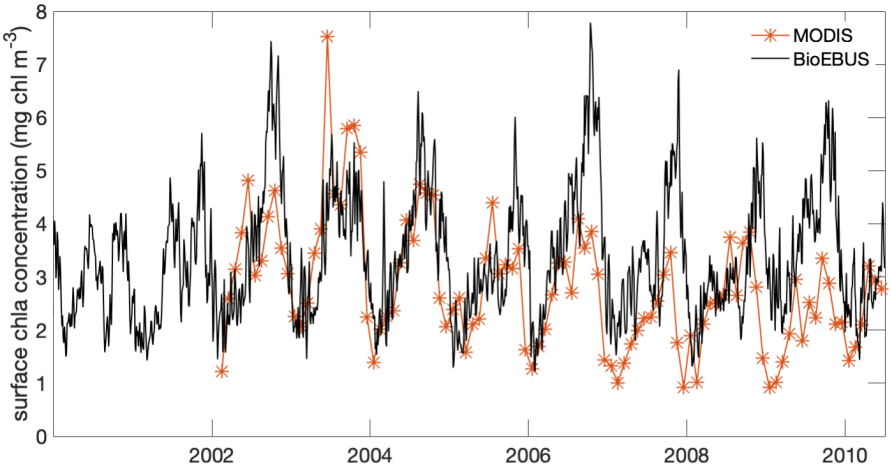

Figure 4.2: Chlorophyll *a* in the model surface layer and in MODIS observations (NASA, 2018), averaged over the closest 2° or about 200 km off the coast of Peru from 15 to 5°S.

tions by Moriarty and O'Brien (2013) and O'Brien and Moriarty (2012), which are provided in carbon units. For model comparison we transformed the observations to nitrogen dividing by a carbon to nitrogen ratio of 4.9 gC/gN (Kiørboe, 2013) and by the nitrogen molar mass of 14 g/mol. Because the model does not parameterise diel vertical migrations, simulated zooplankton is only present where food is available, within the upper 100 m. We therefore compared only the averaged zooplankton in the model and observations over the upper 100 m of the water column. An extensive discussion on the possible causes of mismatch between simulated large zooplankton and mesozooplankton observations observed in an earlier version of BioEBUS is provided by Hill Cruz et al. (2021).

A previous version of the model (José et al., 2017) strongly overestimated zooplankton in comparison to observations (Hill Cruz et al., 2021). Therefore, for the present study, we tuned the model to better match observed concentrations. After tuning the model, large zooplankton is generally of the same order of magnitude as mesozooplankton observations (Figure 4.3). Both, model and observations, show a high concentration of mesozooplankton in the region near the Equator as well as towards the coast of Peru. Within 50 km from the coast, large zooplankton declines in the model. This is not evident in the observations; however, this might be due to the low spatial resolution of samples. Observations show a hotspot of high mesozooplankton concentrations around the Galapagos Islands which is

not visible in the model. This could be either a weakness of the model or it could also be an artefact in the observations due to averaging over very few samples for the whole water column.

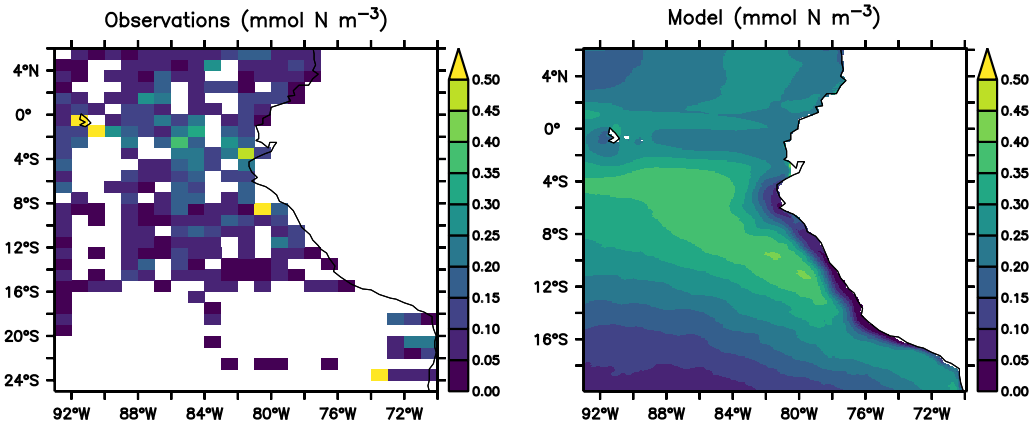

Figure 4.3: Comparison of mesozooplankton observations from the global dataset by O'Brien and Moriarty (2012); Moriarty and O'Brien (2013) and simulated large zooplankton averaged over the upper 100 m depth (mmol N m^{-3}).

4.3.2 OSMOSE model calibration and evaluation

After calibrating and hand adjusting the parameters, simulated biomass and landings show a good fit to observed estimates for most of the groups and are stable for at least 300 years (Figure 4.4). We also evaluated the model performance by comparing the trophic levels simulated by OSMOSE (Figure 4.5) with literature values (Table 4.1). Generally, trophic levels simulated by our model system are very similar to those simulated with Ecopath models (Guénette et al., 2008; Tam et al., 2008). The trophic structure in OSMOSE agrees with the trophic structure of Ecopath. After plankton, euphausiids are the lowest trophic level in the simulation, followed by the small pelagic fish. Humboldt squid and hake are the top predators (Figure 4.5 and Table 4.1). For anchovy, Pizarro et al. (2019) observed a trophic level of 3.23 while, in our model, the trophic level of anchovies lies between 3.1 and 3.4. Pizarro et al. (2019) point out the presence of two groups of anchovies with different diet preferences. One of them, with a mean trophic level of 2.91, prefers to graze on phytoplankton and another carnivorous group has a mean trophic level as high as 3.79 (Pizarro et al., 2019). The smaller trophic level range of anchovy in our study is likely due to having a single feeding preference (predator-prey size ratio range) for all schools of the same age class. We could not find trophic level estimations for squat lobster. However, given that it occupies a similar niche to anchovy (Gutiérrez et al., 2008) we may also expect a trophic level around 3. In OSMOSE we observe that it lies between about 2.5 and 3 (Figure 4.5).

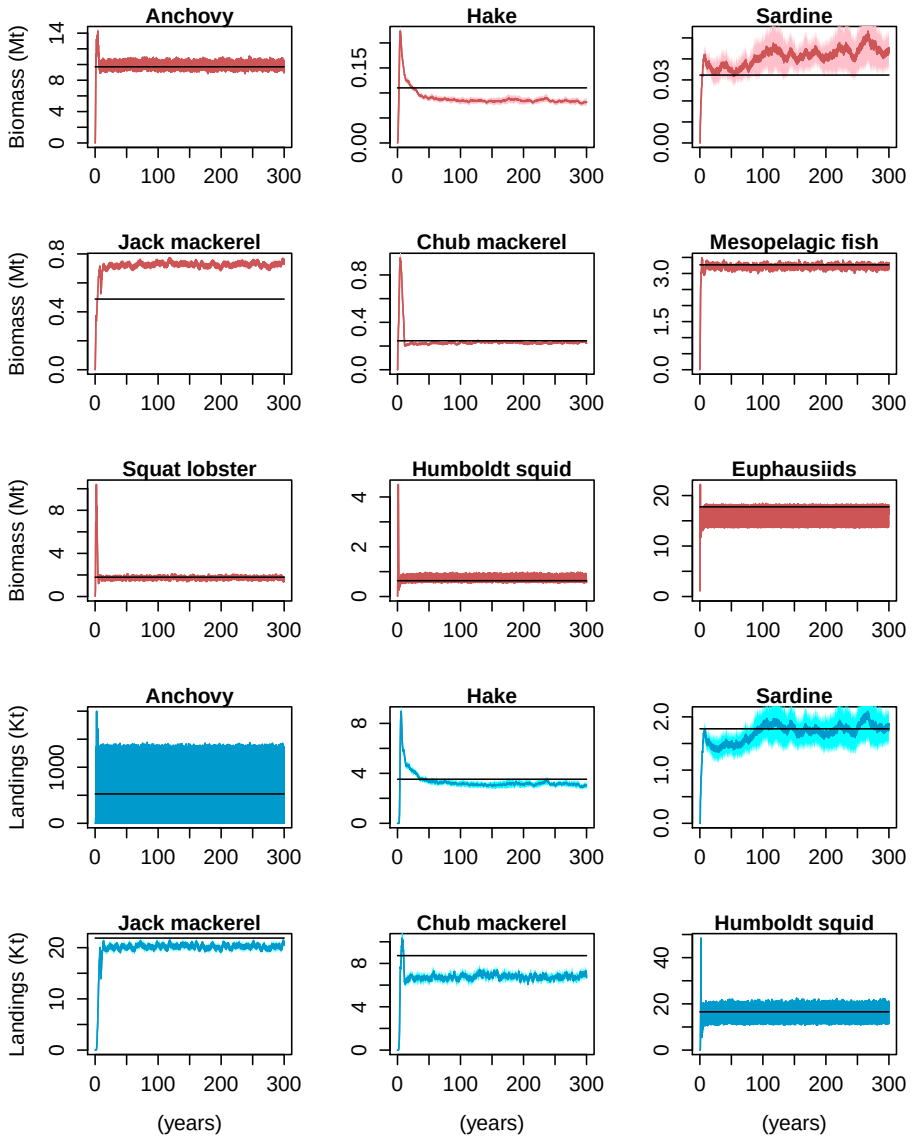

Figure 4.4: Simulated biomass (red) and monthly landings (blue) over 300 years of climatological simulation and observations averaged from 2000 to 2008 (black). These were the observations used to calibrate the model and the model output with the final set of calibrated and adjusted parameters.

4.3.3 Effect of plankton temporal variability, accessibility coefficient and larval mortality on fish biomass

The climatological calibration replicates well the time-averaged biomass of fish and macroinvertebrates for the averaged time period 2000-2008 (Figure 4.4). For most scenarios and groups, simulated biomass lies within the large variability in the observations (Figure 4.6). The hybrid and the interannual configurations show similar results (Figure 4.6), pointing

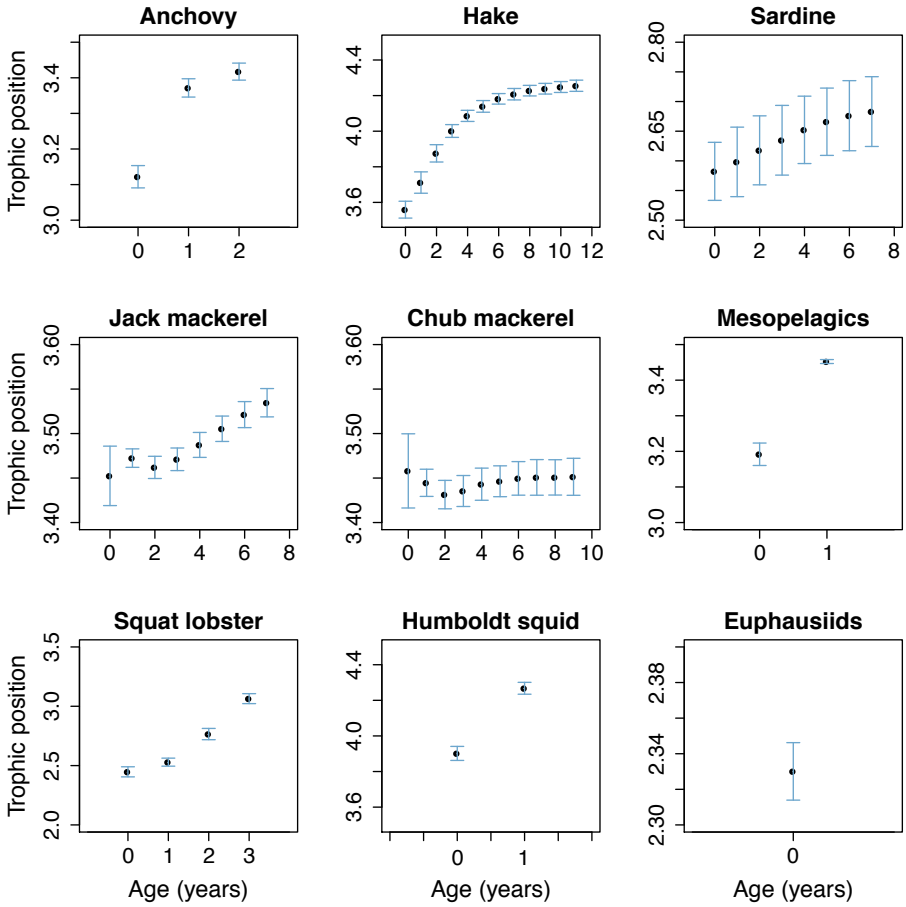

Figure 4.5: Trophic levels per age class (yearly) of every group simulated by OSMOSE, starting from age-class 0. The mean of 25 years of simulation after spin-up is provided and the error bars indicate the standard deviation.

Table 4.1: Trophic levels reported in the literature in Ecopath models of the NHCS (1a, 1b and 2) and observations. Sources: 1a,b Tam et al. (2008). 1a refers to a model of the ecosystem state between 1995–1996, during La-Niña conditions and 1b between 1997–1998 during El-Niño conditions. 2 Guénette et al. (2008). 3 Pizarro et al. (2019).

	(1a)	(1b)	(2)	Observations
Anchovy	2.35	3.17	2.22	3.23 (3)
Hake	3.66-4.32	3.59-4.51	3.33	
Sardine	3.16	2.99	2.98	
Jack mackerel	2.6	3.57	3.3	
Chub mackerel	3.74	3.59	3.18	
Mesopelagics	3.49	3.12		
Squat lobster				
Humboldt squid	4.18	4.14		
Euphausiids	2.50	2.12	2.12	

out that the different spin-ups do not have a considerable impact on the simulation. This is especially evident for the euphausiids (Figure 4.7 right) where both simulations converge after exhibiting different trajectories during the spin-up. This may suggest that the initial conditions are also not so important in OSMOSE once it reaches equilibrium. When comparing these two experiments with the climatological simulation, the effect of introducing interannual variability in food is evidenced by a shift of the mean biomass of euphausiids. In the hybrid configuration, anchovy and euphausiids exhibit a maximum relative interannual variability of 8.8 and 14.6 % of the mean value, respectively. However, in the climatological run, they also exhibit an interannual variability of about 4.1 and 1.1 %, respectively. Therefore, about half of the interannual variability in anchovies comes from the internal dynamics of OSMOSE rather than from the change in plankton forcing. In the case of euphausiids, most of the variability can be directly related to the change in plankton forcing. This is also evident when comparing the hybrid and interannual configuration. Both experiments exhibit almost the same results for the euphausiids, but they differ in the case of anchovies. (Figure 4.7). Such difference does not come from the plankton input but rather from the stochasticity and trophic interactions through the food chain in OSMOSE.

While the hybrid and interannual runs do show a different pattern than the climatological run, their interannual fluctuations tend to be small compared to the high temporal variability in the observations. Other groups show almost no difference between the climatological and the interannual and hybrid configurations. Two important changes in the ecosystem were observed after the El-Niño of 1998: an increase in pelagic squat lobster and a complete collapse of sardines. These are not replicated by the model, which keeps all groups relatively constant before and after the El-Niño (Figure 4.6) and highlights the importance of including other sources of temporal variability in end-to-end models, such as species spatial distribution, in addition to food (see Appendix C.3).

We also investigated the importance of total food concentration on fish biomass by reducing the accessibility coefficient (AC) by 10 %. The reduction leads to a small decrease in fish biomass (Figure 4.6). In contrast, a 10 % increase in the larval mortality (LM) of anchovies has a much larger impact on this species than decreasing the AC (Figure 4.6). Therefore, in this configuration, the LM plays a greater role in controlling the biomass of fish. Finally, we also observe a clear bottom-up effect of reducing anchovy biomass on some of the other species. The effect is especially strong on squat lobster which increases when anchovy decreases, evidencing the same niche utilisation of the two species (Figure 4.6).

4.3.4 Plankton accessibility coefficient effect on model temporal variability

The plankton accessibility coefficient (AC) is a parameter that scales the plankton available for fish to eat. Because the AC was calibrated for each plankton group individually, its differences across plankton groups (low for large zooplankton and higher for the other groups) might mask the impact of seasonal or temporal variability of plankton on fish. To further investigate this issue, in Fig. 4.8, we examined the total amount of plankton (i.e., without multiplication by AC), and the variation of plankton as food (after multiplication by AC). For this specific analysis, we focused on the anchovy habitat. Therefore, we isolated the region inabited by about 90 % of the anchovies (Figure 4.8 right). To isolate this region, we first omitted cells in the averaged climatological distribution map without anchovies and, out of the remaining cells, we selected those where the probability of finding anchovies was larger than the mean over the domain. The maximum interannual variability of total plankton in this region is 21 and 18 % with and without the calibrated plankton accessibility coefficient, respectively, and the maximum seasonal variability is 18 and 19 % (Figure 4.8 left and middle). Thus, the interannual variability of total plankton in this region as food is increased by the AC as much as 3 %. Furthermore, applying a plankton AC shifts the seasonal peak of highest food availability from October to May (Figure 4.8 middle).

Finally, we assessed the effect of applying the same AC to all plankton groups. In OSMOSE, in addition to the AC, the food availability to each fish group is also affected by the predator-prey size ratio, and not all plankton groups are preyed by all planktivorous fish. For example, sardines prey on small particles such as plankton while anchovies prefer euphausiids. The temporal variability of plankton comes directly from the bigoeochemical model; while euphausiids are explicitly represented in OSMOSE and affected by the variability of their main plankton prey but also the trophic interactions with their predators. Therefore, interspecies competition and predation between species of OSMOSE may also play a role, possibly causing non-linear effects. To further investigate this, in a final experiment (Hybrid-eqAC), we set the AC parameter to a constant value of 10 % for every plankton group, thereby omitting any effects caused by the different AC values. For analysis, we focused on the impact of this change on the diet of euphausiids which are the main planktivorous group in OSMOSE and constitue about 85 % of the anchovies diet. The large, homogenous AC of 10 % increases the contribution of large zooplankton to the diet of euphausiids six times, from only 3% to 18.6 % (Table 4.2). Furthermore, setting up an equal AC for all groups also decreases the direct consumption of large phytoplankton by euphausiids by almost half (Table 4.2). This group is replaced by small zooplankton as the main prey of euphausiids. This implies that the temporal variability of zooplankton has a greater impact on euphausiids as well as their subsequent predators.

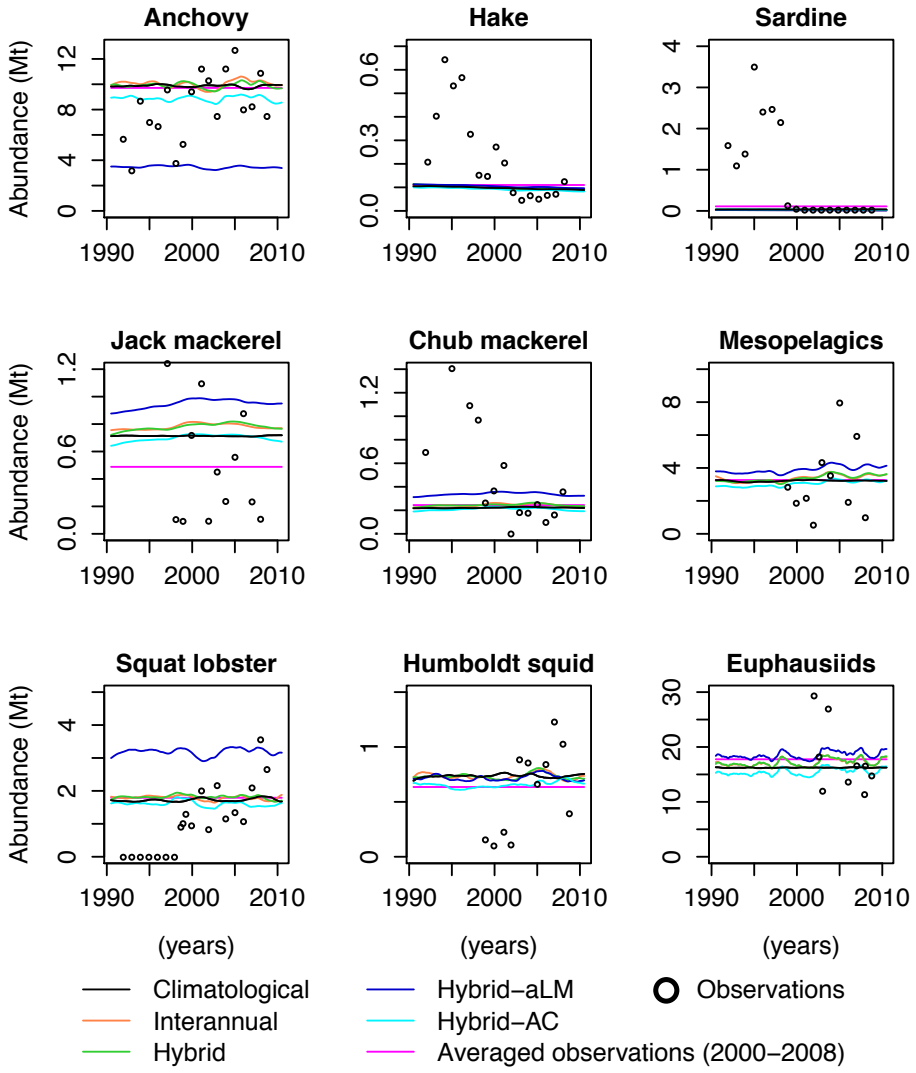

Figure 4.6: Biomass 12-month running mean after spin-up (see Sect. 4.2.3), as well as observations (dots) and 2000 to 2008 averaged observations used to calibrate the model. Observations source: Dimitri Gutierrez, Instituto del Mar del Peru (IMARPE), personal communication. Also available in Oliveros-Ramos et al. (2017), their Fig. 13

Table 4.2: Euphausiids diet proportions

experiment	P_S	P_L	Z_S	Z_L	others
Hybrid	34.3	37.4	24.4	2.9	1.0
Hybrid-eqAC	29.7	19.9	31.0	18.6	0.8

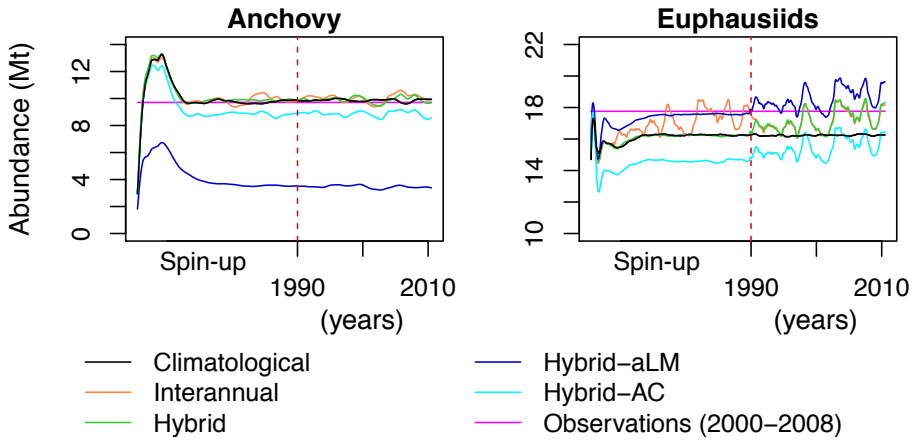

Figure 4.7: Same as Figure 4.6 including spin-up of anchovies and euphausiids.

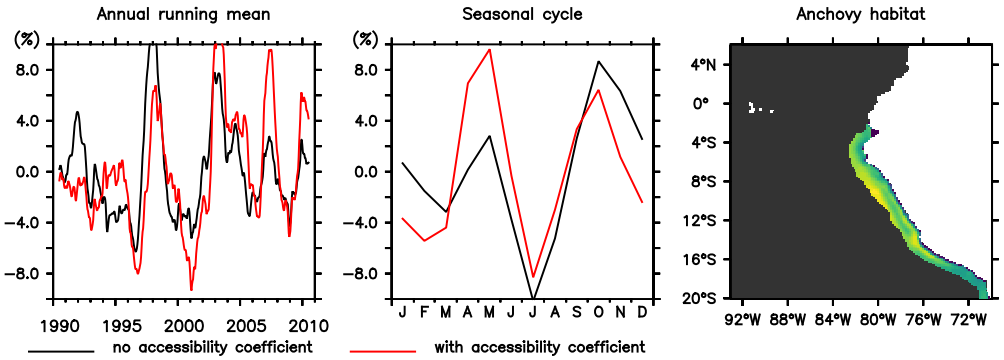

Figure 4.8: Interannual (left) and seasonal (middle) variability of total plankton in the region occupied by about 90 % of anchovies (anchovy habitat in the right panel), calculated taking into account the plankton accessibility coefficient (red) and without plankton accessibility coefficient (black).

4.4 Discussion

Our study shows a weak effect of temporal variability in the biogeochemical model on higher trophic levels (HTL), which may be attributed to several reasons. First, it is possible that the plankton temporal variability in the CROCO-BioEBUS model is, in fact, too weak. Compared to satellite data (see 4.3.1), the surface chlorophyll in the model displays a similar variability. However, as shown in Sect. 4.3.4, the interannual variability in integrated plankton of CROCO-BioEBUS that was provided as forcing to OSMOSE is close to 20 % of the mean. This is small compared to the variability observed for anchovies. A second reason may be that the link between the biogeochemical model CROCO-BioEBUS and the HTL model OSMOSE is too weak. This link is done only through plankton food forcing for juvenile and adult fish. Other possible links may include the effect of oxygen, temperature and food availability on larval survival and through interannually-varying distribution maps. In Appendix C.3, we provide an alternative configuration where additional interannual variability is introduced by applying interannual distribution maps instead of climatological. To our knowledge, the study by Oliveros-Ramos et al. (2017) is the only modelling project that has successfully replicated the regime shift after the El-Niño event of 1998. They achieved this, in addition to including interannual distribution maps, by calibrating time-varying parameters. While such an approach successfully replicates the interannual variability in the system, it masks the interactions between the biogeochemical and HTL because the temporally varying model parameters account for all temporal variability, which is not necessarily justified, not allowing to pinpoint processes. For instance, in Oliveros-Ramos et al. (2017, their Figure 10), anchovy larval mortalities (LM) fluctuated more than 2-fold around the central value. In our study, we found that OSMOSE is very sensitive to the value of LM, with a 10% change decreasing the biomass of anchovy by more than half. The impact is much stronger than the effect caused by a 10 % decrease in available food. This suggests that the key to reproduce the interannual variability of the fisheries in the NHCS may not be in the food provided to adults but rather on the survival of larvae. Finally, it may be that also in the real ocean, there is not a straightforward bottom-up control of HTL as supported by Ayón et al. (2004). They found no significant correlation between zooplankton and anchovy observations off Peru between the period of 1984 to 2001, pointing to other potential drivers than food production. Therefore, the main driver of the interannual variability in the NHCS might not be as simple as adult fish following the trends in plankton concentrations. This may be a peculiarity of the NHCS that makes the modelling of this ecosystem so challenging. Simulating environmental variability in OSMOSE only through changes in plankton food for juvenile and adult fish has, in fact, produced stronger impacts in other ecosystems. Fu et al. (2012) evaluated the effects of interannual variability in plankton input on their OSMOSE model configuration for the Strait of Georgia in British Columbia, Canada. In their study, interannual variability in phytoplankton produced strong effects of more than ±50 % on their small forage fish, her-

ring (Fu et al., 2012, their Figure 5a). This is much larger than the response observed in our study.

The maximum sustainable yield is the maximum amount of fish that can be taken from the system while keeping the population growth at sustainable levels. Past studies emphasize the importance of recruitment and mortality on the growth rate of fish populations (Tsikliras and Froese, 2019). Therefore, understanding the drivers of recruitment is essential to assess the growth of a population and, in turn, its maximum sustainable yield. In OSMOSE, recruitment is controlled by the LM parameter which represents the additional natural mortality during the first 15 days of life of eggs and larvae. It intends to account for processes that happen during the earliest life stages of fish when mortality is very high but hard to estimate from empirical studies. For instance, spatio-temporal match between larvae and plankton allows fish recruitment (Cushing, 1990). In upwelling regions, this occurs at an optimal wind stress (Cury and Roy, 1989; Cushing, 1990). In this way, the LM parameter in OSMOSE also accounts for the impact of environmental processes on larvae such as wind-dependence mixing. Our OSMOSE configuration proved to be highly sensitive to the LM parameter. Following the setting-up of other OSMOSE configurations (e.g., Vergnon et al., 2008; Marzloff et al., 2009; Travers et al., 2009; Fu et al., 2012; Grüss et al., 2015; Halouani et al., 2016), we estimated this parameter during the calibration process of the model. Therefore, it was used, in combination with the plankton accessibility coefficient (AC), to adjust the fish biomass to observed levels. Alternatives to calibrating this parameter may include to find a mechanistic representation of the fine scale larvae dynamics in relation to the physical environment and food availability.

In Tab. 4.3, we compared some larval mortalities used in our configuration against literature values of egg and larval survival compiled by Dahlberg (1979). We compared survival rates of Pacific sardine and jack mackerel (Dahlberg, 1979, , their Table 1). Because Dahlberg (1979) did not provide estimations for Peruvian anchovy, we compared our anchovies LM against Japanese anchovy (Dahlberg, 1979, , their Table 2). The relationship between the daily larval mortality (LM/15 days $= \mu$) and survival (S) in OSMOSE is given by $S = \frac{N(t+\Delta t)}{N(t)} = e^{-\mu \Delta t}$ (using the exponential approach provided in OSMOSE source code: `https://github.com/osmose-model/osmose/tree/master/java`). The daily survival rates in OSMOSE are smaller than in Dahlberg (1979) (Table 4.3). However, this comparison has to be taken with caution since the egg and first-feeding larvae period in OSMOSE (15 days) is shorter than the periods reported by Dahlberg (1979) (Table 4.3). Therefore, the high mortality of the initial days of life of fish is concentrated over a shorter timeframe and it is not surprising that the survival rates are lower.

Finding a mechanistic link between the LM and the environmental drivers will be a crucial step in the development of end-to-end models. Roy (1993) found a relationship between

Table 4.3: Comparison of survival rates (dimensionless) during egg and larval stages (period of estimation provided in days) provided by Dahlberg (1979) and in our configuration. Species provided by Dahlberg (1979): Anchovy, *Engraulis japonica* (Nakai et al., 1955); Jack mackerel, *Trachurus symmetricus* (Farris, 1961); sardine, Pacific sardine (Murphy, 1961, scientific name not provided)

	Species	Anchovy	Sardine	Jack mackerel
Dahlberg (1979)	Period of estimation (days)	31	50	57
	Survival per day	0.799	0.883	0.83
OSMOSE	Period of estimation (days)	15	15	15
	Survival per day	0.555	0.461	0.524

wind speed and recruitment of anchovy and sardine populations in several eastern boundary upwelling systems. This is based on the hypothesis that low wind and upwelling is linked to low primary productivity and recruitment; high wind-speeds, on the other hand, generates strong mixing that disperses larvae away from the food. Therefore, there is an "Optimal Environmental Window" (Cury and Roy, 1989) where the wind is neither too strong, nor too weak and maximum recruitment is achieved (Roy, 1993). From a modelling perspective, Lett et al. (2008) proposed an explicit simulation of the larval stages of fish as a Lagrangian individual-based model with salinity, temperature and velocity inputs. A simple experiment to increase the effect of food availability on fish in OSMOSE is to link the LM to the food availability through a linear relationship. Other potential improvements for the larval parameterisation in OSMOSE may include to either link the LM parameter to environmental conditions, for instance, through the relationship found by Roy (1993); or to include a whole new larval sub-model in OSMOSE, similar to the one proposed by Lett et al. (2008). The time-series of estimated larval mortalities by Oliveros-Ramos et al. (2017) provides a good fitting hindcast. A statistical relationship with the physical parametes and traces of the biogeochemical model could then be derived to produce estimates for future projections. This may not only reduce the uncertainty in the LM but, because LM and AC act in opposite directions, it would potentially also provide insights into better estimations of the AC during the calibration process by reducing the number of parameters to be optimised.

There is no model that fits all purposes but models are useful tools to investigate certain questions. Every question, however, poses specific requirements for the model. OSMOSE was originally developed to investigate trophic interactions among HTL such as fish (Shin and Cury, 2001, 2004). At this time, fish schools were divided into piscivorous and non-piscivorous fish and their maximum populations were regulated by a carrying capacity (Shin and Cury, 2001, 2004). Later on, it was modified to also include explicit food forcing from plankton groups (Travers, 2009) which could be derived from satellite and surveys data

(Marzloff et al., 2009) or biogeochemical models (Travers et al., 2009). At this point, a carrying capacity parameter was not necessary anymore since limited resources were explicitly modelled. However, the AC was implemented to scale the biomass of plankton that is available to the fish. The reasoning behind is that not all plankton in the water-column is available for the fish to feed (Travers et al., 2009). This parameter is, however, poorly understood and it is usually calibrated. A blind calibration of the AC may, however, obscures the interactions between higher and lower trophic levels in the end-to-end model. The study by Travers-Trolet et al. (2014b,a) looked at the combined effects of top-down and bottom-up pressures on a two-way coupled $N_2P_2Z_2D_2$-OSMOSE model system. The fish-to-plankton feedback was achieved by calculating a mortality map of plankton based on the consumption by fish. The maximum consumption of every plankton group was given by the AC which came from a calibration. Since, in a two-way coupling system, fish consumption has a direct impact on zooplankton mortality, the AC might also affect the biogeochemistry of the model. Therefore, special attention has to be taken for the choice of this parameter.

4.5 Conclusion

We set up a climatological configuration for the Northern Humboldt Current System coupling the higher trophic levels model OSMOSE with the physical-biogeochemical model CROCO-BioEBUS. Changing the climatological plankton forcing to an interannual time-series did not replicate the strong fluctuations in fish, especially sardine and anchovy, seen before and after the El-Niño event of 1998. Temporal changes in the habitat of fish may be an additional source of interannual variability. These were included by Oliveros-Ramos et al. (2017) as interannually-varying distribution maps based on statistical methods. In climate projections, these could be directly linked to the variables in the biogeochemical model. Alternative coupling methods linking other environmental drivers, for instance temperature and oxygen, with life stages of higher trophic levels, for instance larvae, may shed light into the main causes of the strong fluctuations of small pelagic fish in the Northern Humboldt Current System. This, in turn, may reduce the uncertainty in the plankton accessibility coefficient which is the most poorly constrained parameter in OSMOSE. When the main goal of using OSMOSE is to explore the interactions between higher trophic levels and biogeochemistry, including plankton, we recommend a thoughtful consideration of what the plankton accessibility coefficient represents in the model. For example, some of the large zooplankton may perform vertical migrations and hide in the oxygen minimum zone. In this case, it would not be available for the fish during part of the day and it would require a different accessibility coefficient. However, if this information is missing while parameters need to be calibrated, for evaluating the link between the biogeochemical processes and OSMOSE, we recommend to calibrate the same accessibility coefficient for all plankton groups.

Chapter 5

Using mixed layer depth to constrain projections of Southern Ocean ecosystem functioning

This chapter is a manuscript in preparation by Xue T., Frenger I., Koeve, W., and Oschlies A.(2022).

Abstract

Phytoplankton, as the base of the food web, photosynthesises in the very upper sunlit ocean, thereby fixing CO_2 to organic carbon, some of which is transferred up the marine food web and exported into the deep ocean. Projected changes in phytoplankton under climate change differ dramatically across different model estimations. We here introduce an observed correlation between mixed layer depth and surface chlorophyll concentration, a proxy for phytoplankton biomass, under present day-climate seasonality in the Southern Ocean, a region with a large mixed layer depth seasonal cycle. We then use this relationship as a constraint on potential variation in surface chlorophyll under climate change. Applying this observational constraint, we expect a 10-16% increase in surface chlorophyll under a high emissions scenario, with a significantly reduced uncertainty from 15% to 6%. Apart from the surface chlorophyll concentration, total phytoplankton biomass within the water column is also expected to slightly increase by 4% while zooplankton reveals a more prominent increase of 12%, that is an amplified response. This future trophic amplification is mainly due to enhanced trophic transfer efficiency as a result of improved zooplankton grazing conditions with shoaling mixed layers. In addition, higher zooplankton biomass in winter, allowing the zooplankton to feed more efficiently on the spring bloom, contributes to the increase in trophic transfer efficiency next to higher prey concentrations. With our findings of improved phytoplankton growth conditions and the stronger grazing pressure as a result of the shoaling mixed layer, we emphasise the potential increasing importance of "top-down" control under climate change.

5.1 Introduction

Marine phytoplankton plays a critical role in the global carbon cycle as it contributes approximately half to the global biological carbon fixation (Field et al., 1998), and, as the base of the marine ecosystem, provides food to the marine food web (Pauly and Christensen, 1995). Phytoplankton growth is thought to be mostly determined by environmental factors (e.g., nutrients, light, and temperature) which are influenced by physical processes (e.g., mixed layer dynamics, upwelling, etc; Behrenfeld et al., 2006). Given that these environmental factors will change under climate change, phytoplankton will inevitably also be influenced by climate change. However, how it will be influenced is not entirely clear, current model projections of phytoplankton biomass and its growth reveal great uncertainties (Lotze et al., 2019; Laufkötter et al., 2015; Frölicher et al., 2016) due to not only the underlying physical forcing, but also different biological and biogeochemical parameterizations of processes in models (Laufkötter et al., 2015). Such uncertainties propagate through the food web and introduce even greater uncertainties to higher trophic level projections due to the simplified depiction of food web mechanisms (Lotze et al., 2019). Food web dynamics is often poorly simulated within global biogeochemical models which hence are unable to cap-

ture the complexities of trophic interactions (Le Quéré et al., 2016). Meanwhile, ecosystem processes that are represented in global biogeochemical models are typically not thoroughly calibrated, such as the functioning of zooplankton (Stock et al., 2014b).

In general, phytoplankton biomass and its growth are expected to decrease with global warming due to enhanced nutrient limitation as a result of shoaling mixed layers, especially in the low-latitude regions (Doney, 2006; Behrenfeld et al., 2006; Boyce et al., 2010). Furthermore, research indicates that the overall trend of declining phytoplankton biomass and primary productivity would be amplified in higher trophic levels such as zooplankton (Chust et al., 2014; Stock et al., 2014a; Kwiatkowski et al., 2019) and fish (Lotze et al., 2019). On the contrary, high-latitude regions show an opposite biological response to shoaling mixed layers due to improving light conditions (Doney, 2006). In response to the phytoplankton increase, zooplankton are projected to maintain a relatively higher biomass in winter, resulting in stronger grazing on the spring bloom (Stock et al., 2014a).

The Southern Ocean is a vast region where models tend to agree that phytoplankton will grow better under global warming, albeit with an uncertain magnitude (Fig. 5.1 Bopp et al., 2013; Laufkötter et al., 2015; Kwiatkowski et al., 2020). At the same time, it is a region where deep ocean carbon is outgassed to the atmosphere (Gruber et al., 2019; Frölicher et al., 2015), and where nutrient characteristics of water masses are reset (Sarmiento et al., 2004; Marinov et al., 2006; Nissen et al., 2021). Upper ocean biology plays an important role in setting these biogeochemical characteristics, and a better understanding of its likely evolution under climate change is required for reliable projections of the nutrient inventories of the water masses formed in the Southern Ocean. Based on contemporary seasonality, we apply an emergent constraint to reduce uncertainties in future surface chlorophyll projections in the Southern Ocean. Moreover, we investigate the consequences of increasing phytoplankton on the ecosystem and further improve our understanding and ability to predict marine ecosystem responses to climate change.

5.2 Methods

5.2.1 Multi-Model Ensemble

To analyse trophic dynamics, we use the output of a Multi-Model Ensemble (MME, Table 5.1) over the Southern Ocean (>45^{o}S). Of the ten models that we used, eight were taken from the Coupled Model Intercomparison Project Phase 6 (CMIP6, downloaded from https://esgf-data.dkrz.de), while the other two (FOCI and UVic) were taken from previous publications (Chien et al., 2022; Yao et al., 2019). The selection of these models is based on the availability of the variables required (mixed layer depth, chlorophyll concentration, phytoplankton biomass concentration, zooplankton biomass concentration,

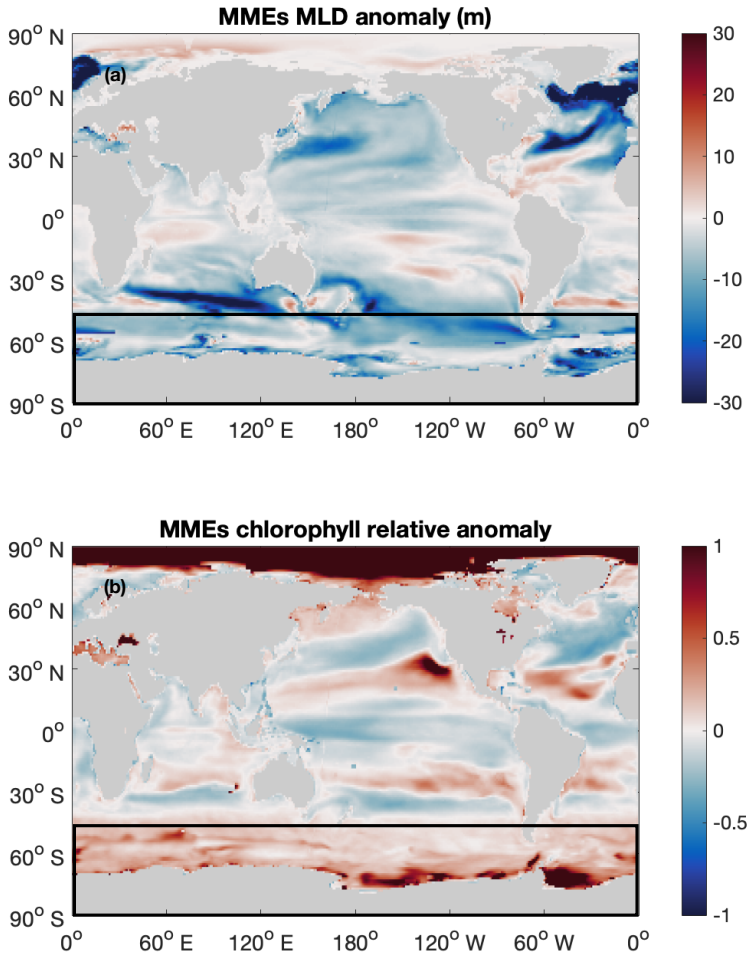

Figure 5.1: The Southern Ocean sticks out as a region with projected shoaling mixed layers and increasing chlorophyll under climate change. Global maps of changes in (a) mixed layer depth (MLD) and (b) surface chlorophyll, with global warming (between the first (2000s) and the last decade (2090s) of the 21st century), with the Southern Ocean highlighted in black lines. Red indicates deepening mixed layers/increasing surface chlorophyll and blue indicates shoaling mixed layers/decreasing surface chlorophyll during the 21st century. MME denotes a multi-model ensemble.

Table 5.1: Overview of the Multi-Model Ensemble (MME) used in this study

Model Name	Ocean Biogeochemistry	Plankton Groups	Simulations Sec. 5.3.2	Simulations Sec. 5.3.3	Reference
ACCESS-ESM1-5	WOMBAT*	P1Z1	✓		Ziehn et al. (2020)
CanESM5	CMOC	P1Z1	✓	✓	Swart et al. (2019)
CanESM5-CanOE	CanOE*	P2Z2	✓	✓	Christian et al. (2021)
CNRM-ESM2-1	PISCESv2-gas*	P2Z2	✓	✓	Séférian et al. (2019)
FOCI1	MOPS	P1Z1	✓		Chien et al. (2022)
IPSL-CM6A-LR	PISCES-v2*	P2Z2	✓	✓	Boucher et al. (2020)
MPI-ESM1.2-LR	HAMOCC6 *	P2Z1	✓	✓	Mauritsen et al. (2019)
MRI-ESM2.0	NPZD	P1Z1	✓	✓	Tsujino et al. (2017)
UKESM1-0-LL	MEDUSA *	P2Z2	✓	✓	Sellar et al. (2019)
UVic (NoFe) †	-	P2Z1	✓		Yao et al. (2022)

* indicates models that explicitly include iron limitation.
† indicates models that still used CMIP5-RCP8.5 forcing; the other models used SSP5-8.5.
Sec. 3.2 and Sec. 3.3 refer to the sections where we used respective model output which was more limited in Sec. 3.3 because higher trophic level information was provided for fewer models.

zooplankton grazing), temporal resolution (monthly), and experimental settings (historical simulation, piControl simulation to control for potential drifts, and SSP5-8.5/RCP8.5 high emission scenarios). The models within the MME are structurally different, cover a range of different parameterizations of processes, and use differing initial conditions. All output fields were regridded on a regular $1^\circ \times 1^\circ$ map before further analysis. Outliers are removed from the results using percentile thresholds [0.1 99.9]. The contemporary (2000 - 2015) seasonal sensitivity of chlorophyll to mixed layer depth changes was calculated for each model based on the monthly mixed layer depth anomaly and the surface chlorophyll fractional changes, relative to the temporal mean values. Further climate change sensitivity is calculated based on the difference between the respective mean values of the first (2015 - 2024) and last decades (2091 - 2100) in the period of 2015 - 2100 under the high emissions scenario.

5.2.2 Observational constraints

To assess the seasonal sensitivity of observational constraint, we used monthly climatological mixed layer depth (MLD) data from WOA (World Ocean Atlas, `https://www.ncei.noaa.gov/products/world-ocean-atlas`, last access: March 2022) and satellite-based monthly climatologies of chlorophyll concentration data from CZCS (product period: 1978 - 1986, `https://oceancolor.gsfc.nasa.gov/l3/`, last access: March 2022), SeaWiFS (product period: 1997 - 2010, `https://oceancolor.gsfc.nasa.gov/l3/`, last access: March 2022) and MODIS (product period: 2002 - present, `https://oceancolor.gsfc.nasa.gov/l3/`,

last access: June 2021).

5.2.3 Emergent constraint

For the emergent constraint, MME contemporary seasonal sensitivities (S_{season}, Eq. 5.1, period: 2000-2014, unit: m^{-1}) and long-term sensitivities (S_{clm}, Eq. 5.2, period: 2015-2100, unit: m^{-1}) of surface chlorophyll are calculated. The contemporary seasonal sensitivities (S_{season}, Eq. 5.1) are computed using the MLD seasonal amplitude and the chlorophyll conditions difference between the month with the deepest mixed layer (mmax) and the month with the shallowest mixed layer (mmin) relative to the annual mean value (mmean). Long-term sensitivities (S_{clm}, Eq. 5.2) are calculated by subtracting the mean values of the last (2090s) and first (2000s) decades.

$$S_{season} = \frac{(Chl_{mmax} - Chl_{mmin})/Chl_{mmean}}{MLD_{mmax} - MLD_{mmin}} \tag{5.1}$$

$$S_{clm} = \frac{(\overline{Chl_{2090s}} - \overline{Chl_{2000s}})/\overline{Chl_{2000s}}}{\overline{MLD_{2090s}} - \overline{MLD_{2000s}}} \tag{5.2}$$

The probability density functions (PDFs) of the long-term sensitivity of the surface chlorophyll were calculated the following way for the unconstrained MME prior and after the CZSZ, SeaWIFS, and MODIS constraints (Fig. 5.4b): Assuming all models have equal probability, the unconstrained MME prior PDF was derived from a Gaussian distribution. Furthermore, we calculated the constrained PDFs as discussed in the review by Williamson et al. (2021) where the mean is picked based on the observations combined with the newly determined correlation of S_{season} and S_{clm}, and the standard deviation is estimated from the correlation.

5.2.4 Trophic transfer efficiency

In Sec. 5.3.3, to further investigate the impact of MLD on ecosystem functioning, we calculate the trophic transfer efficiency as the ratio of depth-integrated monthly-mean biomass of zooplankton (zoo, Eq. 5.3, unit: $mg\ C\ m^{-2}$) to phytoplankton (phy, Eq. 5.3, unit: $mg\ C\ m^{-2}$) following Barnes et al. (2010). The dimensionless notion of trophic transfer efficiency reflects the biomass or energy transfer between trophic levels and is typically estimated based on the biomasses or productivities of trophic levels. Here we pick biomass because it allows for a direct comparison with observations.

$$TTE = \frac{\int zoo}{\int phy} \tag{5.3}$$

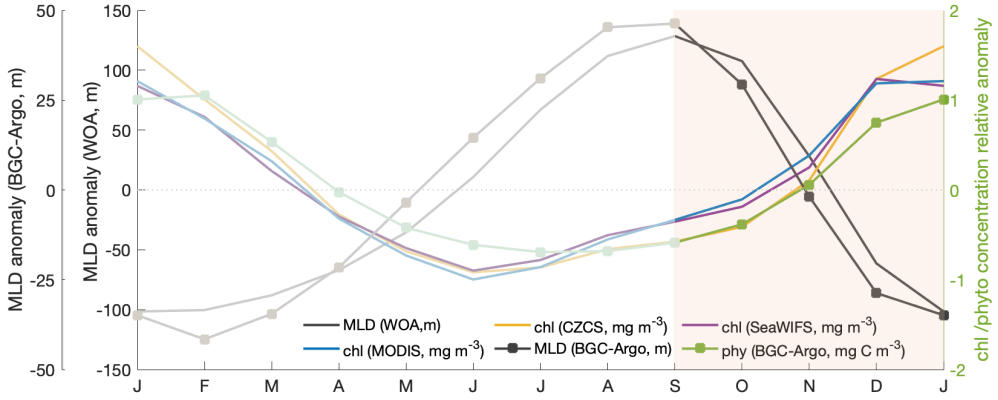

Figure 5.2: The observed surface chlorophyll (chl)/phytoplankton concentration shows a clear seasonal cycle that is correlated with mixed layer depths (MLD). Contemporary seasonal variations of observed MLD (WOA: black) and surface chlorophyll concentration relative to the respective annual means, based on satellite data (CZCS: yellow; SeaWIFS: purple; MODIS: blue) in the Southern Ocean (south of 45°S). Square lines indicate BGC-Argo MLD (black) and phytoplankton concentration (green) seasonality, digitized from Arteaga et al. (2020). Note that the month of January (J) is shown repeatedly to visualize the cyclicity of the seasonal cycle.

5.3 Results

5.3.1 Observed relationship between seasonalities of mixed layer depth and surface chlorophyll

The observed surface chlorophyll concentration in the Southern Ocean peaks during early austral summer (Fig. 5.2) and exhibits a clear seasonal cycle that is related to mixed layer dynamics. Surface chlorophyll concentration is used as a proxy for phytoplankton biomass. It is chosen because it is a comparatively well observed variable, in contrast to biomass. Both MLD and surface chlorophyll display a clear seasonality, with shallow MLD coinciding with relatively high surface chlorophyll and deep MLD coinciding with relatively low surface chlorophyll in austral winter. The observed relationship of surface chlorophyll and MLD on a seasonal scale can be explained by the MLD-driven dilution and light limitation, as suggested by previous studies (Uchida et al., 2019; Arteaga et al., 2020).

We choose the MLD shoaling period (austral spring, Sept-Jan, shaded period in Fig. 5.2) in the following Sec. 5.3.2 to constrain the effect of projected shoaling mixed layer depths on surface chlorophyll under climate change. While the general anticorrelation of the seasonal cycles of MLD and surface chlorophyll concentration is visually striking, there is a lag between the peaks of maximum MLD and minimum chlorophyll in winter prior to the MLD shoaling period in spring. This lag is partially due to poor light conditions in deep MLD triggering an increase of the Chl:C ratio that masks a continued decrease of phytoplankton

biomass concentration in ever deepening MLD (Geider, 1987; Arteaga et al., 2016). Thus, we pick the time period right after MLD peaking, that is, spring, where dilution of chlorophyll is expected to strongly decrease with strong MLD shoaling.

5.3.2 Using observed seasonal cycles to constrain projections of future change of surface chlorophyll

The global climate multi-model ensemble (MME) reproduces well the seasonal anticorrelation of mixed layer depths and surface chlorophyll concentration (Fig. D3). While the MME features slightly reduced amplitudes of the seasonal cycles of MLD and chlorophyll compared to observations, it does show an increase in surface chlorophyll associated with the shoaling of MLD in austral spring (Fig. D3). Also the individual models largely agree with the observations, though with some spread. Such spread is not unexpected given the structural differences of the biogeochemical models that include varying considerations and representations of the Chl:C ratio, grazing, and nutrient limitations (such as iron). Nevertheless, individual models agree in that winter chlorophyll surface concentrations are comparatively lower and increase towards summer, as reflected in the MME and consistent with observations.

For the 21st century, models project shoaling mixed layer depths along with enhanced surface chlorophyll concentrations in the Southern Ocean (Fig. 5.1a,b). By the end of the century, MLD is projected to shoal 23±9 m compared to the beginning of the century (Fig. 5.3a). In response to the shoaling MLD, surface chlorophyll will rise by 14% throughout the 21st century (Fig. 5.3b), that is a sensitivity of chlorophyll to MLD changes of 0.6% m^{-1}. However, model estimates of surface chlorophyll are associated with substantial uncertainties (±15%) which thus include zero or negative changes of surface chlorophyll in the Southern Ocean (Fig. 5.3b).

The seasonal sensitivity (S_{season}) of chlorophyll relative to variations of the MLD and the long-term sensitivity (S_{clm}) have a clear inter-model linear relationship (r=0.78, Fig. 5.4a). This relationship means that models within which surface chlorophyll is more sensitive to MLD changes on a seasonal scale tend to show a larger sensitivity also of surface chlorophyll to MLD changes on a longer-term scale. The mechanisms underpinning the correlation between mixed layer depth and surface chlorophyll on a long-term climate scale are consistent with reduced dilution and an amelioration of "bottom-up" controls similar to the mechanisms at the seasonal scale: when MLD is shoaling and phytoplankton is being compressed in a narrower surface layer (Xue et al., 2022b), they are experiencing better light conditions, and possibly temperature conditions as well (as with global warming). Hence, the seasonal sensitivity of surface chlorophyll to MLD can serve as a proxy for the long-term response.

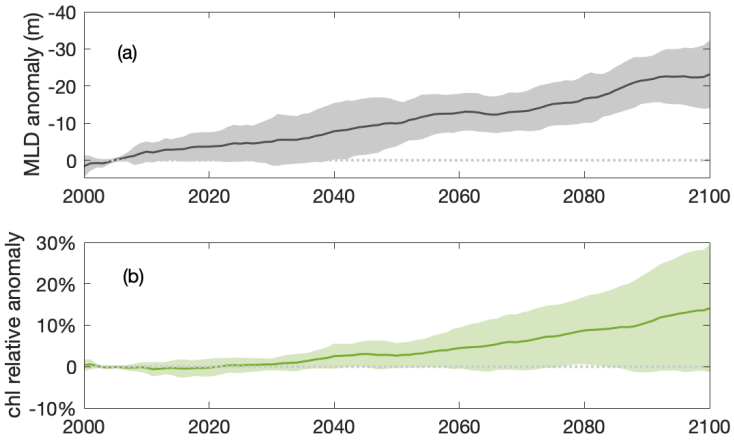

Figure 5.3: Shoaling mixed layer depth (MLD) and increasing surface chlorophyll (chl) towards the end of the century. Multi-model ensemble (MME) projections of annual mean (a) mixed layer depth (grey); and (b) surface chlorophyll concentration relative changes (light green) from 2000 - 2100 to the mean values of first decade of the 21st century (2000 - 2009) with ±1 SD (shaded) under high emission scenarios in the Southern Ocean. The timeseries are filtered using a 10-year moving average.

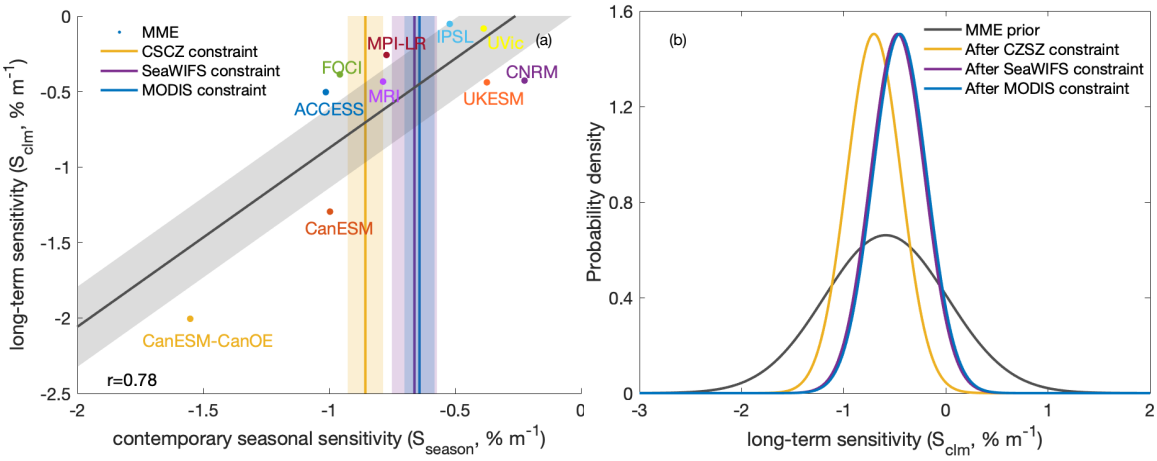

Figure 5.4: Emergent constraint on the long-term sensitivity (S_{clm}) of surface chlorophyll to mixed layer depth based on the seasonal sensitivity (S_{season}). (a) The long-term sensitivity (S_{clm}) of surface chlorophyll relative anomaly to MLD anomalies, against the seasonal sensitivity (S_{season}) of surface chlorophyll relative anomaly to MLD anomalies. Dots indicate the results of the multi-model ensemble (MME). Solid vertical lines indicate observational constraints (CZCS: yellow; SeaWIFS: purple; MODIS: blue) with shaded areas indicating ±1 SD. (b) Probability density functions (PDFs) of the long-term sensitivity of surface chlorophyll relative anomaly to MLD anomaly. The black line shows the "MME prior" PDF, assuming all models are equally likely and from a Gaussian distribution. The colored lines show the observationally constrained PDFs (CZCS: yellow; SeaWIFS: purple; MODIS: blue).

Applying observational constraints to the MME output emergent relationship, estimates of the long-term sensitivity of chlorophyll relative variation to climate-change driven MLD anomalies shift from -0.59±0.6 $\%m^{-1}$ to -0.7±0.3 $\%m^{-1}$ (CZSZ), -0.47±0.3 $\%m^{-1}$ (SeaWIFS) and -0.45±0.3 (MODIS; Fig. 5.4). While the projected mean unconstrained long-term sensitivity (0.6% m^{-1}) is within the constrained estimates, the observational constraints help to substantially reduce the uncertainty from 0.7% m^{-1} to 0.3% m^{-1}. Despite no model predicting a negative long-term climate impact on surface chlorophyll along with shoaling MLD, there is an unconstrained probability of 17% of a decrease in chlorophyll with climate change. This probability is significantly reduced after applying observational constraints (CZCS: 0.4%; SeaWIFS: 4%; MODIS: 5%). Given that the MME mean MLD shoaling is 23 m throughout the 21st century, our emergent constraints imply a 10% (MODIS constraint) to 16% (CZCS constraint) increase in surface chlorophyll concentrations in the Southern Ocean, with 6% uncertainty under the high emissions scenario.

5.3.3 Even greater increase of zooplankton: Trophic amplification

Despite the shoaling MLD, modelled depth-integrated biomass of both phytoplankton and zooplankton reveals an increasing trend, with the zooplankton showing a more prominent increase, which suggests the pattern of trophic amplification (Fig. 5.5a). Future projections of depth-integrated phytoplankton biomass are determined by the competing effects of the shoaling MLD and the increasing phytoplankton concentration. Though with large uncertainty, the contribution from the increasing phytoplankton concentration overrules the shoaling MLD and leads to a 4% MME mean depth-integrated phytoplankton biomass increase. Worth noticing, while depth-integrated phytoplankton biomass reveals a general rising trend, depth-integrated zooplankton biomass exhibits three times (12%) the phytoplankton increase. The phenomenon of a higher trophic level revealing greater change than the lower trophic level is known as trophic amplification (Kirby and Beaugrand, 2009).

Trophic amplification, which is also reflected in an increasing trophic transfer efficiency, is mainly driven by increasing zooplankton grazing due to the enhanced phytoplankton (prey) concentration. Higher predator and prey concentrations in a thinner layer allow the predator to graze more efficiently due to a high encounter efficiency. Hence a shallower mixed layer supports a high specific grazing rate for the predator. This mechanism is apparent in a significant correlation between prey concentration and the grazing from the predator (Fig. D4), which previously has been suggested to occur on a seasonal scale in present-day productive systems (Xue et al., 2022a).

The trophic transfer efficiency (Eq. 5.3) increases most prominently from late winter to early spring as a result of zooplankton's more efficient feeding on phytoplankton spring bloom (Fig. 5.6b). Future MLD seasonality will be weakened as the deep mixed layer in

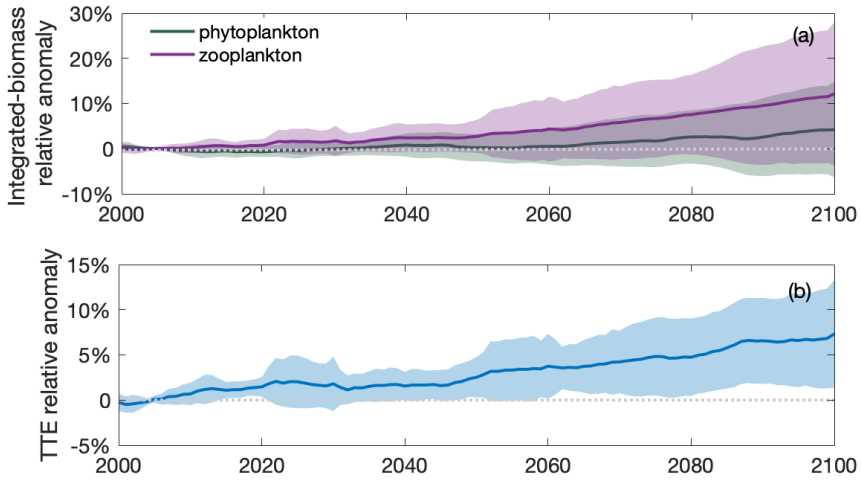

Figure 5.5: Both total phytoplankton and zooplankton biomass within the water column reveal an increasing trend towards the end of the century, with zooplankton showing a more prominent relative increase. Multi-model ensemble (MME) projections of the relative anomalies of (a) depth-integrated phytoplankton (dark green) and zooplankton (purple) biomasses; and (b) trophic transfer efficiency (blue; see Equ. 5.3) from 2000 - 2100 under the SSP5-8.5 scenario with ±1 SD (shaded), referencing the respective mean values of first decade of the 21st century (2000-2009) in the Southern Ocean. The timeseries are filtered using a 10-year moving average.

winter is shoaling more substantially compared to summer (Fig. 5.6a): the MME mean MLD shoaling of 23 m by the last decade of the 21st century relative to the first decade (Fig. 5.3) is unevenly distributed seasonally, with MLD shoaling the most in austral winter and the least in summer. The resulting improving winter growth conditions for phytoplankton cause an increase in phytoplankton biomass, that is zooplankton prey, and a subsequent zooplankton biomass increase. In addition, compared to contemporary conditions, zooplankton biomass stays relatively elevated in winter, allowing it to respond faster to the phytoplankton spring bloom. These mechanisms are in agreement with the arguments by Stock et al. to explain future trophic amplification (Stock et al., 2014a).

Despite MLD shoals to some extent also in austral summer, phytoplankton biomass in summer does not change much by the end of the century, indicating a balance between the changing ”bottom-up” and ”top-down” controls. Interestingly, the seasonality of phytoplankton will be somewhat attenuated throughout the century, which is consistent with the pattern demonstrated by the satellite products from consecutive time periods (Fig. 5.2). Apart from better growth conditions (under the assumption of a nutrient replenished upwelling system), a shoaling MLD would also increase grazing pressure for phytoplankton. This suggests an increasing importance of ”top-down” control in the Southern Ocean ecosystem under climate change.

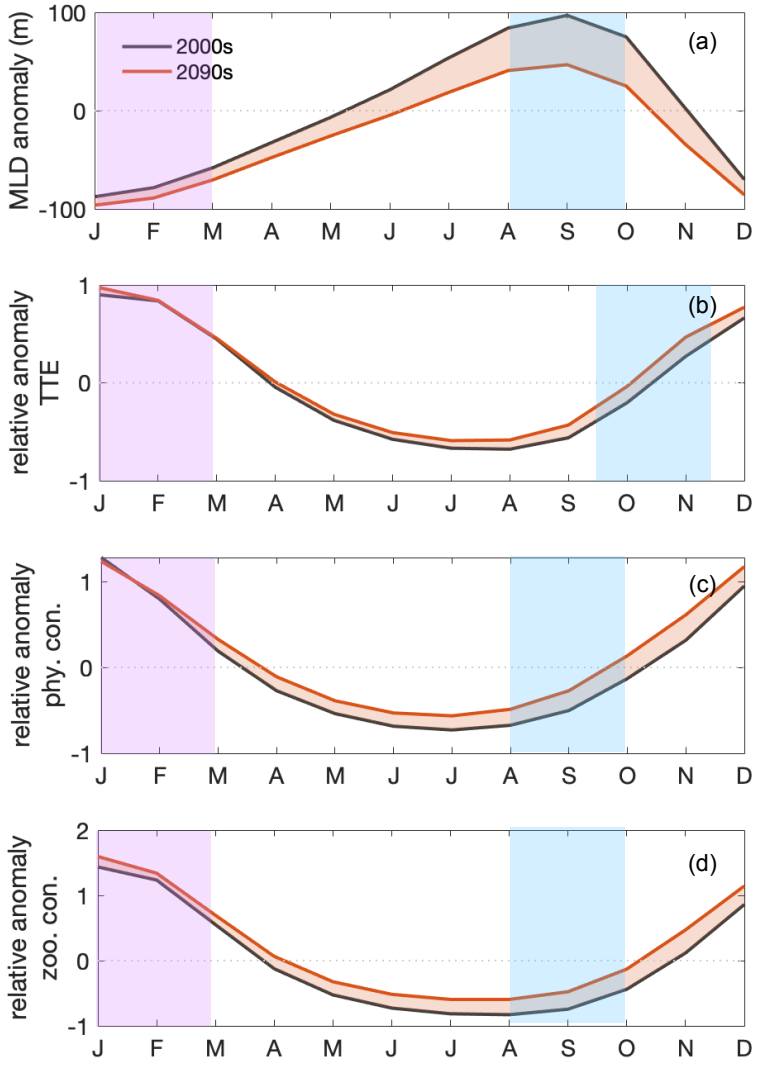

Figure 5.6: The trophic transfer efficiency increase mainly originates from late winter and early spring as a result of zooplankton's more efficient feeding on phytoplankton spring bloom (blue shading). Despite the predominant shoaling of mixed layer depth (MLD) throughout the year, in austral summer phytoplankton does not clearly change (purple shading), indicating a balance between "bottom-up" and "top-down" controls. Seasonal variations of (a) MLD anomaly; (b) trophic transfer efficiency; (c) surface phytoplankton and (d) zooplankton concentration for the first (2000-2009, black) and last decades (2090-2099, red) of the twenty-first century, relative to the annual mean of the first (2000-2009) decade. Red shaded area indicates the change.

5.4 Discussion

5.4.1 Emergent constraint on surface chlorophyll and its potential limitations

We here developed an emergent constraint on surface chlorophyll concentration based on its contemporary seasonal sensitivity to mixed layer depth, to better project its future variation under climate change. Within the Southern Ocean, opposite seasonalities of phytoplankton concentration and mixed layer depth are mainly introduced by changes in dilution and the effect of light limitation on phytoplankton growth. Both mechanisms are expected to regulate phytoplankton and its growth also on a longer timescale, assuming nutrients are in surplus in contemporary climate and shoaling mixed layers will alleviate the light limitation (Bopp et al., 2001; Doney, 2006), supporting the notion of a long-term sensitivity of phytoplankton concentration (chlorophyll) to the mixed layer depth. To reduce the uncertainty of future projections of surface chlorophyll, we use the approach of an emergent constraint, which has previously been used to constrain future projections of variables of interest (e.g., tropical marine primary productivity (Kwiatkowski et al., 2017), ocean carbon sink (Terhaar et al., 2021; Kessler and Tjiputra, 2016), ocean acidification (Terhaar et al., 2020)).

A caveat of the concept of emergent constraints is the ignorance of relevant processes in ESMs (Hall et al., 2019; Williamson et al., 2021). For instance, iron, a commonly-agreed primary limiting micro-nutrient in the Southern Ocean, is not included in all models of the MME (Table 5.1). Hamilton et al. (2020) projected a weaker iron limitation with progressing climate change, as soluble iron deposition is expected to increase due to more frequent and intense wildfires (Bowman et al., 2020), an important iron source for the Southern Ocean. The observation of widespread phytoplankton blooms downwind of the 2019 – 2020 Australian wildfires in the Southern Ocean (Tang et al., 2021) corroborates this notion. Solely considering the availability of iron, future phytoplankton will likely experience reduced growth limitation and further biomass increase relative to present conditions. Hence, we expect that future changes in iron availability will not oppose the trend of increasing surface chlorophyll concentration under climate change.

5.4.2 Constraining trophic amplification

The feature of trophic amplification with ocean warming affecting more strongly the higher trophic level than lower trophic levels has been previously found on both seasonal (Xue et al., 2022a) and longer-term climate scale (Kirby and Beaugrand, 2009; Chust et al., 2014; Stock et al., 2014a; Kwiatkowski et al., 2019; Lotze et al., 2019). Different responses of different trophic levels are projected by climate models for different regions with global warming. In the tropical regions, negative trophic amplification is projected with zooplankton biomass decreasing more than phytoplankton (Chust et al., 2014; Kwiatkowski et al., 2019). This

could be explained by increased nutrient limitation due to increasing stratification, which further leads to zooplankton starvation (Stock et al., 2014a). In temperate regions, trophic attenuation tends to be projected with phytoplankton biomass decreasing more than zooplankton biomass (Chust et al., 2014; Kwiatkowski et al., 2019). Interestingly, only polar regions reveal a signal of positive trophic amplification with a zooplankton biomass increase that is larger than the phytoplankton biomass (Chust et al., 2014; Kwiatkowski et al., 2019).

The mechanism behind the positive trophic amplification on the present-day seasonal scale could potentially be used to constrain trophic amplification under climate change. The seasonal sensitivities of the trophic transfer efficiency to the MLD could thus be used as predictors for changes under climate change. Unfortunately, future trophic transfer efficiency emergent constraints would have to be based on not only a more comprehensive observational system, in particular of zooplankton quantities such as biomass and grazing rates, but also larger and better calibrated model ensembles where zooplankton-related variables are saved as standard model output.

5.4.3 Implications for carbon export to the deeper ocean

Based on our findings of modelled future ecosystem functioning, we suggest that the projected shoaling mixed layers in the Southern Ocean with global warming may promote the export of organic material to the deep ocean. Our findings indicate that the shoaling of the mixed layer depth will lead to an overall increase in phytoplankton biomass. Along with the improved growth conditions, this would inevitably lead to enhanced primary production, which would affect the export to the deep ocean from the starting point (Henson et al., 2022). In addition to the phytoplankton biomass, we emphasize that the ratio of zooplankton to phytoplankton biomass is projected to increase in models across the Southern Ocean as a result of positive trophic amplification (Chust et al., 2014). Previous studies have highlighted the importance of zooplankton for organic carbon export due to their fast-sinking fecal pellets and vertical migration (Cavan et al., 2015, 2017). Therefore, with an increasing ratio of zooplankton to phytoplankton biomass under climate change, we expect not only higher export but also a higher export efficiency.

5.5 Conclusions

In this study, we used observable correlations between mixed layer depth (MLD) and surface chlorophyll concentration on a seasonal scale to constrain future projections of surface chlorophyll concentration under climate change in the Southern Ocean. The application of observational constraints substantially reduces the uncertainty of future chlorophyll projections from 15% to 6%. Based on the multi model mean projection under a high emission scenario that MLD will shoal 23 m throughout the 21st century, our emergent constraints

imply a 10 - 16% increase in surface chlorophyll concentration under the high emissions scenario. In addition, our confidence in the long-term effect of shoaling mixed layers on surface chlorophyll substantially increases with the emergence of constraints on projections. While our results increase our confidence that chlorophyll will increase, they also suggest that the most extreme projected chlorophyll decrease is less likely than previously thought.

We further extended our findings of a future increase in surface chlorophyll to a possible implication for ecosystem functioning. Despite the shoaling of the mixed layer, the phytoplankton biomass within the water column is projected to rise in the Southern Ocean. Overall zooplankton biomass is increasing more significantly (12%) than phytoplankton (4%), indicating trophic amplification under climate change, consistent with previous findings for high-latitude oceans (Chust et al., 2014; Stock et al., 2014a; Kwiatkowski et al., 2019). We suggest that trophic amplification in the Southern Ocean under climate change is due to enhanced trophic transfer efficiency (TTE), as a result of improved grazing conditions (higher prey density) for zooplankton. This mechanism matches what has been found in present-day conditions for productive systems on a seasonal scale (Xue et al., 2022a). We note that TTE increases most prominently in the late winter and early spring. We suggest that this is because zooplankton will sustain a relatively higher biomass in winter in the future, allowing it to react faster and more efficiently to the spring bloom.

Our findings highlight the need to understand the underlying mechanisms of "bottom-up" and, particularly "top-down" processes, which have long been understudied. "Top-down" control is typically used as a closure term in biogeochemical models and is relevant to lower trophic level ecosystem functioning. To improve our understanding will necessitate significant efforts in terms of both observations and model simulations. We expect the importance of "top-down" control in the Southern Ocean will continue to grow until the end of the 21st century. The growing importance of "top-down" control may only change once the system reaches the point of nutrient limitation (Lewandowska et al., 2014). Overall, our findings suggest a key role for mixed layer depth in simulating trophodynamic processes.

Chapter 6

Conclusion and Outlook

6.1 Conclusion

In this thesis, we used model simulations to identify the critical role of mixed layer depth for the marine ecosystem in the contemporary climate (chapters 2 & 3), determining that the fish biomass fluctuation is not driven by food consumption (chapter 4), and using the findings from the contemporary climate to better constrain and understand ecosystem simulations under climate change (chapter 5). The four chapters address the fourfold aims of this thesis, respectively, outlined in the introduction section:

(1) The driving mechanisms of phytoplankton seasonality
In chapter 2, we used a regional physical-biogeochemical model (CROCO-BioEBUS) to reproduce the "seasonal paradox" with an opposite seasonality between surface chlorophyll and upwelling intensity in the Humboldt upwelling system. In our simulation, the seasonal cycle of surface chlorophyll concentration is mostly driven by MLD-related processes, notably dilution and light-limitation. We also find that upwelling-related processes such as temperature limitation and phytoplankton advective loss provide secondary contributions. Moreover, phytoplankton seasonality propagates up the food chain and influences the trophodynamics and ecosystem functioning (e.g., export efficiency). Despite the considerable effect of upwelling, our research shows that phytoplankton seasonality in the Humboldt system is still driven by mixed layer dynamics. This demonstrates that in a productive ecosystem the mixed layer depth is the driving mechanism of phytoplankton seasonality.

(2) How does the phytoplankton seasonality transfer up to the zooplankton?
In chapter 3, we employed the same model setup as in chapter 2 to further investigate seasonal trophic amplification induced by mixed layer dynamics in the Humboldt and other productive systems with high chlorophyll concentrations. The mixed layer depth alters the vertical distribution of phytoplankton and, therefore, the zooplankton-phytoplankton en-

counters, with fewer encounters in a deeper mixed layer where phytoplankton are diluted. Additionally, we find the same mechanism applies to other ocean biomes with high chlorophyll concentrations, such as coastal and high latitude oceans. The food chain efficiency exhibits opposite seasonal trends to that of the mixed layer depth, with trophic transfer from phytoplankton to zooplankton being less efficient in the deep mixed layer and vice versa. This result indicates that the mixed layer depth alters the trophic transfer from phytoplankton to zooplankton via the dilution effect and plays a crucial role in the ecosystem functioning in the Humboldt and other productive systems.

(3) How do changes in the planktonic community affect higher trophic levels?

In chapter 4, we used a one-way coupled physical-biogeochemical-fish model (CROCO-BioEBUS-OSMOSE) to explore the link between the planktonic community and higher trophic levels in the Humboldt system. However, the simulated fish biomass forced by the plankton food displays much weaker interannual variation compared to the strong fluctuations in observation, especially the regime-shift following the El Niño event. Worth noticing, two other biological parameters appear to have a stronger influence on the fish than the plankton food. This implies that other biological processes may be more important to fish biomass variation. Therefore, plankton food does not affect the interannual fluctuation of higher trophic levels significantly in this model.

(4) Use current climate to understand and constrain ecosystem simulations under climate change

In chapter 5, we applied results from chapter 2 regarding the impact of MLD on phytoplankton in current climate along with the observed correlations to constrain simulations of a multi-model ensemble towards the Southern Ocean ecosystem under climate change. Observations of correlations between MLD and surface chlorophyll on a seasonal scale were applied to constrain the future projection of surface chlorophyll concentration under climate change using a newly developed approach known as emergent constraints. There is a significant reduction in the uncertainty of future chlorophyll projections (from 15% to 6%) due to the observational constraints. Considering MLD will shoal 23 m over the 21$^{\text{st}}$st century, this implies a 10-16% increase in the concentration of surface chlorophyll under high emission scenarios.

We then used findings from chapter 3 regarding the impact of MLD on trophic transfer in productive ecosystems under the current climate to better understand the potential changes in the Southern Ocean ecosystem due to global warming. It is noteworthy that zooplankton biomass exhibits a greater increase (12%) than phytoplankton biomass (4%) over the 21$^{\text{st}}$st century, which implies trophic amplification. This could be explained by the same mechanism we found under contemporary seasonality, as the shoaling mixed layer

boosts trophic transfer efficiency by increasing zooplankton prey density. Given the improving growth conditions and increasing grazing pressure on phytoplankton due to the shoaling mixed layer, "top-down" control will continue to be more critical in the Southern Ocean until the end of the 21stst century. This study uses findings from contemporary seasonality to better understand and constrain ecosystem projections towards climate change in a productive ecosystem.

Taken as a whole, this thesis emphasizes the critical role of mixed layer depth in productive marine ecosystems, thereby its potential to improve ecosystem simulations under climate change. The findings contribute in several ways to our understanding of the conceptual mechanisms underlying "bottom-up" and "top-down" processes in the current climate and provide a basis for better understanding and projection towards productive ecosystems under climate change.

6.2 Outlook

This thesis links together the broad and complex physical-biological interactions on different timescales. Gaps and future perspectives emerging from this thesis need to be taken into consideration, notably:

Monitoring and Modelling: While ocean ecosystem monitoring and modelling abilities have been significantly improved over the past decades, there is considerable room for further improvement. For example, gaps remain in the observation and simulation of zooplankton. As a foundation for learning about trophodynamics and constraining model simulations, a comprehensive systematic zooplankton observational system should be established. For instance, as an important part of the plankton community, observations of microzooplankton are surprisingly lacking. Continued efforts are needed to make observations more accessible and easier to implement in the model. One example is that observations of plankton are commonly measured with abundance, whereas models only take biomass. Moreover, current biogeochemical models, especially with global coverage and with respect to zooplankton simulations, tend to be poorly calibrated, partly due to a lack of observations and have a simplified depiction of food web mechanisms. This makes it difficult to enhance our understanding of the processes and their relevance, posing a large obstacle for future ecosystem projections.

Marine Phenological Responses: Complementary to our first-step attempt in chapter 5, more comprehensive studies to resolve the plankton phenological responses (e.g., bloom timing) under climate change are needed since they have the potential to lead to trophic level decoupling. According to previous research (Burrows et al., 2011), phenological changes may occur more quickly in marine ecosystems than in terrestrial ones. Ocean

warming has induced an earlier spring and thus earlier plankton seasonal cycles (Edwards and Richardson, 2004). However, plankton consumers (e.g., fish) may not adjust their phenology following plankton, which may result in mismatches with prey and further affect the fisheries (Asch, 2015). Therefore, we recommend more comprehensive studies of marine phenological responses to climate change and their mechanistic drivers to be followed to advance our understanding towards the potential changes and adjust the relevant fishing tactics.

Foreseeable Tipping Point: Despite this thesis exclusively discusses productive ecosystems, given the continuous shoaling mixed layer under climate change, there might come a time when the current "productive ecosystem" will transform into a "nutrient-limited ecosystem". Previous research has found that an ecosystem's response to climate change is dependent on nutrient regimes (like shown in Fig. 1.3; Doney, 2006; Lewandowska et al., 2014). In a "productive ecosystem", warming is generally associated with a release of "bottom-up" control along with increased "top-down" regulation of phytoplankton biomass as a result of the shoaling mixed layer (chapter 5). However, once the tipping point has passed, the ecosystem structure may shift dramatically and respond completely differently to climate change. Under these conditions for a "nutrient-limited ecosystem", warming generally means enhanced "bottom-up" regulation of phytoplankton biomass, which has been already observed in oligotrophic regions by Behrenfeld et al. (2006) and Polovina et al. (2008). Phytoplankton growth and size structure are to a large degree controlled from the "bottom-up" through nutrient inputs (Edwards et al., 2012), and these factors have concomitant influences on zooplankton (Stibor et al., 2004). Future work will hopefully enable us to evaluate governance regimes and predict the upcoming tipping point and potential consequences in advance.

A. Supporting Information for 'Mixed layer depth dominates over upwelling in regulating the seasonality of ecosystem functioning in the Peruvian Upwelling System'

A.1 Methods

A.1.1 Two-way nesting approach

Figure A.1 visualises the coarser-resolution parent domain and nested finer-resolution child domain that contains the focus region. The variables in section A.2 are shown for the child domain.

A.1.2 Adjustment of biogeochemical model parameters

The parameter setting is the same as in José et al. (2017), with only a few biological parameters adjusted to make the ecology (phyto- and zooplankton biomasses, productivity) better fit observational data. The changed parameters along with value ranges from literature are listed in Table A.1 and will be further explained below.

Here, we assign a higher mortality rate for large phytoplankton to simulate the potential impact of virus infection during bloom conditions (Suttle, 2005). Simulated phytoplankton biomass and its seasonality has been calibrated and evaluated against chlorophyll concentration data from MODIS monthly climatology data (https://oceancolor.gsfc.nasa.gov/). Nitrate has been evaluated based on World Ocean Atlas (WOA; Garcia et al., 2019) and cruise data (M92 and M93; Thomsen et al., 2016) while simulated MLD has been validated against the ARGO mixed layer database (http://mixedlayer.ucsd.edu/; Holte et al., 2017).

Table A.1: Adjusted biological parameters and range of published parameter values

Parameters	Symbols	Units	Value	Range
Max growth rate of P_L	a_{P_L}	d^{-1}	0.6	0.6[a]-3.0[b]
Mortality rate of P_L	μ_{P_L}	d^{-1}	0.15	0.027[c]-0.2[d]
Preference of Z_S for P_S	$e_{Z_S P_S}$	-	0.65	see references[e]
Preference of Z_S for P_L	$e_{Z_S P_L}$	-	0.35	see references[e]
Preference of Z_L for P_S	$e_{Z_L P_S}$	-	0.1	see references[f,g]
Preference of Z_L for P_L	$e_{Z_L P_L}$	-	0.4	see references[f,g]
Preference of Z_L for Z_S	$e_{Z_L Z_S}$	-	0.5	see references[f,g]
Excretion rate of Z_S	γ_{Z_S}	d^{-1}	0.1	0.03[h]-0.1[i]
Excretion rate of Z_L	γ_{Z_L}	d^{-1}	0.1	0.05[h]-0.1[i]
Mortality rate of Z_L	μ_{Z_L}	$mmol\, N\, m^{-3}\, d^{-1}$	0.135	0.05[a]-0.25[j]

The values for diet preferences were picked based on a combination of calibrating the model against observations of plankton biomasses and observed qualitative diet preferences in the references.

[a] Gutknecht et al. (2013)
[b] Andersen et al. (1987)
[c] Koné et al. (2005)
[d] Taylor et al. (1991)
[e] Bohata (2016)
[f] Kleppel (1993)
[g] Schukat et al. (2014)
[h] Aumont et al. (2015)
[i] Fennel et al. (2006)
[j] Lima and Doney (2004)

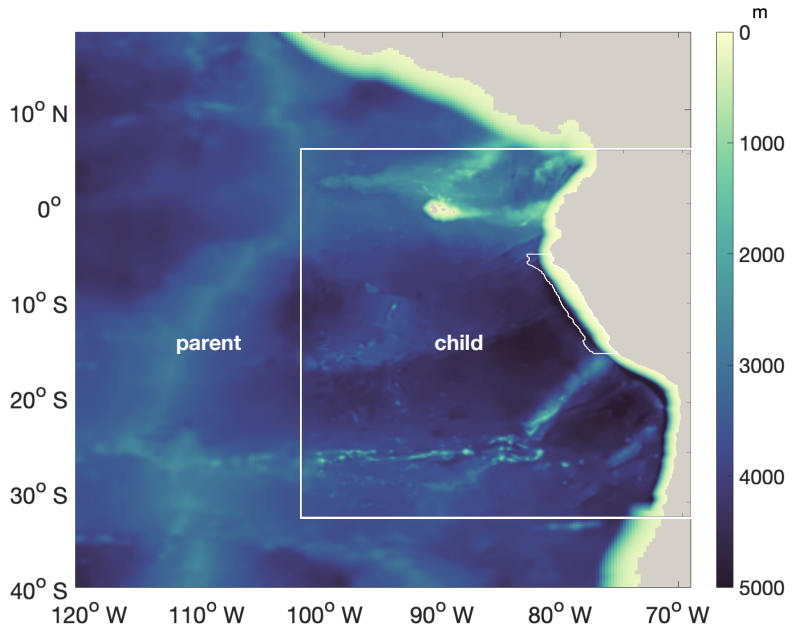

Figure A.1: Bathymetry of the "parent" (1/4° resolution) and "child" (1/12° resolution) domains. White lines near the coast highlight the focus region.

A.2 Model evaluation

A.2.1 Surface chlorophyll concentration

The large-scale spatial pattern of annual average surface chlorophyll of the monthly climatology of MODIS data and CROCO-BioEBUS are similar (Fig. A.3), with higher chlorophyll concentrations in coastal regions and lower concentrations offshore (note that chlorophyll is shown in log-scale). The satellite data features a higher cross-shore chlorophyll concentration gradient compared to the model simulation. The model's overestimation of the low offshore chlorophyll and hence weaker cross-shore gradient potentially is due to the lack of iron limitation in the model. Apart from that, the model is also not able to correctly capture the alongshore pattern (Fig. A.3), i.e. it misses two observed high surface chlorophyll concentration patches between 8°S to 10°S and 12°S to 14°S (Bruland et al., 2005). Within a 200 km band near the coast, both satellite data and the model simulation show a similar seasonality with maximum chlorophyll concentrations exceeding 4 mg /m^3 from March to April and minimum concentrations around 2 mg /m^3 in August. In general, simulated surface chlorophyll concentrations agree reasonably well with satellite data.

A.2.2 Surface nitrate concentration

The simulated surface nitrate distribution shows the same seasonality as observations from the World Ocean Atlas (WOA; Garcia et al., 2019) (Fig. A.4). The simulated surface nitrate

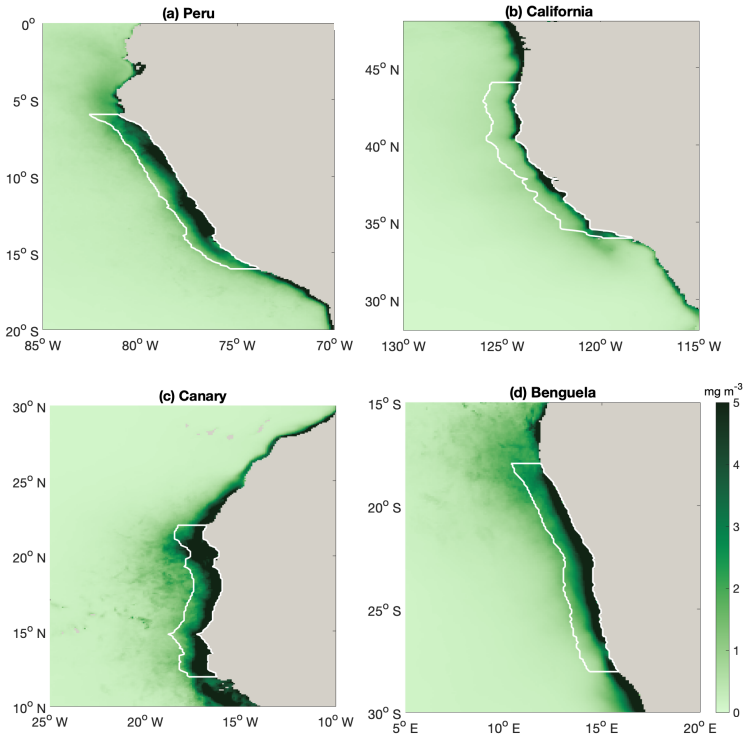

Figure A.2: Map of annual mean surface chlorophyll ($mg\,chl\,m^{-3}$) with white lines highlight the regions that we average over in our analyses in Fig.2.2. Coastal EBUS regions picking here are the same as Chavez and Messié (2009)

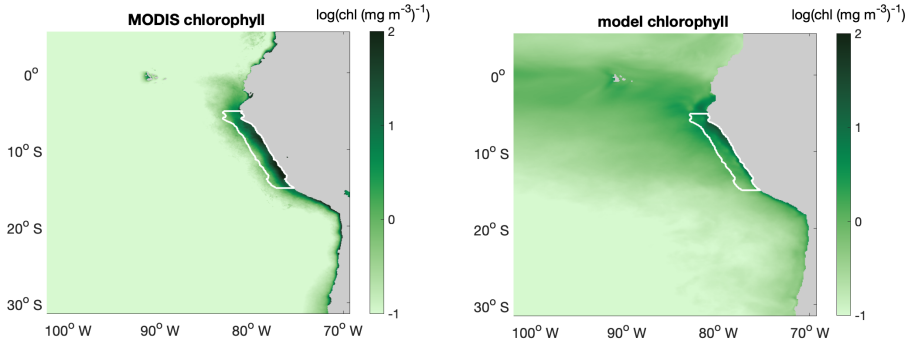

Figure A.3: Annual mean surface chlorophyll concentration (in $log(chl\,(mg\,m^{-3})^{-1})$) distribution of (a) MODIS and (b) CROCO-BioEBUS. White lines highlight the focus region.

concentration in the coastal region is biased high compared to the WOA data. This may be partly due to the WOA data failing to capture high-nitrate concentrations due to coastal upwelling. This notion is supported by nitrate concentration data from two cruises (M92 and M93; Thomsen et al., 2016) in austral summer that show nitrate concentrations in the coastal region are high compared to the model data.

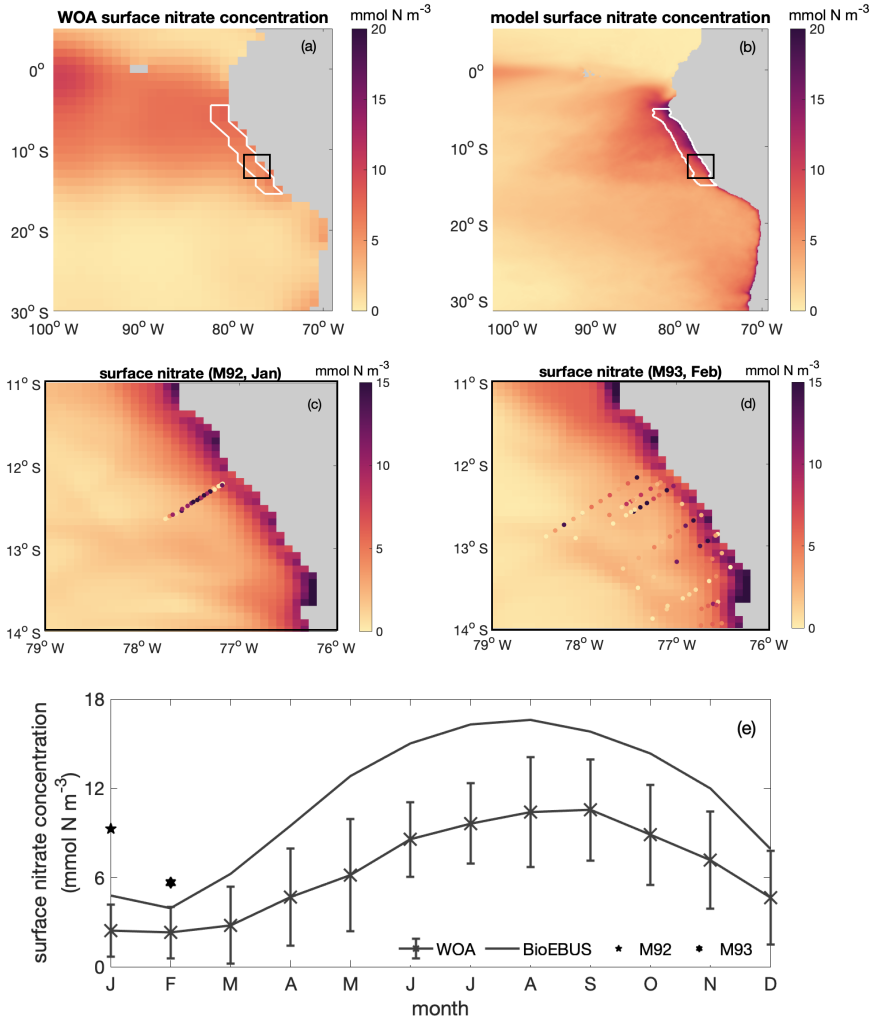

Figure A.4: Spatial distribution of surface nitrate concentration based on (a) WOA and (b) CROCO-BioEBUS; (c) January and (d) February as simulated by CROCO-BioEBUS. Dots indicate measurements from the cruises M92 (January) and M93 (February); (e) Seasonal cycle of surface nitrate concentration from WOA (cross), CROCO-BioEBUS (line) and cruises (pentagram, hexagram) within the focus region. White lines highlight the focus region. The black box indicates the maps of panel c-d.

A.2.3 Mixed layer depth

We validate the simulated MLD against both the gridded ARGO mixed layer dataset (http://mixedlayer.ucsd.edu/; Holte et al., 2017), and the de Boyer Montégut climatology mixed layer data available from the IFREMER/LOS Mixed Layer Depth Climatology website (www.ifremer.fr/cerweb/deboyer/mld) within the research area (Fig. A.5). All observational data and simulated MLD are calculated as the depth where a 0.2^oC difference to the surface temperature is reached. The annually averaged spatial distribution of MLD within the research area presents the same features as ARGO: shallower MLD in the coastal region (around 20 m) and deeper MLD in the offshore region (around 80 m). The simulated seasonal variability of MLD within the research region generally follows the seasonal trend of the ARGO and the Boyer Montégut climatology data. The water column within the research region is most stratified in February to March and most deeply mixed in August. Although simulated MLD in austral winter is somewhat deeper than Argo and the de Boyer Montégut climatology data, the simulated MLD and the de Boyer Montégut climatology data are largely within the range of the ARGO data. Deeper simulated MLD compare to observation could partially come from not including chlorophyll shading effect on water cooling (Echevin et al., 2021).

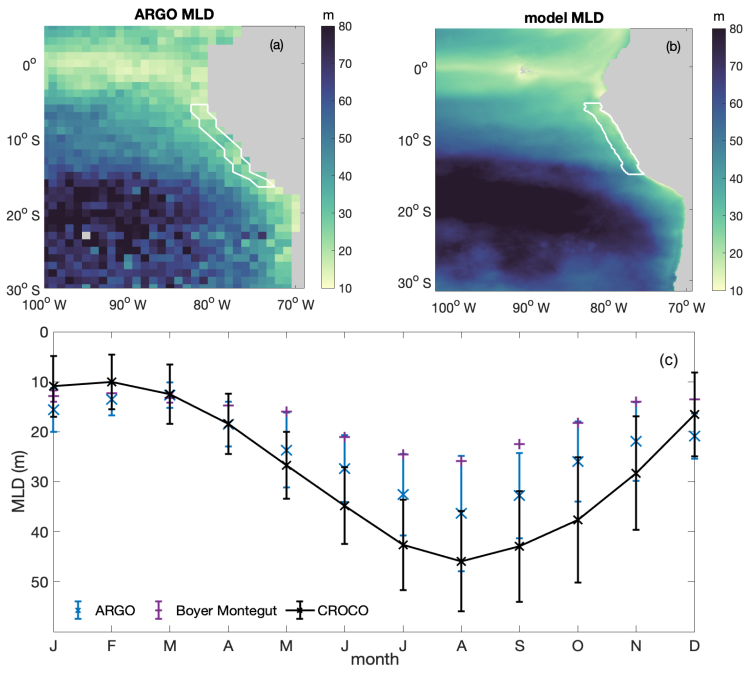

Figure A.5: Annual average spatial distribution of mixed layer depth (MLD) from (a) ARGO and (b) CROCO-BioEBUS; (c) Seasonal variation of average mixed layer depth from ARGO (blue), the de Boyer Montégut climatology (purple) and model simulation (black) with error bar indicating the standard deviation within focus region. White lines highlight the focus region.

A.2.4 Sea surface temperature

The simulated SST has been validated against monthly climatological MODIS data in terms of both spatial pattern and seasonal variability within the research area (Fig. A.6). The annually averaged spatial distribution of SST is well simulated by the model. The model successfully captures the cold coastal upwelled water as well as slightly warmer water masses further offshore. The simulated SST seasonality within the research region generally follows the seasonal trend of the observations, with a cool bias of less than 1^oC. The surface waters within the research region are warmest in February to March matching the modelled/observed shallowest mixed layers and coldest from August to October. In general, the simulated SST matches the observations well both in terms of spatial pattern and seasonal variation.

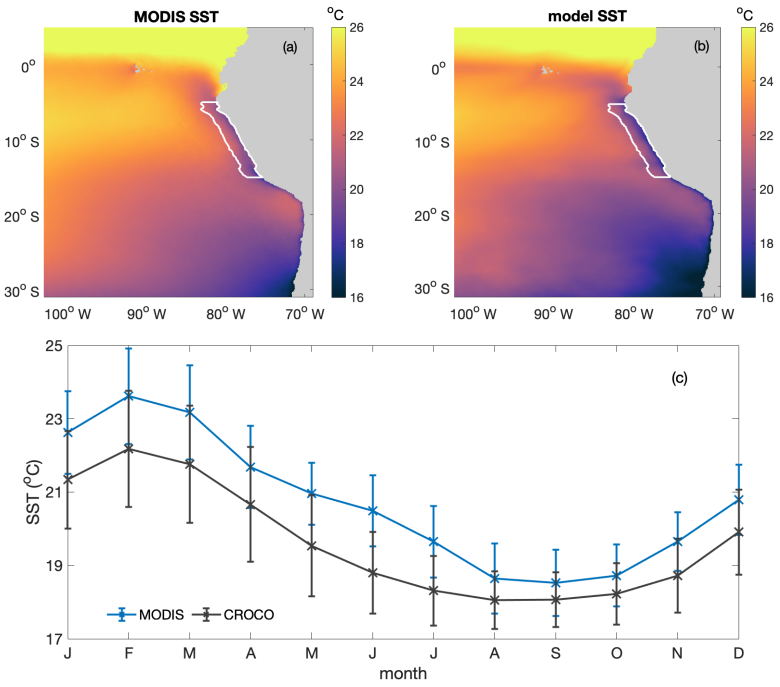

Figure A.6: Annual average spatial distribution of sea surface temperature (SST, in ^oC) from (a) MODIS and (b) CROCO-BioEBUS; (c) Seasonal variation of average sea surface temperature (SST) from MODIS (cross) and model simulation (line) within focus region. White lines highlight the focus region.

A.2.5 Mesozooplankton distribution

In addition, we calibrated zooplankton in the BioEBUS model against observational estimates (Fig. A.7). Calibration and assessment of simulated zooplankton is often omitted, despite the central role of zooplankton parameterisations on plankton dynamics (Anderson et al., 2010; Prowe et al., 2012). While the observations show a large spread, the simulated large-scale spatial distribution of mesozooplankton generally follows the observed pattern,

with high mesozooplankton biomass in the upwelling region and low biomass further offshore. The overestimated simulated zooplankton biomass compared to the observational data in the offshore region is likely partially related to the overestimated offshore phytoplankton biomass, which in turn presumably results from the lack of iron limitation in the model. As shown in Fig. A.7c, most data points fall close to the 1:1 line. However, the model is not able to capture the few data points with very high zooplankton biomass. The model simulates a stripe of low zooplankton biomass concentrations in the focus region near the coast (due to offshore advection combined with slow mesozooplankton growth) that is difficult to assess, as observations near the coast are sparse. This feature may be apparent to some extent in the observations in the southern focus region. Note that observational zooplankton biomass estimates are based on a wide range of methods and accordingly have a large uncertainty that is difficult to quantify (O'Brien, 2007). An agreement of model and observations in magnitude and large scale pattern is therefore a meaningful result.

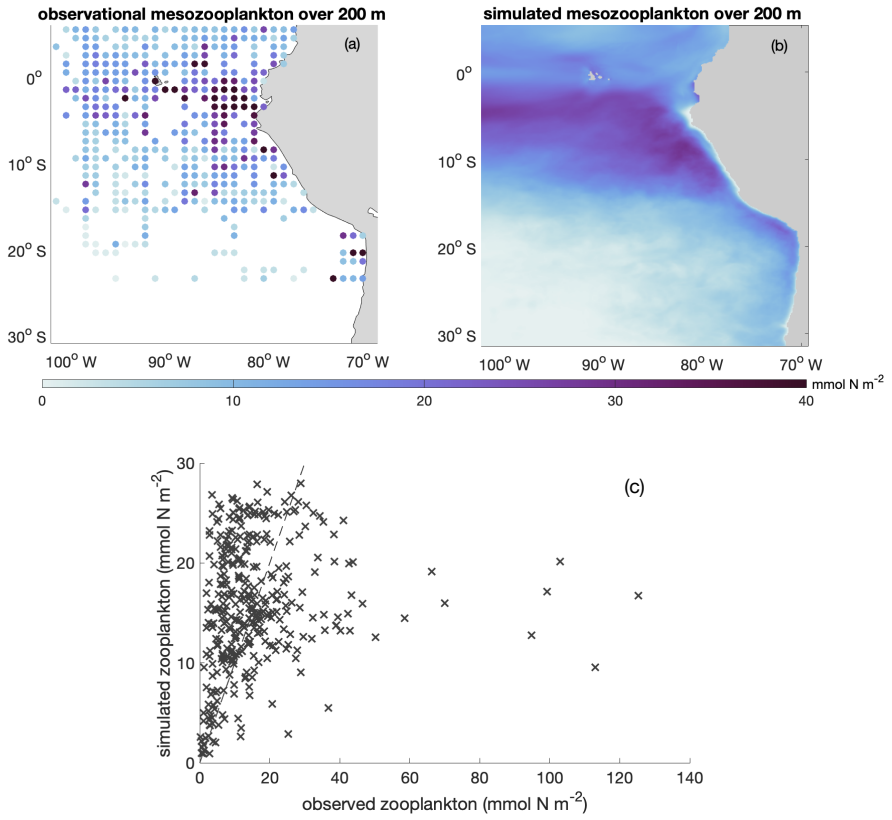

Figure A.7: Annual average spatial distribution of integrated mesozooplankton biomass over upper 200 m based on (a) observational data (Moriarty and O'Brien, 2013, https://doi.org/10.5194/essd-5-45-2013) and (b) model simulation. (c) Scatter plot of observed and simulated integrated mesozooplankton biomass over upper 200 m (in $mmol\ N\ m^{-2}$). The dashed line indicates the 1:1 line.

A.3 Additional Figures

The whole time series of temperature and nitrate concentration at 10 m and 100 m are shown in Fig. A.8a-b. Surface fields are spun up after one year while water at 100 m takes 3-10 years longer to reach a steady state. In the meanwhile, mixed layer and surface layer chlorophyll are also spun up after one year (Fig. A.8c-d).

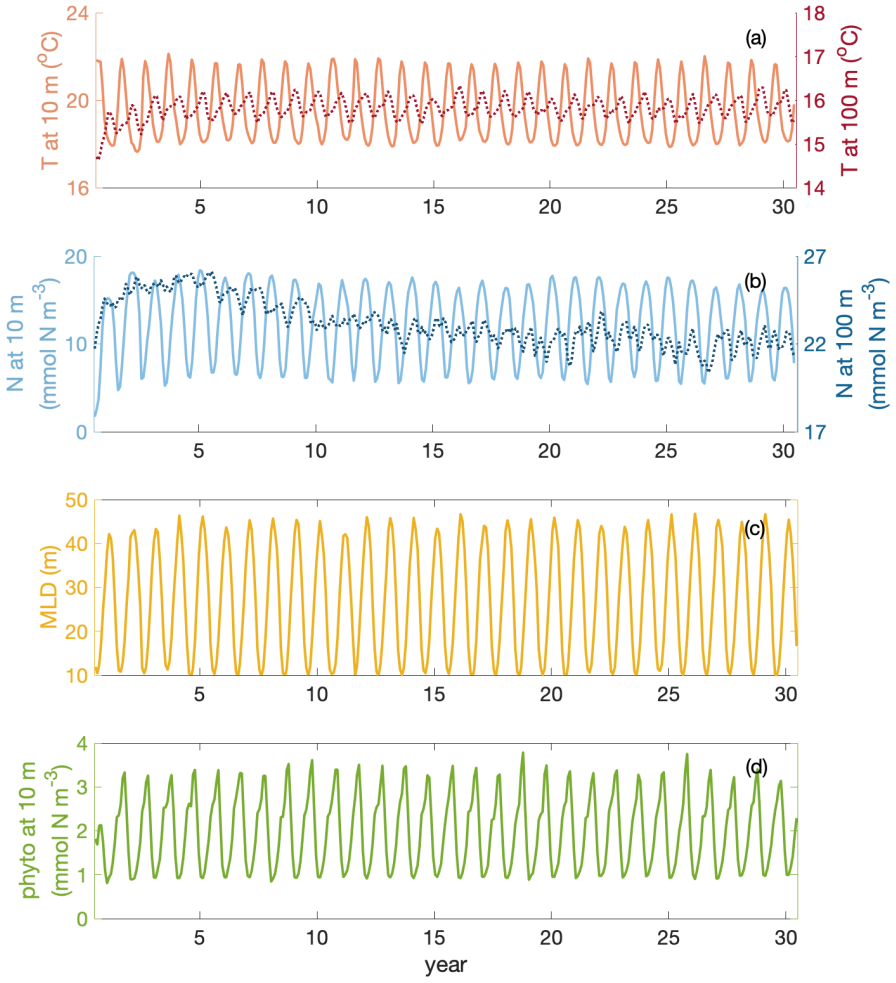

Figure A.8: Time series of temperature T (at 10 m & 100 m depth), nitrate N (at 10 m & 100 m depth), mixed layer depth MLD and phytoplankton phyto (at 10 m) over 30 years of simulation in the focus region.

Apart from above mentioned mixed layer depth and upwelling intensity, short-wave surface radiation and surface net heat flux are of second-order importance to light- and temperature-related variance during the decline phase respectively (Fig.A.9).

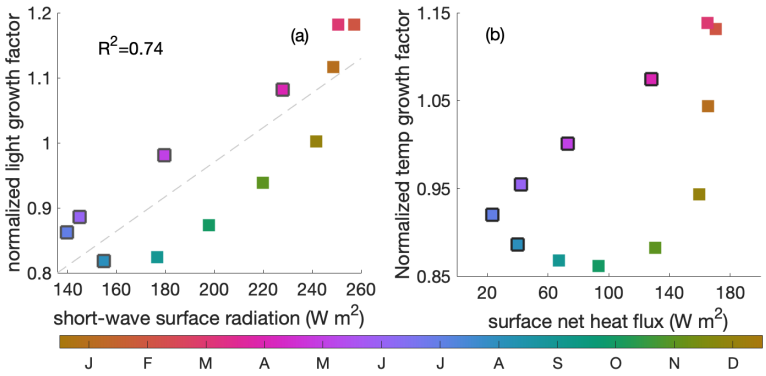

Figure A.9: (a) Correlation between surface short-wave radiation (Wm^{-2}) and the averaged light-related growth factor within mixed layer; (b) Correlation between the surface heat forcing (in $^oCd^{-1}$) and averaged temperature-related growth factor within mixed layer. Colour indicates the time of the year and black edges the decline phase.

Phytoplankton net advection flux over the mixed layer closely follows the upwelling intensity during the decline phase (Fig.A.10, $R^2 = 0.81$). When the mixed layer depth is relatively shallow, the correlation between upwelling intensity and phytoplankton convergence of advection over the mixed layer is insignificant.

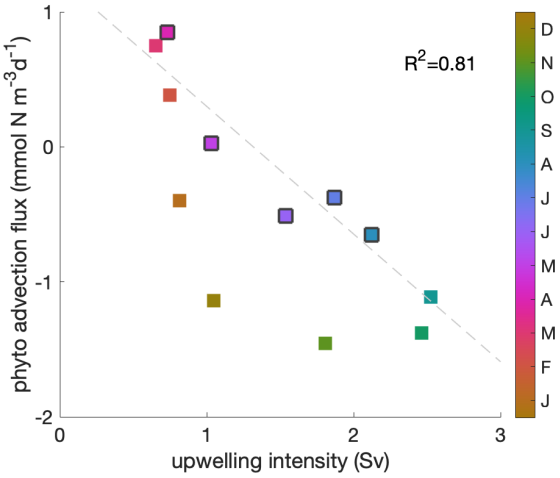

Figure A.10: Correlation between upwelling intensity and phytoplankton convergence of advection over the mixed layer. A negative convergence equals a divergence of phytoplankton biomass due to the combined effect of upwelling and lateral transports. Color indicates the time of the year and black edges the decline phase. The correlation coefficient (R^2=0.81) is shown for the decline phase.

B. Supporting Information for 'Mixed layer depth promotes trophic amplification on a seasonal scale'

B.1 Sensitivity studies

To assess how food chain length affects trophic amplification, we purposely modify the predator diet and thus food chain length in sensitivity runs with model CROCO-BioEBUS. We perform simulations LZOO and SZOO in which we remove the linkage between small phytoplankton and mesozooplankton or the linkage between large phytoplankton and microzooplankton, respectively. Both LZOO and SZOO simulations have the same set-up as the reference simulation except for altered zooplankton diet preferences through parameter settings (Table. B.1).

A comparison with the reference study (Fig. B.3a), of the run where we remove the linkage between small phytoplankton and mesozooplankton (Fig. B.3b) or the linkage between large phytoplankton and microzooplankton (Fig. B.3c), shows that the food chain length, FCL, lengthens or shortens, respectively. The dominant role of predator-prey encounter efficiency due to mixed layer dilution is not affected by such a deliberate change in the food chain length (Fig. B.4), which agrees with what was previously found by D'Alelio et al. (2016).

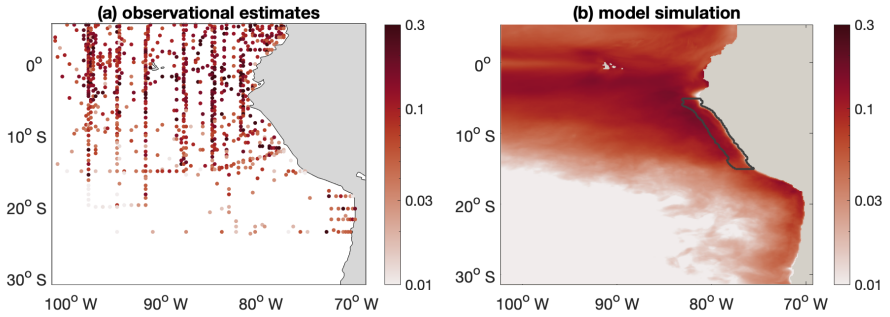

Figure B.1: Annual average spatial distribution of the food chain efficiency based on (a) observational estimates (derived from COPEPOD and MODIS temperature and productivity data (calculated the same way as in Stock and Dunne (2010)) and (b) model simulation. The black lines highlight the focus region)

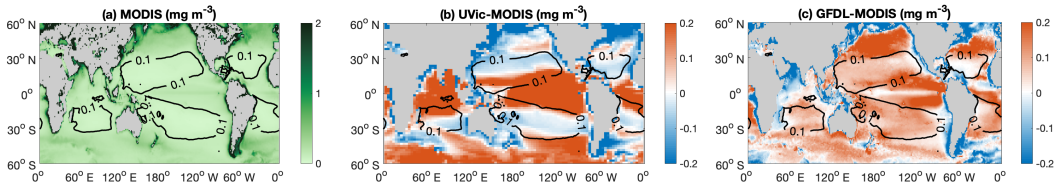

Figure B.2: Maps of (a) annual-mean surface chlorophyll concentration from MODIS; and simulated bias of the (b) UVic-model and (c) GFDL-model. Black contour lines in the three panels indicate the observational biome threshold (MODIS surface chlorophyll concentration equaling 0.1 $mg\ m^{-3}$).

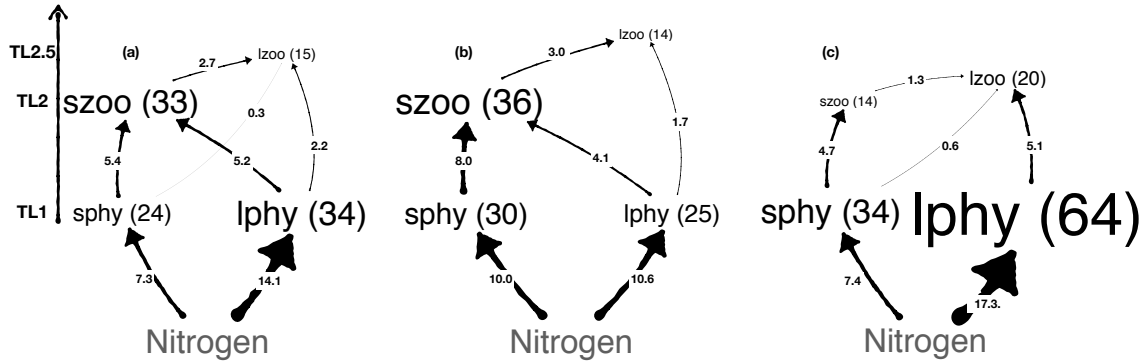

Figure B.3: Food web structure of (a) reference simulation (b) LZOO simulation (removal of small phytoplankton - mesozooplankton link) and (c) SZOO simulation (removal of large phytoplankton - microzooplankton link). All variables shown are integrated over the water column. The plankton groups are shown in the unit of mmol N m^{-2}. The fluxes are shown in the unit of mmol N m^{-2} d^{-1}

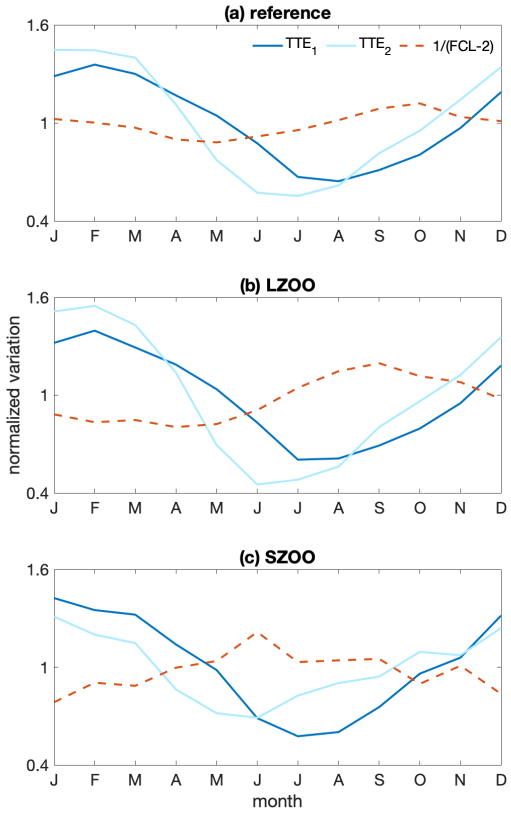

Figure B.4: Normalized seasonal variation of trophic transfer efficiency (TTE) between trophic level 1 and 2 (TTE_1, light blue) and trophic level 2 and 3 (TTE_2, dark blue) along with the reciprocal of the food chain length ($1/(FCL-2)$, red) over the water column within the focus region based on (a) reference simulation (b) LZOO simulation (removal of small phytoplankton-mesozooplankton link) and (c) SZOO simulation (removal of large phytoplankton-microzooplankton link).

Table B.1: Adjusted diet preferences in sensitivity runs

Sensitivity studies	reference	LZOO	SZOO
Preference of Z_S for P_S	0.65	0.65	1
Preference of Z_S for P_L	0.35	0.35	0
Preference of Z_L for P_S	0.1	0	0.1
Preference of Z_L for P_L	0.4	0.5	0.4
Preference of Z_L for Z_S	0.5	0.5	0.5

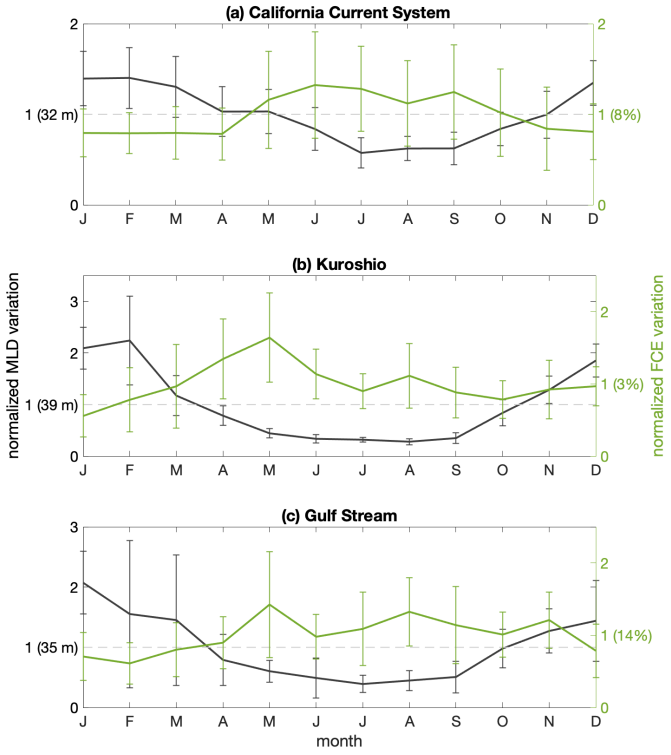

Figure B.5: Average observational estimates of seasonal cycles of normalized MLD (black) and food chain efficiency(FCE, the ratio of net mesozooplankton production to primary production; green) for (a) California Current System; (b) Kuroshio and (c) Gulf Stream. Values in brackets indicate the absolute values of annual means. Error bars indicates the standard deviation.

C. Supporting Information for 'Understanding the drivers of fish variability in an end-to-end model of the Northern Humboldt Current System'

C.1 Higher trophic levels model parameters

Tab. C.1 provides the parameters used to run OSMOSE. The original name of each parameter as it is read by the model is provided. Fig. C.1 provides the seasonality of the anchovy landings. Additional parameters and the distribution maps are provided in the Supplement.

Table C.1: Parameters. Species and groups are: a for anchovy, h for hake, s for sardine, jm for jack mackerel, chm for chub mackerel, m for mesopelagics, sl for squat lobster, hs for Humboldt squid, e for euphausiids. For a detailed explanation on each parameter please refer to Shin and Cury (2004), as well as the official OSMOSE documentation: `http://documentation.osmose-model.org/index.html`. Source: Oliveros-Ramos and Lujan-Paredes, personal communication, based on the configuration by Oliveros-Ramos et al. (2017). *Marzloff et al. (2009) **Tam et al. (2008) ***Adjusted ****Calibrated.

Parameter	Unit	a	h	s	jm	chm	m	sl	hs	e
simulation.ncschool	n	24	12	12	24	12	148	4	48	148
species.lInf	cm	19.5	68	38.71	81.6	40.6	8	4.2	95	2.6
species.K	1/yr	0.76	0.,025	0.22	0.,167	0.41	1.15	0.,375	1.1	1.8
species.t0	years	- 0.14	- 0.,269	- 1.34	- 0.28	- 0.05	- 0.06	- 328	- 0.09	- 198
species.vonbertalanffy.threshold.age	years	0.35	0.5	0.5	0.5	0.5	0.35	0.5	1	0.1
species.length2weight.condition.factor	g/cm	0.0065	0.,007	0.0089	0.0135	0.0086	0.00832	0.,174	0.,005	0.00925
species.length2weight.allometric.power	—	3	3.05	2.99	2.9248	3.26	3.15	3.03	3.4	3
species.relativefecundity	—					1				
species.egg.size	cm					0.1				
species.egg.weight	g					0.0005386				
species.sexratio	—	0.5	0.5	0.5	0.5	0.5	0.5	0.5	0.5	0.5
species.maturity.size	cm	12	35	21	29	29	2.5	1.9	66	0.8
species.lifespan	years	3	12	8	8	10	2	4	1.5	1
mortality.starvation.rate.max	1/ts	1	0.05	0.1	0.15	0.05	0.5	0.1	0.1	0.5
predation.efficiency.critical	—	0.57	0.57	0.57	0.57	0.57	0.57	0.57	0.57	0.57
predation.ingestion.rate.max	g food/g fish/year	3.5	3.5	3.5	3.5	3.5	3.5	3.5	3.5	3.5
predation.predPrey.sizeRation.max	—	8,6	3, 2.5	25, 150	20, 15	20, 15	3.5	2	2.5, 2, 1	15, 10
predation.predPrey.sizeRation.min	—	800, 200	50, 50	1000, 10000	300, 200	300, 200	100	150	35, 55, 70	3000, 2000
predation.predPrey.stage.threshold	cm	10	18	13	20	20	—	—	30, 60	0.6
movement.distribution.method	—					maps				
movement.randomwalk.range	cells/ts					1				
mortality.algorithm	—					stochastic				
mortality.fishing.recruitment.size	cm	12	35	21	26	26	2.5	1.9	30	0.8
mortality.natural.rate*	1/yr	0.34	0.3	0.3***	0.24	0.25	1.19	0.3	6.27	0.954**
mortality.fishing.rate*	1/yr	1.1	0.3	0.4	0.3	0.5	0	0	0.11***	0
mortality.natural.larva.rate****	1/ts	8.83	9.63	11.6***	9.7	9.16	4.63	0.61	4.47	2.6
q-factor (see main text)	—	0.87	0.41	0.74	0.54	0.76	0.16	0.88	0.31	0.5
population.seeding.biomass	(tons)	$8x10^6$	$2.1x10^5$	$1x10^{4}$***	$4.36x10^6$	$9x10^5$	$1.5x10^7$	$1x10^7$	$3x10^6$	$4x10^7$

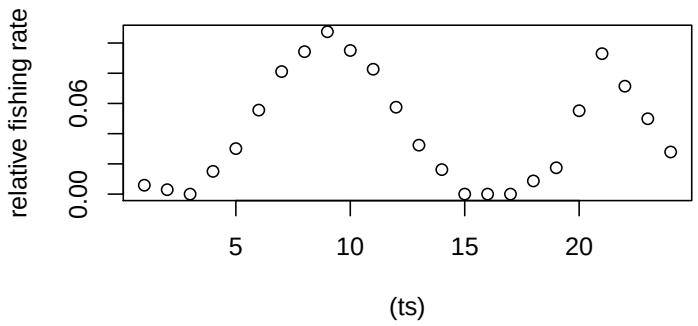

Figure C.1: Seasonal variability in the fishing rate. The sum of all points for 24 time-steps in one year is 1. These were calculated from monthly landings data provided by Gutierrez-Aguilar and Instituto del Mar del Peru (IMARPE) (personal communication).

C.2 Calibration evolution

The calibration ran for 400 generations using 75 individuals. The global fitness function evolved from an original global fitness of 521.59 on the first generation, to 0.29 on generation 200. From here, it only decreased to 0.26 at generation 400. Figs. C.2 and C.3 show the evolution of the parameter sets over the first half of the calibration.

C.3 Configuration with interannual distribution maps

In this section we examine the hybrid configuration (see Section 4.2.3) running with interannually-varying distribution maps from 1992 to 2008 instead of climatological distribution maps. The initalisation, food forcing and parameters are the same as in the hybrid configuration. The interannual distribution maps are the same as used by Oliveros-Ramos et al. (2017).

Applying interannual variability to the distribution maps has a visible impact on the fish when compared to using climatological maps (Figure C.4). Compared to the hybrid configuration, in the configuration with interannual maps, some of the groups, for instance Humboldt squid, exhibit a stronger interannual variability (Figure C.4).

C.4 Plankton interannual and seasonal variability

Plankton has interannual and seasonal variability. These are highly affected by the accessibility coefficient (intV = 13 % and 9.1 % and seasV = 19 % and 27 %, Figure C.5) in the full domain. On the other hand, the accessibility coefficient has a smaller effect when

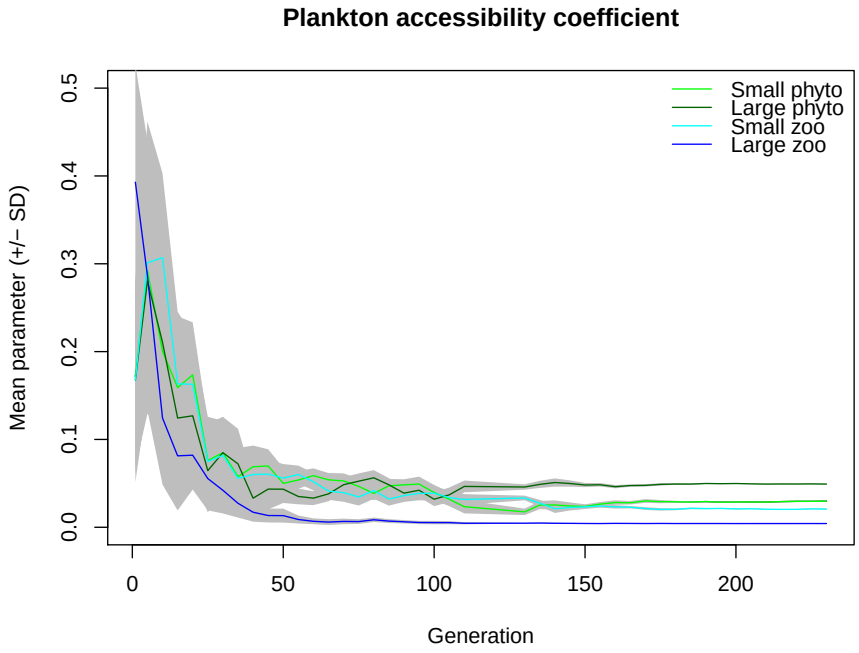

Figure C.2: Mean plankton accessibility coefficient (dimensionless) and standard deviation (shaded area) of the parameters in the 75 individuals of the calibration.

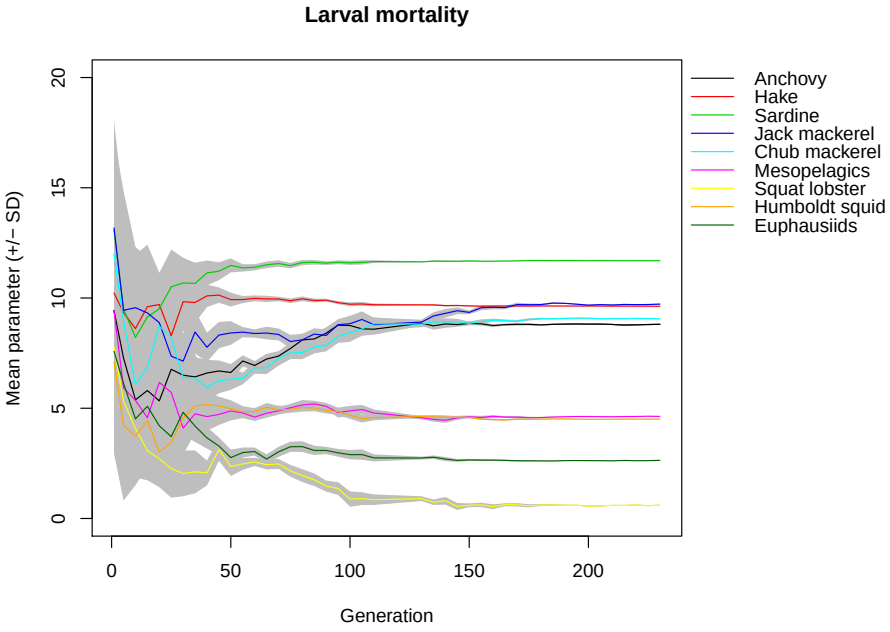

Figure C.3: Same as Fig. C.2 for the larval mortality (1/ts)

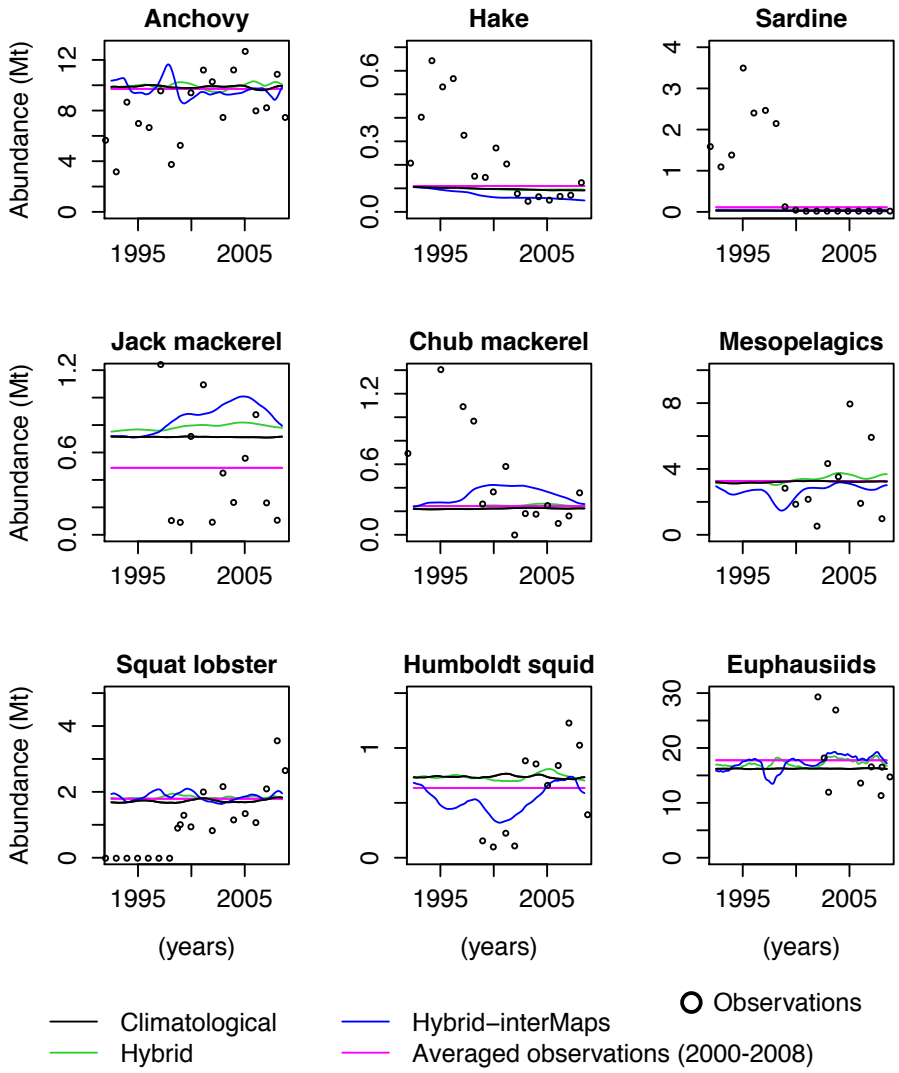

Figure C.4: Biomass 12-month running mean after spin-up of the climatological and hybrid configurations (see Sect. 4.2.3), and the hybrid configuration with interannual distribution maps from 1992 to 2008 (Hybrid-interMaps), as well as observations (dots) and 2000 to 2008 averaged observations used to calibrate the model. Observations source: Dimitri Gutierrez, Instituto del Mar del Peru (IMARPE), personal communication. Also available in Oliveros-Ramos et al. (2017), their Fig. 13

considering only the anchovy habitat (see Sect. 4.3 for a description of the anchovy habitat; intV and seasV differences are only 3 and 1 %, respectively, Figure C.5).

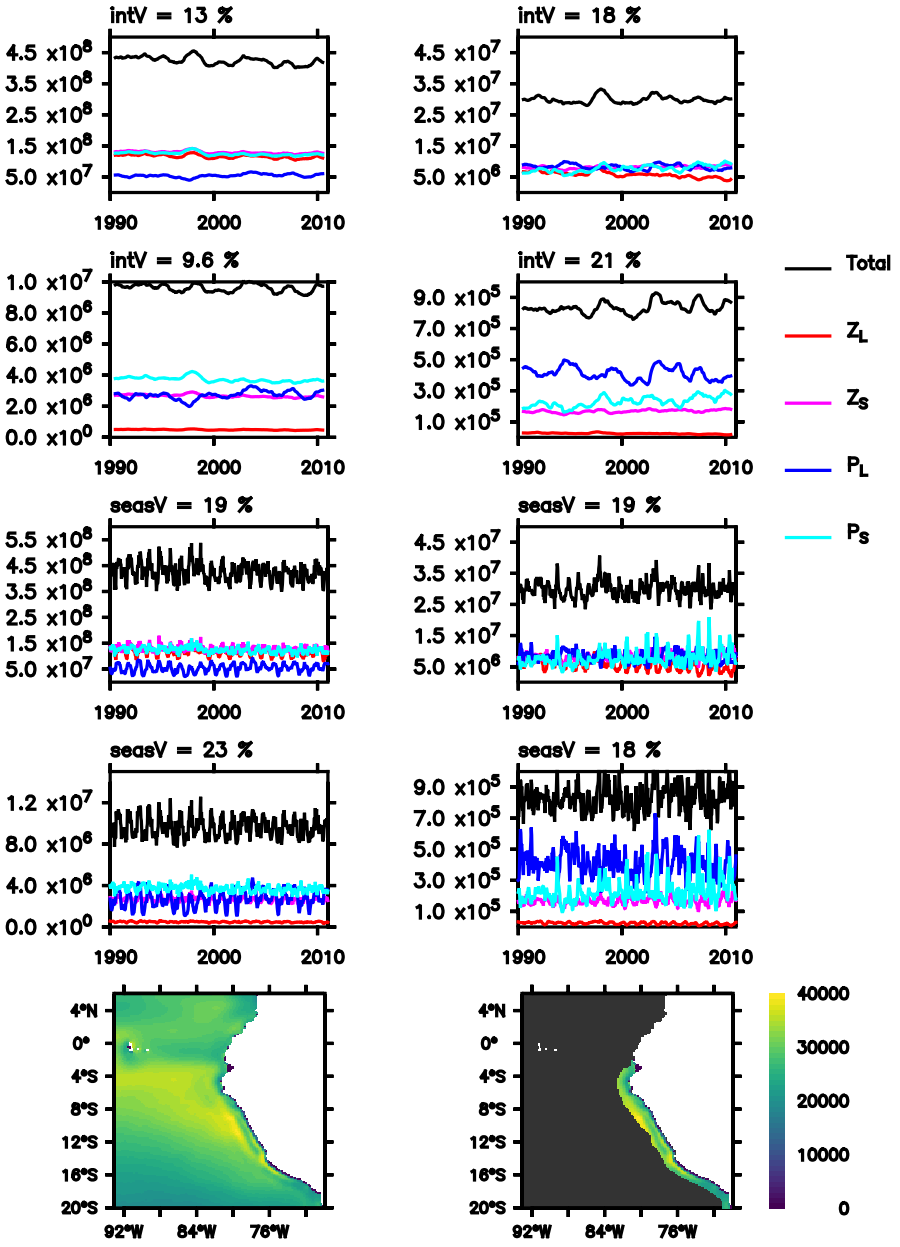

Figure C.5: Rows top to bottom: annual running mean of plankton, annual running mean of plankton multiplied by their respective accessibility coefficients, plankton time-series multiplied by their respective accessibility coefficients (tonnes) and time-averaged total plankton (tonnes per grid cell). intV and seasV refer to the relative difference between the maximum and minimum of the annual running mean and the seasonal cycle, respectively. Columns: plankton in the whole domain (left) and plankton in the region where 90 % of the anchovies live.

D. Supporting Information for 'Using mixed layer depth to constrain projections of Southern Ocean ecosystem functioning'

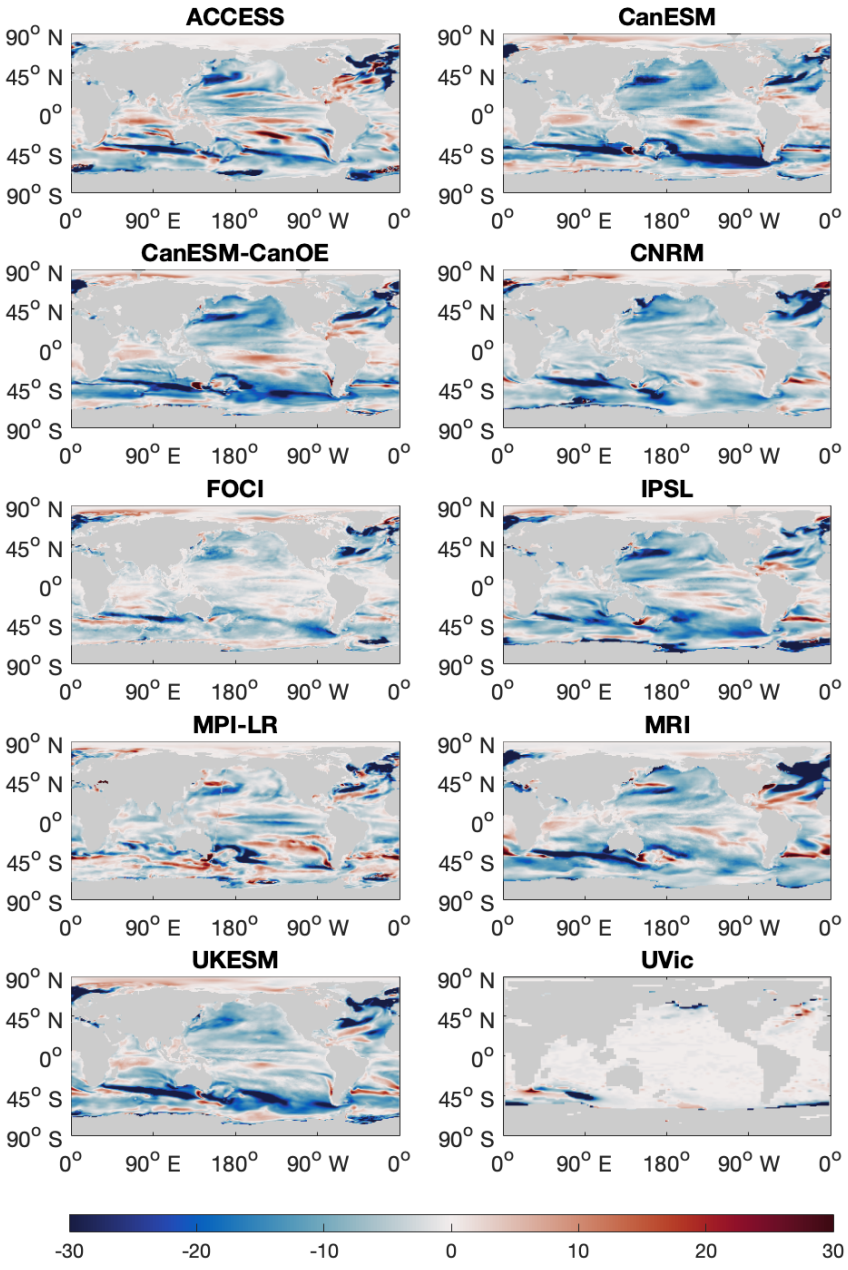

Figure D.1: Maps showing mixed layer depth anomaly from first (2000s) to last decades (2090s) of 21st century referencing the mean value of the first decade. Red indicates deepening and blue indicates shoaling mixed layer during 21st century.

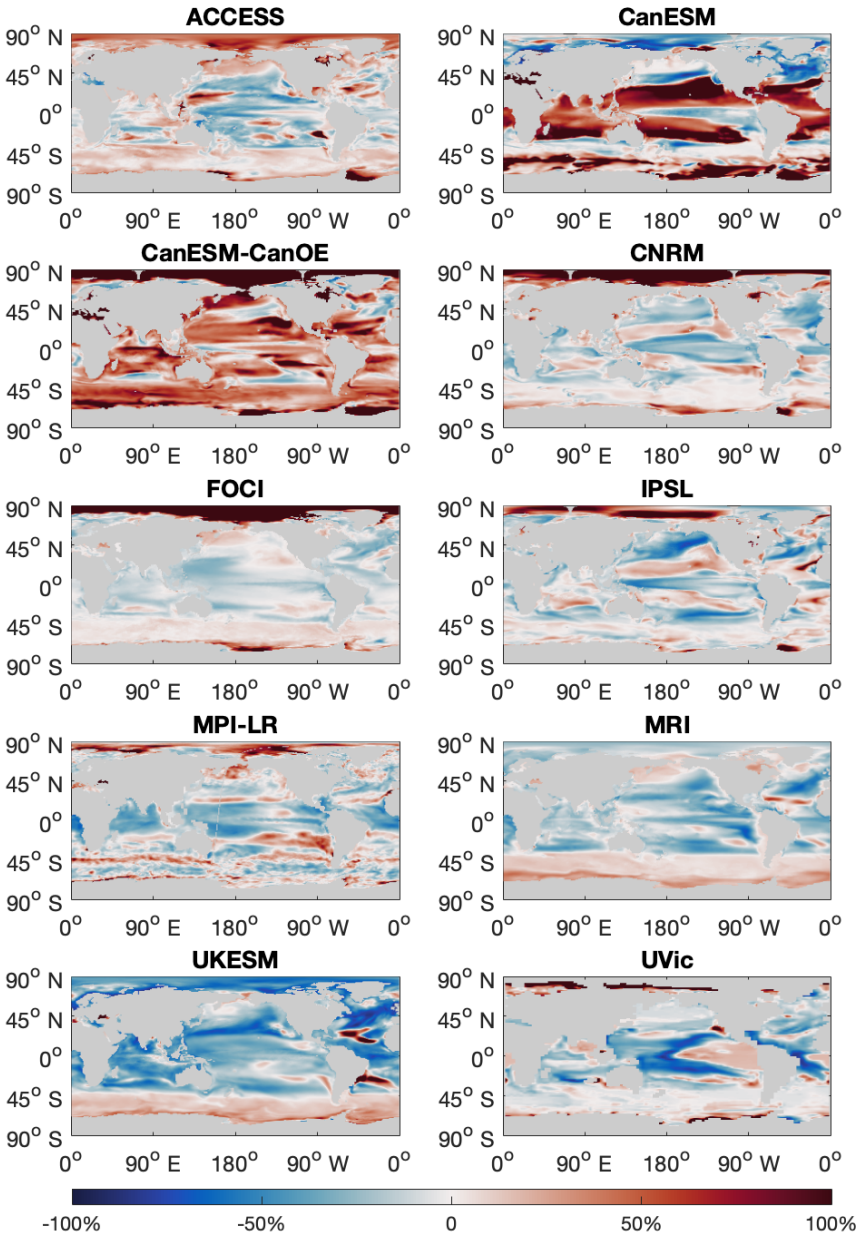

Figure D.2: Maps showing relative variation of surface chlorophyll from first (2000s) to last decades (2090s) of 21st century referencing the mean value of the first decade. Red indicates increasing and blue indicates decreasing surface chlorophyll during 21st century.

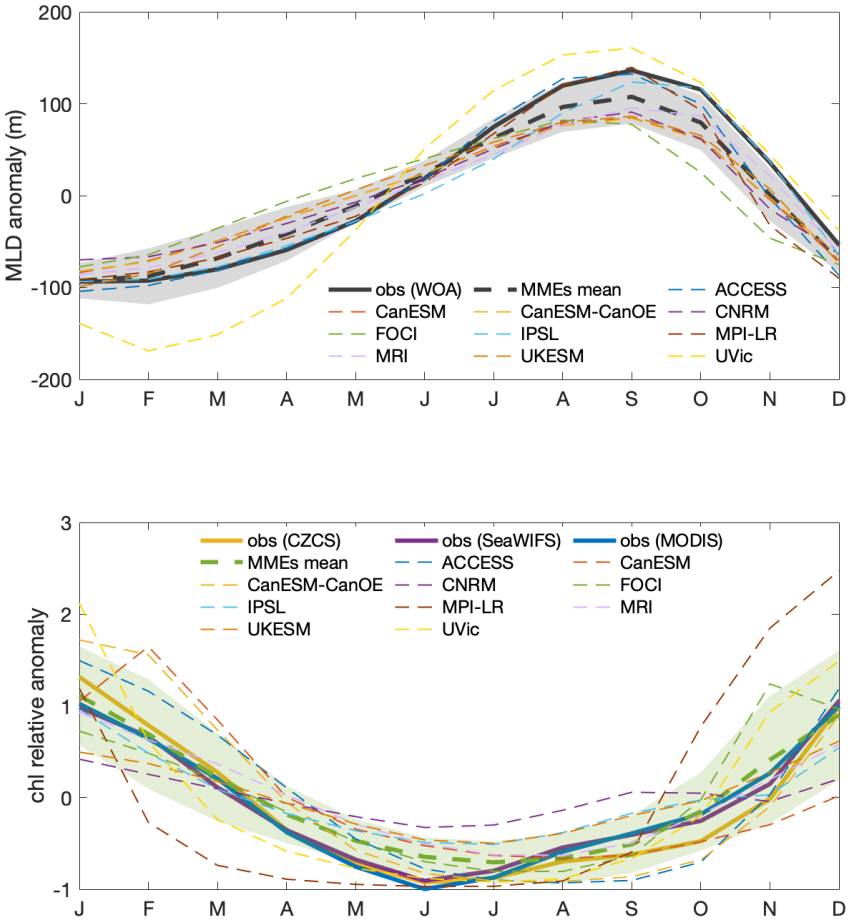

Figure D.3: Seasonal cycles of mixed layer depth anomaly (top, m) and relative chlorophyll anomaly (bottom) based on observation (solid lines) and model simulations (dash lines). Shaded areas indicate the standard deviation of the model simulations.

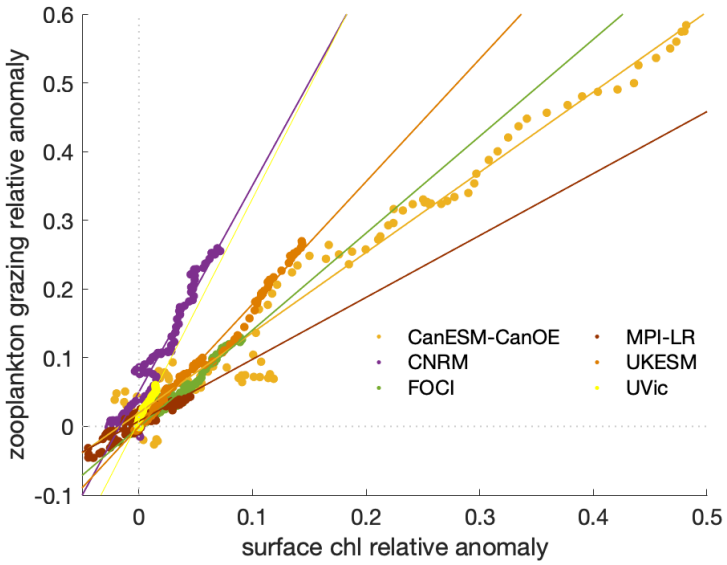

Figure D.4: Correlations of the relative anomalies of surface chlorophyll and zooplankton grazing from 2000-2100 under high emission scenarios referencing the mean values of first decade of the 21st century (2000-2009) in the Southern Ocean. The timeseries are filtered using a 10-year moving average.

Bibliography

Albert, A., Echevin, V., Lévy, M., and Aumont, O. (2010). Impact of nearshore wind stress curl on coastal circulation and primary productivity in the Peru upwelling system. *Journal of Geophysical Research: Oceans*, 115(C12).

Alheit, J. and Niquen, M. (2004). Regime shifts in the Humboldt Current ecosystem. *Progress in Oceanography*, 60(2-4):201–222.

Andersen, V., Nival, P., and Harris, R. P. (1987). Modelling of a planktonic ecosystem in an enclosed water column. *Journal of the Marine Biological Association of the United Kingdom*, 67(2):407–430.

Anderson, T. R., Gentleman, W. C., and Sinha, B. (2010). Influence of grazing formulations on the emergent properties of a complex ecosystem model in a global ocean general circulation model. *Progress in Oceanography*, 87(1-4):201–213.

Aranda, M. (2009). Evolution and state of the art of fishing capacity management in Peru: The case of the anchoveta fishery. *Pan-American Journal of Aquatic Sciences*, 4(2):146–153.

Arteaga, L., Pahlow, M., and Oschlies, A. (2016). Modeled Chl: C ratio and derived estimates of phytoplankton carbon biomass and its contribution to total particulate organic carbon in the global surface ocean. *Global Biogeochemical Cycles*, 30(12):1791–1810.

Arteaga, L. A., Boss, E., Behrenfeld, M. J., Westberry, T. K., and Sarmiento, J. L. (2020). Seasonal modulation of phytoplankton biomass in the Southern Ocean. *Nature Communications*, 11(1):1–10.

Asch, R. G. (2015). Climate change and decadal shifts in the phenology of larval fishes in the California Current ecosystem. *Proceedings of the National Academy of Sciences*, 112(30):E4065–E4074.

Aumont, O., Éthé, C., Tagliabue, A., Bopp, L., and Gehlen, M. (2015). PISCES-v2: an ocean biogeochemical model for carbon and ecosystem studies. *Geoscientific Model Development*, 8(8):2465–2513.

Ayón, P., Purca, S., and Guevara-Carrasco, R. (2004). Zooplankton volume trends off Peru between 1964 and 2001. *ICES Journal of Marine Science*, 61(4):478–484.

Azam, F., Fenchel, T., Field, J. G., Gray, J. S., Meyer-Reil, L.-A., and Thingstad, F. (1983). The ecological role of water-column microbes in the sea. *Marine Ecology Progress Series*, pages 257–263.

Bakun, A. (1973). Coastal upwelling indices, west coast of North America, 1946-71.

Bakun, A. (1990). Global climate change and intensification of coastal ocean upwelling. *Science*, 247(4939):198–201.

Bakun, A. (1997). Patterns in the ocean: ocean processes and marine population dynamics. *Oceanographic Literature Review*, 5(44):530.

Bakun, A. and Broad, K. (2003). Environmental 'loopholes' and fish population dynamics: comparative pattern recognition with focus on El Niño effects in the Pacific. *Fisheries Oceanography*, 12(4-5):458–473.

Bakun, A., Field, D. B., Redondo-Rodriguez, A., and Weeks, S. J. (2010). Greenhouse gas, upwelling-favorable winds, and the future of coastal ocean upwelling ecosystems. *Global Change Biology*, 16(4):1213–1228.

Bakun, A. and Weeks, S. J. (2008). The marine ecosystem off Peru: What are the secrets of its fishery productivity and what might its future hold? *Progress in Oceanography*, 79(2-4):290–299.

Bănaru, D., Diaz, F., Verley, P., Campbell, R., Navarro, J., Yohia, C., Oliveros-Ramos, R., Mellon-Duval, C., and Shin, Y.-J. (2019). Implementation of an end-to-end model of the Gulf of Lions ecosystem (NW Mediterranean Sea). I. Parameterization, calibration and evaluation. *Ecological Modelling*, 401:1–19.

Banse, K. (1992). Grazing, temporal changes of phytoplankton concentrations, and the microbial loop in the open sea. In *Primary Productivity and Biogeochemical Cycles in the Sea*, pages 409–440. Springer.

Barber, R. T. and Chavez, F. P. (1983). Biological consequences of El Niño. *Science*, 222(4629):1203–1210.

Barnes, C., Maxwell, D., Reuman, D. C., and Jennings, S. (2010). Global patterns in predator–prey size relationships reveal size dependency of trophic transfer efficiency. *Ecology*, 91(1):222–232.

Barrett, R. C., Caulkins, J. P., Yates, A. J., and Elliott, D. (1985). Population dynamics of the Peruvian anchovy. *Mathematical Modelling*, 6(6):525–548.

Barton, S. and Yvon-Durocher, G. (2019). Quantifying the temperature dependence of growth rate in marine phytoplankton within and across species. *Limnology and Oceanography*, 64(5):2081–2091.

Behrenfeld, M. J. (2010). Abandoning Sverdrup's critical depth hypothesis on phytoplankton blooms. *Ecology*, 91(4):977–989.

Behrenfeld, M. J. (2014). Climate-mediated dance of the plankton. *Nature Climate Change*, 4(10):880–887.

Behrenfeld, M. J. and Falkowski, P. G. (1997). Photosynthetic rates derived from satellite-based chlorophyll concentration. *Limnology and Oceanography*, 42(1):1–20.

Behrenfeld, M. J., O' Malley, R. T., Siegel, D. A., McClain, C. R., Sarmiento, J. L., Feldman, G. C., Milligan, A. J., Falkowski, P. G., Letelier, R. M., and Boss, E. S. (2006). Climate-driven trends in contemporary ocean productivity. *Nature*, 444(7120):752–755.

Belcher, S. E., Grant, A. L., Hanley, K. E., Fox-Kemper, B., Van Roekel, L., Sullivan, P. P., Large, W. G., Brown, A., Hines, A., Calvert, D., and et al. (2012). A global perspective on Langmuir turbulence in the ocean surface boundary layer. *Geophysical Research Letters*, 39(18).

Benoit-Bird, K. J. and McManus, M. A. (2012). Bottom-up regulation of a pelagic community through spatial aggregations. *Biology Letters*, 8(5):813–816.

Bertrand, A., Segura, M., Gutiérrez, M., and Vásquez, L. (2004). From small-scale habitat loopholes to decadal cycles: a habitat-based hypothesis explaining fluctuation in pelagic fish populations off Peru. *Fish and Fisheries*, 5(4):296–316.

Bindoff, N. L., Cheung, W. W., Kairo, J. G., Arístegui, J., Guinder, V. A., Hallberg, R., Hilmi, N. J. M., Jiao, N., Karim, M. S., Levin, L., and et al. (2019). Changing ocean, marine ecosystems, and dependent communities. *IPCC Special Report on the Ocean and Cryosphere in a Changing Climate*, pages 477–587.

Boerema, L. K. and Gulland, J. A. (1973). Stock Assessment of the Peruvian Anchovy (Engraulis ringens) and Management of the Fishery. *Journal of the Fisheries Research Board of Canada*, 30(12):2226–2235.

Bohata, K. (2016). Microzooplankton of the northern Benguela Upwelling System. *PhD thesis*.

Bopp, L., Lévy, M., Resplandy, L., and Sallée, J.-B. (2015). Pathways of anthropogenic carbon subduction in the global ocean. *Geophysical Research Letters*, 42(15):6416–6423.

Bopp, L., Monfray, P., Aumont, O., Dufresne, J.-L., Le Treut, H., Madec, G., Terray, L., and Orr, J. C. (2001). Potential impact of climate change on marine export production. *Global Biogeochemical Cycles*, 15(1):81–99.

Bopp, L., Resplandy, L., Orr, J. C., Doney, S. C., Dunne, J. P., Gehlen, M., Halloran, P., Heinze, C., Ilyina, T., Seferian, R., and et al. (2013). Multiple stressors of ocean ecosystems in the 21st century: projections with CMIP5 models. *Biogeosciences*, 10(10):6225–6245.

Boucher, O., Servonnat, J., Albright, A. L., Aumont, O., Balkanski, Y., Bastrikov, V., Bekki, S., Bonnet, R., Bony, S., Bopp, L., and et al. (2020). Presentation and evaluation of the IPSL-CM6A-LR climate model. *Journal of Advances in Modeling Earth Systems*, 12(7):e2019MS002010.

Bowman, D. M., Kolden, C. A., Abatzoglou, J. T., Johnston, F. H., van der Werf, G. R., and Flannigan, M. (2020). Vegetation fires in the Anthropocene. *Nature Reviews Earth & Environment*, 1(10):500–515.

Boyce, D. G., Frank, K. T., and Leggett, W. C. (2015). From mice to elephants: overturning the 'one size fits all' paradigm in marine plankton food chains. *Ecology Letters*, 18(6):504–515.

Boyce, D. G., Lewis, M. R., and Worm, B. (2010). Global phytoplankton decline over the past century. *Nature*, 466(7306):591–596.

Boyd, P. and Newton, P. (1999). Does planktonic community structure determine downward particulate organic carbon flux in different oceanic provinces? *Deep Sea Research Part I: Oceanographic Research Papers*, 46(1):63–91.

Boyd, P. W., Claustre, H., Levy, M., Siegel, D. A., and Weber, T. (2019). Multi-faceted particle pumps drive carbon sequestration in the ocean. *Nature*, 568(7752):327–335.

Bruland, K. W., Rue, E. L., Smith, G. J., and DiTullio, G. R. (2005). Iron, macronutrients and diatom blooms in the Peru upwelling regime: brown and blue waters of Peru. *Marine Chemistry*, 93(2-4):81–103.

Buesseler, K. O. (1998). The decoupling of production and particulate export in the surface ocean. *Global Biogeochemical Cycles*, 12(2):297–310.

Buesseler, K. O., Boyd, P. W., Black, E. E., and Siegel, D. A. (2020). Metrics that matter for assessing the ocean biological carbon pump. *Proceedings of the National Academy of Sciences*, 117(18):9679–9687.

Burrows, M. T., Schoeman, D. S., Buckley, L. B., Moore, P., Poloczanska, E. S., Brander, K. M., Brown, C., Bruno, J. F., Duarte, C. M., Halpern, B. S., and et al. (2011). The pace of shifting climate in marine and terrestrial ecosystems. *Science*, 334(6056):652–655.

Calbet, A. and Landry, M. R. (2004). Phytoplankton growth, microzooplankton grazing, and carbon cycling in marine systems. *Limnology and Oceanography*, 49(1):51–57.

Caldeira, K. and Duffy, P. B. (2000). The role of the Southern Ocean in uptake and storage of anthropogenic carbon dioxide. *Science*, 287(5453):620–622.

Calienes, R., Guillén, O., Lostaunau, N., and et al. (1985). Variabilidad espacio-temporal de clorofila, producción primaria y nutrientes frente a la costa peruana. *Boletin Instituto del Mar del Peru*, 10(1):1–44.

Carr, M.-E. (2002). Estimation of potential productivity in Eastern Boundary Currents using remote sensing. *Deep Sea Research Part II*, 49(1):59–80.

Carr, M.-E. and Kearns, E. J. (2003). Production regimes in four Eastern Boundary Current systems. *Deep Sea Research Part II: Topical Studies in Oceanography*, 50(22-26):3199–3221.

Carton, J. A. and Giese, B. S. (2008). A reanalysis of ocean climate using Simple Ocean Data Assimilation (SODA). *Monthly Weather Review*, 136(8):2999–3017.

Cavan, E., Le Moigne, F. A., Poulton, A. J., Tarling, G. A., Ward, P., Daniels, C. J., Fragoso, G. M., and Sanders, R. J. (2015). Attenuation of particulate organic carbon flux in the scotia sea, southern ocean, is controlled by zooplankton fecal pellets. *Geophysical Research Letters*, 42(3):821–830.

Cavan, E. L., Henson, S. A., Belcher, A., and Sanders, R. (2017). Role of zooplankton in determining the efficiency of the biological carbon pump. *Biogeosciences*, 14(1):177–186.

Chavez, F. P. (1995). A comparison of ship and satellite chlorophyll from California and Peru. *Journal of Geophysical Research: Oceans*, 100(C12):24855–24862.

Chavez, F. P., Bertrand, A., Guevara-Carrasco, R., Soler, P., and Csirke, J. (2008). The northern Humboldt Current System: Brief history, present status and a view towards the future. *Progress in Oceanography*, 79:95–105.

Chavez, F. P. and Messié, M. (2009). A comparison of eastern boundary upwelling ecosystems. *Progress in Oceanography*, 83(1-4):80–96.

Chavez, F. P., Ryan, J., Lluch-Cota, S. E., and Ñiquen C, M. (2003). From anchovies to sardines and back: multidecadal change in the Pacific Ocean. *Science*, 299(5604):217–221.

Chen, B. and Laws, E. A. (2017). Is there a difference of temperature sensitivity between marine phytoplankton and heterotrophs? *Limnology and Oceanography*, 62(2):806–817.

Chen, D., Busalacchi, A. J., and Rothstein, L. M. (1994). The roles of vertical mixing, solar radiation, and wind stress in a model simulation of the sea surface temperature seasonal cycle in the tropical Pacific Ocean. *Journal of Geophysical Research: Oceans*, 99(C10):20345–20359.

Chien, C.-T., Durgadoo, J. V., Ehlert, D., Frenger, I., Keller, D. P., Koeve, W., Kriest, I., Landolfi, A., Patara, L., Wahl, S., and et al. (2022). FOCI-MOPS v1–Integration of Marine Biogeochemistry within the Flexible Ocean and Climate Infrastructure version 1 (FOCI 1) Earth system model. *Geoscientific Model Development Discussions*, pages 1–58.

Chisholm, S. W. (2000). Stirring times in the Southern Ocean. *Nature*, 407(6805):685–686.

Christensen, V., de la Puente, S., Sueiro, J. C., Steenbeek, J., and Majluf, P. (2014). Valuing seafood: The Peruvian fisheries sector. *Marine Policy*, 44:302–311.

Christian, J. R., Denman, K. L., Hayashida, H., Holdsworth, A. M., Lee, W. G., Riche, O. G., Shao, A. E., Steiner, N., and Swart, N. C. (2021). Ocean biogeochemistry in the Canadian Earth System Model version 5.0. 3: CanESM5 and CanESM5-CanOE. *Geoscientific Model Development Discussions*, pages 1–68.

Chust, G., Allen, J. I., Bopp, L., Schrum, C., Holt, J., Tsiaras, K., Zavatarelli, M., Chifflet, M., Cannaby, H., Dadou, I., and Irigoien, X. (2014). Biomass changes and trophic amplification of plankton in a warmer ocean. *Global Change Biology*, 20(7):2124–2139.

Cury, P., Bakun, A., Crawford, R. J., Jarre, A., Quinones, R. A., Shannon, L. J., and Verheye, H. M. (2000). Small pelagics in upwelling systems: patterns of interaction and structural changes in "wasp-waist" ecosystems. *ICES Journal of Marine Science*, 57(3):603–618.

Cury, P. and Roy, C. (1989). Optimal Environmental Window and Pelagic Fish Recruitment Success in Upwelling Areas. *Canadian Journal of Fisheries and Aquatic Sciences*, 46(4):670–680.

Cury, P. M., Shin, Y.-J., Planque, B., Durant, J. M., Fromentin, J.-M., Kramer-Schadt, S., Stenseth, N. C., Travers, M., and Grimm, V. (2008). Ecosystem oceanography for global change in fisheries. *Trends in Ecology & Evolution*, 23(6):338–346.

Cushing, D. (1990). Plankton production and year-class strength in fish populations: an update of the match/mismatch hypothesis. In *Advances in Marine Biology*, volume 26, pages 249–293. Elsevier.

Dahlberg, M. D. (1979). A review of survival rates of fish eggs and larvae in relation to impact assessments. *Marine Fisheries Review*, 41.

D'Alelio, D., Libralato, S., Wyatt, T., and d' Alcalà, M. R. (2016). Ecological-network models link diversity, structure and function in the plankton food-web. *Scientific Reports*, 6(1):1–13.

de Boyer Montégut, C., Madec, G., Fischer, A. S., Lazar, A., and Iudicone, D. (2004). Mixed layer depth over the global ocean: An examination of profile data and a profile-based climatology. *Journal of Geophysical Research: Oceans*, 109(C12).

Debreu, L., Marchesiello, P., Penven, P., and Cambon, G. (2012). Two-way nesting in split-explicit ocean models: Algorithms, implementation and validation. *Ocean Modelling*, 49:1–21.

Delworth, T. L., Rosati, A., Anderson, W., Adcroft, A. J., Balaji, V., Benson, R., Dixon, K., Griffies, S. M., Lee, H.-C., Pacanowski, R. C., and Zhang, R. (2012). Simulated climate and climate change in the GFDL CM2. 5 high-resolution coupled climate model. *Journal of Climate*, 25(8):2755–2781.

Diaz, F., Bănaru, D., Verley, P., and Shin, Y.-J. (2019). Implementation of an end-to-end model of the Gulf of Lions ecosystem (NW Mediterranean Sea). II. Investigating the effects of high trophic levels on nutrients and plankton dynamics and associated feedbacks. *Ecological Modelling*, 405:51–68.

Dickman, E. M., Newell, J. M., González, M. J., and Vanni, M. J. (2008). Light, nutrients, and food-chain length constrain planktonic energy transfer efficiency across multiple trophic levels. *Proceedings of the National Academy of Sciences*, 105(47):18408–18412.

Doney, S. C. (2006). Plankton in a warmer world. *Nature*, 444(7120):695–696.

Du Pontavice, H., Gascuel, D., Reygondeau, G., Maureaud, A., and Cheung, W. W. (2020). Climate change undermines the global functioning of marine food webs. *Global Change Biology*, 26(3):1306–1318.

Duboz, R., Versmisse, D., Travers, M., Ramat, E., and Shin, Y.-J. (2010). Application of an evolutionary algorithm to the inverse parameter estimation of an individual-based model. *Ecological Modelling*, 221(5):840–849.

Ducklow, H. W., Steinberg, D. K., and Buesseler, K. O. (2001). Upper ocean carbon export and the biological pump. *Oceanography*, 14(4):50–58.

Echevin, V., Aumont, O., Ledesma, J., and Flores, G. (2008). The seasonal cycle of surface chlorophyll in the Peruvian upwelling system: A modelling study. *Progress in Oceanography*, 79(2-4):167–176.

Echevin, V., Gévaudan, M., Espinoza-Morriberón, D., Tam, J., Aumont, O., Gutierrez, D., and Colas, F. (2020). Physical and biogeochemical impacts of RCP8. 5 scenario in the Peru upwelling system. *Biogeosciences*, 17(12):3317–3341.

Echevin, V., Hauschildt, J., Colas, F., Thomsen, S., and Aumont, O. (2021). Impact of Chlorophyll Shading on the Peruvian Upwelling System. *Geophysical Research Letters*, page e2021GL094429.

Edwards, K. F., Thomas, M. K., Klausmeier, C. A., and Litchman, E. (2012). Allometric scaling and taxonomic variation in nutrient utilization traits and maximum growth rate of phytoplankton. *Limnology and Oceanography*, 57(2):554–566.

Edwards, M. and Richardson, A. J. (2004). Impact of climate change on marine pelagic phenology and trophic mismatch. *Nature*, 430(7002):881–884.

Eppley, R. W. (1972). Temperature and phytoplankton growth in the sea. *Fish. Bull*, 70(4):1063–1085.

Eppley, R. W., Rogers, J. N., and McCarthy, J. J. (1969). Half-saturation constants for uptake of nitrate and ammonium by marine phytoplankton 1. *Limnology and Oceanography*, 14(6):912–920.

Espinoza, P. and Bertrand, A. (2008). Revisiting Peruvian anchovy (Engraulis ringens) trophodynamics provides a new vision of the Humboldt Current system. *Progress in Oceanography*, 79(2-4):215–227.

Evans, G. T. and Parslow, J. S. (1985). A model of annual plankton cycles. *Biological Oceanography*, 3(3):327–347.

FAO (2020). The state of world fisheries and aquaculture 2020. Sustainability in action. *Rome*.

Farris, D. A. (1961). Abundance and distribution of eggs and larvae of jack mackerel (Trachurus symmetricus). *Fishery Bulletin U.S.*, 61:247–279.

Fennel, K., Wilkin, J., Levin, J., Moisan, J., O'Reilly, J., and Haidvogel, D. (2006). Nitrogen cycling in the Middle Atlantic Bight: Results from a three-dimensional model and implications for the North Atlantic nitrogen budget. *Global Biogeochemical Cycles*, 20(3).

Field, C. B., Behrenfeld, M. J., Randerson, J. T., and Falkowski, P. (1998). Primary production of the biosphere: integrating terrestrial and oceanic components. *Science*, 281(5374):237–240.

Friederich, G. E., Ledesma, J., Ulloa, O., and Chavez, F. P. (2008). Air–sea carbon dioxide fluxes in the coastal southeastern tropical Pacific. *Progress in Oceanography*, 79(2-4):156–166.

Friedland, K. D., Stock, C., Drinkwater, K. F., Link, J. S., Leaf, R. T., Shank, B. V., Rose, J. M., Pilskaln, C. H., and Fogarty, M. J. (2012). Pathways between primary production and fisheries yields of large marine ecosystems. *PloS One*, 7(1):e28945.

Frölicher, T. L., Rodgers, K. B., Stock, C. A., and Cheung, W. W. (2016). Sources of uncertainties in 21st century projections of potential ocean ecosystem stressors. *Global Biogeochemical Cycles*, 30(8):1224–1243.

Frölicher, T. L., Sarmiento, J. L., Paynter, D. J., Dunne, J. P., Krasting, J. P., and Winton, M. (2015). Dominance of the Southern Ocean in anthropogenic carbon and heat uptake in CMIP5 models. *Journal of Climate*, 28(2):862–886.

Fu, C., Shin, Y., Perry, R., King, J., and Liu, H. (2012). *Exploring Climate and Fishing Impacts in an Ecosystem Model of the Strait of Georgia, British Columbia*, pages 65–86. Alaska Sea Grant, University of Alaska Fairbanks.

Fuenzalida, R., Schneider, W., Garcés-Vargas, J., Bravo, L., and Lange, C. (2009). Vertical and horizontal extension of the oxygen minimum zone in the eastern South Pacific Ocean. *Deep Sea Research Part II: Topical Studies in Oceanography*, 56(16):992–1003.

Fulton, E. A. (2010). Approaches to end-to-end ecosystem models. *Journal of Marine Systems*, 81(1):171–183. Contributions from Advances in Marine Ecosystem Modelling Research II 23-26 June 2008, Plymouth, UK.

Fulton, E. A., Fuller, M., Smith, A., and Punt, A. (2004). Ecological indicators of the ecosystem effects of fishing.

Fung, I. Y., Meyn, S. K., Tegen, I., Doney, S. C., John, J. G., and Bishop, J. K. (2000). Iron supply and demand in the upper ocean. *Global Biogeochemical Cycles*, 14(1):281–295.

Garcia, H., Weathers, K., Paver, C., Smolyar, I., Boyer, T., Locarnini, M., Zweng, M., Mishonov, A., Baranova, O., Seidov, D., and et al. (2019). World Ocean Atlas 2018. Vol. 4: Dissolved Inorganic Nutrients (phosphate, nitrate and nitrate+ nitrite, silicate).

Geider, R. J. (1987). Light and temperature dependence of the carbon to chlorophyll a ratio in microalgae and cyanobacteria: implications for physiology and growth of phytoplankton. *New Phytologist*, pages 1–34.

Gervais, F. and Riebesell, U. (2001). Effect of phosphorus limitation on elemental composition and stable carbon isotope fractionation in a marine diatom growing under different co2 concentrations. *Limnology and Oceanography*, 46(3):497–504.

Getzlaff, J., Dietze, H., and Oschlies, A. (2016). Simulated effects of southern hemispheric wind changes on the Pacific oxygen minimum zone. *Geophysical Research Letters*, 43(2):728–734.

Grémillet, D., Lewis, S., Drapeau, L., van Der Lingen, C. D., Huggett, J. A., Coetzee, J. C., Verheye, H. M., Daunt, F., Wanless, S., and Ryan, P. G. (2008). Spatial match–mismatch in the Benguela upwelling zone: should we expect chlorophyll and sea-surface temperature to predict marine predator distributions? *Journal of Applied Ecology*, 45(2):610–621.

Gruber, N., Lachkar, Z., Frenzel, H., Marchesiello, P., Münnich, M., McWilliams, J. C., Nagai, T., and Plattner, G.-K. (2011). Eddy-induced reduction of biological production in eastern boundary upwelling systems. *Nature Geoscience*, 4(11):787–792.

Gruber, N., Landschützer, P., and Lovenduski, N. S. (2019). The variable Southern Ocean carbon sink. *Annual Review of Marine Science*, 11:159–186.

Grüss, A., Schirripa, M. J., Chagaris, D., Drexler, M., Simons, J., Verley, P., Shin, Y.-J., Karnauskas, M., Oliveros-Ramos, R., and Ainsworth, C. H. (2015). Evaluation of the trophic structure of the West Florida Shelf in the 2000s using the ecosystem model OSMOSE. *Journal of Marine Systems*, 144:30–47.

Guénette, S., Christensen, V., and Pauly, D. (2008). Trophic modelling of the Peruvian upwelling ecosystem: Towards reconciliation of multiple datasets. *Progress in Oceanography*, 79(2):326–335. The Northern Humboldt Current System: Ocean Dynamics, Ecosystem Processes, and Fisheries.

Guillen, O. and Calienes, R. (1981). Upwelling off chimbote. *Coastal Upwelling*, 1:312–326.

Gutiérrez, M., Ramirez, A., Bertrand, S., Móron, O., and Bertrand, A. (2008). Ecological niches and areas of overlap of the squat lobster 'munida' (Pleuroncodes monodon) and anchoveta (Engraulis ringens) off Peru. *Progress in Oceanography*, 79(2):256–263. The Northern Humboldt Current System: Ocean Dynamics, Ecosystem Processes, and Fisheries.

Gutknecht, E., Dadou, I., Le Vu, B., Cambon, G., Sudre, J., Garçon, V., Machu, E., Rixen, T., Kock, A., Flohr, A., and Lavik, G. (2013). Coupled physical/biogeochemical modeling including O2-dependent processes in the Eastern Boundary Upwelling Systems: application in the Benguela. *Biogeosciences*, 10(6):3559–3591.

Hall, A., Cox, P., Huntingford, C., and Klein, S. (2019). Progressing emergent constraints on future climate change. *Nature Climate Change*, 9(4):269–278.

Hall, A. and Qu, X. (2006). Using the current seasonal cycle to constrain snow albedo feedback in future climate change. *Geophysical Research Letters*, 33(3).

Halouani, G., Lasram, F., Shin, Y.-J., Velez, L., Verley, P., Hattab, T., Oliveros-Ramos, R., Diaz, F., Ménard, F., Baklouti, M., Guyennon, A., Ms, R., and Le Loc'h, F. (2016). Modelling food web structure using an end-to-end approach in the coastal ecosystem of the Gulf of Gabes (Tunisia). *Ecological Modelling*, 339:45–57.

Hamilton, D. S., Moore, J. K., Arneth, A., Bond, T. C., Carslaw, K. S., Hantson, S., Ito, A., Kaplan, J. O., Lindsay, K., Nieradzik, L., and et al. (2020). Impact of changes to the atmospheric soluble iron deposition flux on ocean biogeochemical cycles in the Anthropocene. *Global Biogeochemical Cycles*, 34(3):e2019GB006448.

Hays, G. C. (2003). A review of the adaptive significance and ecosystem consequences of zooplankton diel vertical migrations. *Migrations and Dispersal of Marine Organisms*, pages 163–170.

Heath, M. R. (2012). Ecosystem limits to food web fluxes and fisheries yields in the North Sea simulated with an end-to-end food web model. *Progress in Oceanography*, 102:42–66.

Heneghan, R. F., Everett, J. D., Blanchard, J. L., and Richardson, A. J. (2016). Zooplankton are not fish: improving zooplankton realism in size-spectrum models mediates energy transfer in food webs. *Frontiers in Marine Science*, 3:201.

Henson, S., Le Moigne, F., and Giering, S. (2019). Drivers of carbon export efficiency in the global ocean. *Global Biogeochemical Cycles*, 33(7):891–903.

Henson, S. A., Laufkötter, C., Leung, S., Giering, S. L., Palevsky, H. I., and Cavan, E. L. (2022). Uncertain response of ocean biological carbon export in a changing world. *Nature Geoscience*, pages 1–7.

Henson, S. A., Sanders, R., and Madsen, E. (2012). Global patterns in efficiency of particulate organic carbon export and transfer to the deep ocean. *Global Biogeochemical Cycles*, 26(1).

Hill Cruz, M., Kriest, I., José, J., Kiko, R., Hauss, H., and Oschlies, A. (2021). Zooplankton mortality effects on the plankton community of the northern Humboldt Current System: sensitivity of a regional biogeochemical model. *Biogeosciences*, 18:2891–2916.

Hirst, A. and Bunker, A. (2003). Growth of marine planktonic copepods: global rates and patterns in relation to chlorophyll a, temperature, and body weight. *Limnology and Oceanography*, 48(5):1988–2010.

Holte, J., Talley, L. D., Gilson, J., and Roemmich, D. (2017). An Argo mixed layer climatology and database. *Geophysical Research Letters*, 44(11):5618–5626.

Jahncke, J., Checkley, D. M., and Hunt, G. L. (2004). Trends in carbon flux to seabirds in the Peruvian upwelling system: effects of wind and fisheries on population regulation. *Fisheries Oceanography*, 13(3):208–223.

José, Y. S., Dietze, H., and Oschlies, A. (2017). Linking diverse nutrient patterns to different water masses within anticyclonic eddies in the upwelling system off Peru. *Biogeosciences*, 14(6):1349–1364.

José, Y. S., Stramma, L., Schmidtko, S., and Oschlies, A. (2019). ENSO-driven fluctuations in oxygen supply and vertical extent of oxygen-poor waters in the oxygen minimum zone of the Eastern Tropical South Pacific. *Biogeosciences Discussions*, 2019:1–20.

Kämpf, J. and Chapman, P. (2016). *Upwelling Systems of the World*. Springer.

Karstensen, J., Stramma, L., and Visbeck, M. (2008). Oxygen minimum zones in the eastern tropical Atlantic and Pacific oceans. *Progress in Oceanography*, 77(4):331–350. A New View of Water Masses After WOCE. A Special Edition for Professor Matthias Tomczak.

Kawasaki, T. (1983). Why do some pelagic fishes have wide fluctuations in their numbers? Biological basis of fluctuation from the viewpoint of evolutionary ecology. *FAO Fisheries Report*, 291(3):1065–1080.

Keeling, R. F., Körtzinger, A., Gruber, N., et al. (2010). Ocean deoxygenation in a warming world. *Annu. Rev. Mar. Sci*, 2(1):199–229.

Keller, D., Oschlies, A., and Eby, M. (2012). A new marine ecosystem model for the University of Victoria Earth System Climate Model. *Geoscientific Model Development*, 5(5):1195–1220.

Kelly, T. B., Goericke, R., Kahru, M., Song, H., and Stukel, M. R. (2018). CCE II: Spatial and interannual variability in export efficiency and the biological pump in an eastern boundary current upwelling system with substantial lateral advection. *Deep Sea Research Part I: Oceanographic Research Papers*, 140:14–25.

Kessler, A. and Tjiputra, J. (2016). The Southern Ocean as a constraint to reduce uncertainty in future ocean carbon sinks. *Earth System Dynamics*, 7(2):295–312.

Kiørboe, T. (2013). Zooplankton body composition. *Limnology and Oceanography*, 58(5):1843–1850.

Kirby, R. R. and Beaugrand, G. (2009). Trophic amplification of climate warming. *Proceedings of the Royal Society B: Biological Sciences*, 276(1676):4095–4103.

Kleppel, G. (1993). On the diets of calanoid copepods. *Marine Ecology-Progress Series*, 99:183–183.

Koné, n. V., Machu, E., Penven, P., Andersen, V., Garçon, V., Fréon, P., and Demarcq, H. (2005). Modeling the primary and secondary productions of the southern Benguela upwelling system: A comparative study through two biogeochemical models. *Global Biogeochemical Cycles*, 19(4).

Kwiatkowski, L., Aumont, O., and Bopp, L. (2019). Consistent trophic amplification of marine biomass declines under climate change. *Global Change Biology*, 25(1):218–229.

Kwiatkowski, L., Bopp, L., Aumont, O., Ciais, P., Cox, P. M., Laufkötter, C., Li, Y., and Séférian, R. (2017). Emergent constraints on projections of declining primary production in the tropical oceans. *Nature Climate Change*, 7(5):355–358.

Kwiatkowski, L., Torres, O., Bopp, L., Aumont, O., Chamberlain, M., Christian, J. R., Dunne, J. P., Gehlen, M., Ilyina, T., John, J. G., and et al. (2020). Twenty-first century ocean warming, acidification, deoxygenation, and upper-ocean nutrient and primary production decline from cmip6 model projections. *Biogeosciences*, 17(13):3439–3470.

Lachkar, Z. and Gruber, N. (2011). What controls biological production in coastal upwelling systems? insights from a comparative modeling study. *Biogeosciences*, 8(10):2961–2976.

Lalli, C. and Parsons, T. (1997). *Biological Oceanography: An Introduction*. Elsevier.

Lathuilière, C., Echevin, V., Lévy, M., and Madec, G. (2010). On the role of the mesoscale circulation on an idealized coastal upwelling ecosystem. *Journal of Geophysical Research: Oceans*, 115(C9).

Laufkötter, C., Vogt, M., Gruber, N., Aita-Noguchi, M., Aumont, O., Bopp, L., Buitenhuis, E., Doney, S. C., Dunne, J., Hashioka, T., and et al. (2015). Drivers and uncertainties of future global marine primary production in marine ecosystem models. *Biogeosciences*, 12(23):6955–6984.

Le Quéré, C., Aumont, O., Monfray, P., and Orr, J. (2003). Propagation of climatic events on ocean stratification, marine biology, and CO2: Case studies over the 1979–1999 period. *Journal of Geophysical Research: Oceans*, 108(C12).

Le Quéré, C., Buitenhuis, E. T., Moriarty, R., Alvain, S., Aumont, O., Bopp, L., Chollet, S., Enright, C., Franklin, D. J., Geider, R. J., and et al. (2016). Role of zooplankton dynamics for southern ocean phytoplankton biomass and global biogeochemical cycles. *Biogeosciences*, 13(14):4111–4133.

Legendre, L. and Rassoulzadegan, F. (1996). Food-web mediated export of biogenic carbon in oceans: hydrodynamic control. *Marine Ecology Progress Series*, 145:179–193.

Lett, C., Verley, P., Mullon, C., Parada, C., Brochier, T., Penven, P., and Blanke, B. (2008). A Lagrangian tool for modelling ichthyoplankton dynamics. *Environmental Modelling & Software*, 23(9):1210–1214.

Lewandowska, A. M., Boyce, D. G., Hofmann, M., Matthiessen, B., Sommer, U., and Worm, B. (2014). Effects of sea surface warming on marine plankton. *Ecology Letters*, 17(5):614–623.

Lima, I. D. and Doney, S. C. (2004). A three-dimensional, multinutrient, and size-structured ecosystem model for the North Atlantic. *Global Biogeochemical Cycles*, 18(3).

Lindeman, R. L. (1942). The trophic-dynamic aspect of ecology. *Ecology*, 23(4):399–417.

Link, J. S., Yemane, D., Shannon, L. J., Coll, M., Shin, Y.-J., Hill, L., and Borges, M. d. F. (2010). Relating marine ecosystem indicators to fishing and environmental drivers: an elucidation of contrasting responses. *ICES Journal of Marine Science*, 67(4):787–795.

Liu, W. T., Tang, W., and Polito, P. S. (1998). NASA scatterometer provides global ocean-surface wind fields with more structures than numerical weather prediction. *Geophysical Research Letters*, 25(6):761–764.

Locarnini, M., Mishonov, A., Baranova, O., Boyer, T., Zweng, M., Garcia, H., Seidov, D., Weathers, K., Paver, C., Smolyar, I., and et al. (2018). World ocean atlas 2018, volume 1: Temperature.

López de la Lama, R., de la Puente, S., Sueiro, J. C., and Chan, K. M. A. (2021). Reconnecting with the past and anticipating the future: A review of fisheries-derived cultural ecosystem services in pre-Hispanic Peru. *People and Nature*, 3(1):129–147.

Lotze, H. K., Tittensor, D. P., Bryndum-Buchholz, A., Eddy, T. D., Cheung, W. W., Galbraith, E. D., Barange, M., Barrier, N., Bianchi, D., Blanchard, J. L., and Worm, B. (2019). Global ensemble projections reveal trophic amplification of ocean biomass declines with climate change. *Proceedings of the National Academy of Sciences*, 116(26):12907–12912.

Majkut, J. D., Carter, B. R., Frölicher, T. L., Dufour, C. O., Rodgers, K. B., and Sarmiento, J. L. (2014). An observing system simulation for Southern Ocean carbon dioxide uptake. *Philosophical Transactions of the Royal Society A: Mathematical, Physical and Engineering Sciences*, 372(2019):20130046.

Majluf, P. and Reyes, J. (1989). The Marine Mammals of Peru: A Review. In Pauly, D., Muck, P., Mendo, J., and Tsukayama, I., editors, *The Peruvian upwelling ecosystem: dynamics and interactions. ICLARM Conference Proceedings 18*. Instituto del Mar del Peru (IMARPE) Callao, Peru; Deutsche Gesellschaft fuer Technische Zusammenarbeit (GIZ), GmbH, Eschbom, Federal Republic of Germany; and International Center for Living Aquatic Resources Management (ICLARM), Manila Philippines.

Mann, K. H. and Lazier, J. R. (2013). *Dynamics of Marine Ecosystems: Biological-Physical Interactions in the Oceans*. John Wiley & Sons.

Marañón, E., Lorenzo, M. P., Cermeño, P., and Mouriño-Carballido, B. (2018). Nutrient limitation suppresses the temperature dependence of phytoplankton metabolic rates. *The ISME Journal*, 12(7):1836–1845.

Marinov, I., Gnanadesikan, A., Toggweiler, J., and Sarmiento, J. L. (2006). The Southern Ocean biogeochemical divide. *Nature*, 441(7096):964–967.

Marzloff, M., Shin, Y.-J., Tam, J., Travers, M., and Bertrand, A. (2009). Trophic structure of the Peruvian marine ecosystem in 2000-2006: Insights on the effects of management scenarios for the hake fishery using the IBM trophic model OSMOSE. *Journal of Marine Systems*, 75(1-2):290–304.

Massing, J. C., Schukat, A., Auel, H., Auch, D., Kittu, L., Pinedo Arteaga, E. L., Correa Acosta, J., and Hagen, W. (2022). Toward a solution of the "Peruvian Puzzle" : Pelagic Food-Web Structure and Trophic Interactions in the Northern Humboldt Current Upwelling System Off Peru. *Frontiers in Marine Science*, 8:Art–Nr.

Mauritsen, T., Bader, J., Becker, T., Behrens, J., Bittner, M., Brokopf, R., Brovkin, V., Claussen, M., Crueger, T., Esch, M., and et al. (2019). Developments in the MPI-M Earth System Model version 1.2 (MPI-ESM1. 2) and its response to increasing CO2. *Journal of Advances in Modeling Earth Systems*, 11(4):998–1038.

Maury, O. (2010). An overview of APECOSM, a spatialized mass balanced "Apex Predators ECOSystem Model" to study physiologically structured tuna population dynamics in their ecosystem. *Progress in Oceanography*, 84(1):113–117. Special Issue: Parameterisation of Trophic Interactions in Ecosystem Modelling.

McGowan, J. A. and Hayward, T. L. (1978). Mixing and oceanic productivity. *Deep Sea Research*, 25(9):771–793.

McQuatters-Gollop, A., Reid, P. C., Edwards, M., Burkill, P. H., Castellani, C., Batten, S., Gieskes, W., Beare, D., Bidigare, R. R., Head, E., and et al. (2011). Is there a decline in marine phytoplankton? *Nature*, 472(7342):E6–E7.

Messié, M. and Chavez, F. P. (2015). Seasonal regulation of primary production in eastern boundary upwelling systems. *Progress in Oceanography*, 134:1–18.

Messié, M., Ledesma, J., Kolber, D. D., Michisaki, R. P., Foley, D. G., and Chavez, F. P. (2009). Potential new production estimates in four eastern boundary upwelling ecosystems. *Progress in Oceanography*, 83(1-4):151–158.

Mitra, A., Castellani, C., Gentleman, W. C., Jónasdóttir, S. H., Flynn, K. J., Bode, A., Halsband, C., Kuhn, P., Licandro, P., Agersted, M. D., and John, M. S. (2014). Bridging the gap between marine biogeochemical and fisheries sciences; configuring the zooplankton link. *Progress in Oceanography*, 129:176–199.

Moloney, C. L., St John, M. A., Denman, K. L., Karl, D. M., Köster, F. W., Sundby, S., and Wilson, R. P. (2011). Weaving marine food webs from end to end under global change. *Journal of Marine Systems*, 84(3-4):106–116.

Montes, I., Dewitte, B., Gutknecht, E., Paulmier, A., Dadou, I., Oschlies, A., and Garçon, V. (2014). High-resolution modeling of the Eastern Tropical Pacific oxygen minimum zone: Sensitivity to the tropical oceanic circulation. *Journal of Geophysical Research: Oceans*, 119(8):5515–5532.

Morán, X. A. G., Calvo-Díaz, A., Arandia-Gorostidi, N., and Huete-Stauffer, T. M. (2018). Temperature sensitivities of microbial plankton net growth rates are seasonally coherent and linked to nutrient availability. *Environmental Microbiology*, 20(10):3798–3810.

Moriarty, R. and O'Brien, T. (2013). Distribution of mesozooplankton biomass in the global ocean. *Earth System Science Data*, 5(1):45–55.

Moullec, F., Barrier, N., Drira, S., Guilhaumon, F., Marsaleix, P., Somot, S., Ulses, C., Velez, L., and Shin, Y.-J. (2019a). An End-to-End Model Reveals Losers and Winners in a Warming Mediterranean Sea. *Frontiers in Marine Science*, 6:345.

Moullec, F., Velez, L., Verley, P., Barrier, N., Ulses, C., Carbonara, P., Esteban, A., Follesa, C., Gristina, M., Jadaud, A., Ligas, A., Díaz, E. L., Maiorano, P., Peristeraki, P., Spedicato, M. T., Thasitis, I., Valls, M., Guilhaumon, F., and Shin, Y.-J. (2019b). Capturing the big picture of mediterranean marine biodiversity with an end-to-end model of climate and fishing impacts. *Progress in Oceanography*, 178:102179.

Muck, Peter, D. P. (1987). Monthly anchoveta consumption of guano birds, 1953 to l982. In Pauly, D. and Tsukayama, I., editors, *The Peruvian anchoveta and its upwelling ecosystem: three decades of change. ICLARM Studies and Reviews 15*, pages 219–233. Instituto del Mar del Peru (IMARPE) Callao, Peru; Deutsche Gesellschaft fuer Technische Zusammenarbeit (GIZ), GmbH, Eschbom, Federal Republic of Germany; and International Center for Living Aquatic Resources Management (ICLARM), Manila Philippines., Instituto del Mar del Peru (IMARPE) Callao, Peru; Deutsche Gesellschaft fuer Technische Zusammenarbeit (GIZ), GmbH, Eschbom, Federal Republic of Germany; and International Center for Living Aquatic Resources Management (ICLARM), Manila Philippines.

Murphy, G. I. (1961). Oceanography and variations in the Pacific sardine population. *California Cooperative Oceanic Fisheries Investigation Report*, 8:55–64.

Murray, J. W., Young, J., Newton, J., Dunne, J., Chapin, T., Paul, B., and McCarthy, J. J. (1996). Export flux of particulate organic carbon from the central equatorial pacific determined using a combined drifting trap-234th approach. *Deep Sea Research Part II: Topical Studies in Oceanography*, 43(4-6):1095–1132.

Nakai, Z., Usami, S., and Hattori, S. (1955). *Progress Report of the Cooperative Iwashi Resources Investigations: April 1949-December 1951.* Fisheries Agency, Tokai Regional Fisheries Research Laboratory.

NASA Goddard Space Flight Center, Ocean Ecology Laboratory, Ocean Biology Processing Group (2018). Moderate-resolution Imaging Spectroradiometer (MODIS) Aqua Chlorophyll Data; 2018 Reprocessing.

Nissen, C., Gruber, N., Münnich, M., and Vogt, M. (2021). Southern Ocean phytoplankton community structure as a gatekeeper for global nutrient biogeochemistry. *Global Biogeochemical Cycles*, 35(8):e2021GB006991.

O'Brien, T. and Moriarty, R. (2012). Global distributions of mesozooplankton abundance and biomass - Gridded data product (NetCDF) - Contribution to the MAREDAT World Ocean Atlas of Plankton Functional Types.

O'Brien, T. D. (2007). COPEPOD, a global plankton database: A review of the 2007 database contents and new quality control methodology.

Oliveros-Ramos, R. and Shin, Y.-J. (2016). Calibrar: an R package for fitting complex ecological models. *arXiv*.

Oliveros-Ramos, R., Verley, P., Echevin, V., and Shin, Y.-J. (2017). A sequential approach to calibrate ecosystem models with multiple time series data. *Progress in Oceanography*, 151:227–244.

O'Reilly, J. E., Maritorena, S., Mitchell, B. G., Siegel, D. A., Carder, K. L., Garver, S. A., Kahru, M., and McClain, C. (1998). Ocean color chlorophyll algorithms for SeaWiFS. *Journal of Geophysical Research: Oceans*, 103(C11):24937–24953.

Oschlies, A., Brandt, P., Stramma, L., and Schmidtko, S. (2018). Drivers and mechanisms of ocean deoxygenation. *Nature Geoscience*, 11(7):467–473.

Paredes, C. E. and Gutierrez, M. E. (2008). The peruvian anchovy sector: Costs and benefits. an analysis of recent behavior and future challenges. In Shriver, A. L., editor, *Proceedings of the Fourteenth Biennial Conference of the International Institute of Fisheries Economics & Trade, July 22-25, 2008, Nha Trang, Vietnam: Achieving a Sustainable Future: Managing Aquaculture, Fishing, Trade and Development*, page 10, Corvallis, Oregon, USA. International Institute of Fisheries Economics & Trade.

Pasciak, W. J. and Gavis, J. (1974). Transport limitation of nutrient uptake in phytoplankton 1. *Limnology and Oceanography*, 19(6):881–888.

Pauly, D. and Christensen, V. (1995). Primary production required to sustain global fisheries. *Nature*, 374(6519):255–257.

Pauly, D., Christensen, V., Dalsgaard, J., Froese, R., and Torres, F. (1998). Fishing down marine food webs. *Science*, 279(5352):860–863.

Pauly, D., Vildoso, A. C., Mejia, J., Samame, M., and Palomares, M. L. (1987). Population dynamics and estimated anchoveta consumption of bonito (sarda chiliensis) off per. In Pauly, D. and Tsukayama, I., editors, *The Peruvian anchoveta and its upwelling ecosystem: three decades of change. ICLARM Studies and Reviews 15*, pages 325–342. Instituto del Mar del Peru (IMARPE) Callao, Peru; Deutsche Gesellschaft fuer Technische Zusammenarbeit (GIZ), GmbH, Eschbom, Federal Republic of Germany; and International Center for Living Aquatic Resources Management (ICLARM), Manila Philippines.

Pennington, J. T., Mahoney, K. L., Kuwahara, V. S., Kolber, D. D., Calienes, R., and Chavez, F. P. (2006). Primary production in the eastern tropical Pacific: A review. *Progress in Oceanography*, 69(2-4):285–317.

Penven, P. (2019). Croco tools.

Pikitch, E. K., Santora, C., Babcock, E. A., Bakun, A., Bonfil, R., Conover, D. O., Dayton, P., Doukakis, P., Fluharty, D., Heneman, B., Houde, E. D., Link, J., Livingston, P. A., Mangel, M., McAllister, M. K., Pope, J., and Sainsbury, K. J. (2004). Ecosystem-Based Fishery Management. *Science*, 305(5682):346–347.

Pizarro, J., Docmac, F., and Harrod, C. (2019). Clarifying a trophic black box: stable isotope analysis reveals unexpected dietary variation in the peruvian anchovy *Engraulis ringens*. *PeerJ*, 7:e6968.

Polovina, J. J., Howell, E. A., and Abecassis, M. (2008). Ocean's least productive waters are expanding. *Geophysical Research Letters*, 35(3).

Prowe, A. F., Pahlow, M., Dutkiewicz, S., Follows, M., and Oschlies, A. (2012). Top-down control of marine phytoplankton diversity in a global ecosystem model. *Progress in Oceanography*, 101(1):1–13.

Prowe, A. F., Visser, A. W., Andersen, K. H., Chiba, S., and Kiørboe, T. (2019). Biogeography of zooplankton feeding strategy. *Limnology and Oceanography*, 64(2):661–678.

Raven, J., Caldeira, K., Elderfield, H., Hoegh-Guldberg, O., Liss, P., Riebesell, U., Shepherd, J., Turley, C., and Watson, A. (2005). *Ocean acidification due to increasing atmospheric carbon dioxide*. The Royal Society.

Reynolds, C. S. (2006). *The Ecology of Phytoplankton*. Cambridge University Press.

Ridgway, K., Dunn, J., and Wilkin, J. (2002). Ocean interpolation by four-dimensional weighted least squares—Application to the waters around Australasia. *Journal of Atmospheric and Oceanic Technology*, 19(9):1357–1375.

Riebesell, U., Schulz, K. G., Bellerby, R., Botros, M., Fritsche, P., Meyerhöfer, M., Neill, C., Nondal, G., Oschlies, A., Wohlers, J., and Zöllner, E. (2007). Enhanced biological carbon consumption in a high CO2 ocean. *Nature*, 450(7169):545–548.

Riebesell, U., Zondervan, I., Rost, B., Tortell, P. D., Zeebe, R. E., and Morel, F. M. (2000). Reduced calcification of marine plankton in response to increased atmospheric CO2. *Nature*, 407(6802):364–367.

Rose, K. A., Fiechter, J., Curchitser, E. N., Hedstrom, K., Bernal, M., Creekmore, S., Haynie, A., ichi Ito, S., Lluch-Cota, S., Megrey, B. A., Edwards, C. A., Checkley, D., Koslow, T., McClatchie, S., Werner, F., MacCall, A., and Agostini, V. (2015). Demonstration of a fully-coupled end-to-end model for small pelagic fish using sardine and anchovy in the California Current. *Progress in Oceanography*, 138:348–380. Combining Modeling and Observations to Better Understand Marine Ecosystem Dynamics.

Rose, K. A., Gutiérrez, D., Breitburg, D., Conley, D., Craig, K. J., Froehlich, H. E., Jeyabaskaran, R., Kripa, V., Mbaye, B. C., Mohamed, K., et al. (2019). Impacts of ocean deoxygenation on fisheries.

Roy, C. (1993). The optimal environmental window hypothesis: A non linear environmental process affecting recruitment success. *ICES Journal of Marine Science*, 76:1–13.

Ruiz-Cooley, R. I., Gerrodette, T., Fiedler, P. C., Chivers, S. J., Danil, K., and Ballance, L. T. (2017). Temporal variation in pelagic food chain length in response to environmental change. *Science Advances*, 3(10):e1701140.

Ryther, J. H. (1969). Photosynthesis and fish production in the sea. *Science*, 166(3901):72–76.

Sallée, J.-B., Pellichero, V., Akhoudas, C., Pauthenet, E., Vignes, L., Schmidtko, S., Garabato, A. N., Sutherland, P., and Kuusela, M. (2021). Summertime increases in upper-ocean stratification and mixed-layer depth. *Nature*, 591(7851):592–598.

Sallée, J.-B., Shuckburgh, E., Bruneau, N., Meijers, A. J., Bracegirdle, T. J., and Wang, Z. (2013). Assessment of Southern Ocean mixed-layer depths in CMIP5 models: Historical bias and forcing response. *Journal of Geophysical Research: Oceans*, 118(4):1845–1862.

Sarmiento, J. L., Slater, R., Barber, R., Bopp, L., Doney, S., Hirst, A., Kleypas, J., Matear, R., Mikolajewicz, U., Monfray, P., and et al. (2004). Response of ocean ecosystems to climate warming. *Global Biogeochemical Cycles*, 18(3).

Schukat, A., Auel, H., Teuber, L., Lahajnar, N., and Hagen, W. (2014). Complex trophic interactions of calanoid copepods in the Benguela upwelling system. *Journal of Sea Research*, 85:186–196.

Schukat, A., Hagen, W., Dorschner, S., Acosta, J. C., Arteaga, E. L. P., Ayón, P., and Auel, H. (2021). Zooplankton ecological traits maximize the trophic transfer efficiency of the Humboldt Current upwelling system. *Progress in Oceanography*, 193:102551.

Schwartzlose, R. A., Alheit, J., Bakun, A., Baumgartner, T. R., Cloete, R., Crawford, R. J. M., Fletcher, W. J., Green-Ruiz, Y., Hagen, E., Kawasaki, T., Lluch-Belda, D., Lluch-Cota, S. E., MacCall, A. D., Matsuura, Y., Nevárez-Martínez, M. O., Parrish, R. H., Roy, C., Serra, R., Shust, K. V., Ward, M. N., and Zuzunaga, J. Z. (1999). Worldwide large-scale fluctuations of sardine and anchovy populations. *South African Journal of Marine Science*, 21(1):289–347.

Séférian, R., Nabat, P., Michou, M., Saint-Martin, D., Voldoire, A., Colin, J., Decharme, B., Delire, C., Berthet, S., Chevallier, M., and et al. (2019). Evaluation of CNRM earth system model, CNRM-ESM2-1: Role of earth system processes in present-day and future climate. *Journal of Advances in Modeling Earth Systems*, 11(12):4182–4227.

Sellar, A. A., Jones, C. G., Mulcahy, J. P., Tang, Y., Yool, A., Wiltshire, A., O'connor, F. M., Stringer, M., Hill, R., Palmieri, J., and et al. (2019). UKESM1: Description and evaluation of the UK Earth System Model. *Journal of Advances in Modeling Earth Systems*, 11(12):4513–4558.

Shchepetkin, A. F. and McWilliams, J. C. (2005). The regional oceanic modeling system (ROMS): a split-explicit, free-surface, topography-following-coordinate oceanic model. *Ocean Modelling*, 9(4):347–404.

Shifrin, N. S. and Chisholm, S. W. (1981). Phytoplankton lipids: Interspecific differences and effects of nitrate, silicate and light-dark cycles 1. *Journal of Phycology*, 17(4):374–384.

Shin, Y.-J. and Cury, P. (2001). Exploring fish community dynamics through size-dependent trophic interactions using a spatialized individual-based model. *Aquatic Living Resources*, 14(2):65–80.

Shin, Y.-J. and Cury, P. (2004). Using an individual-based model of fish assemblages to study the response of size spectra to changes in fishing. *Canadian Journal of Fisheries and Aquatic Sciences*, 61(3):414–431.

Simpson, J. H. and Sharples, J. (2012). *Introduction to the Physical and Biological Oceanography of Shelf Seas*. Cambridge University Press.

Steinberg, D. K. and Landry, M. R. (2017). Zooplankton and the ocean carbon cycle. *Annual Review of Marine Science*, 9:413–444.

Stibor, H., Vadstein, O., Diehl, S., Gelzleichter, A., Hansen, T., Hantzsche, F., Katechakis, A., Lippert, B., Løseth, K., Peters, C., and et al. (2004). Copepods act as a switch between alternative trophic cascades in marine pelagic food webs.

Stock, C. and Dunne, J. (2010). Controls on the ratio of mesozooplankton production to primary production in marine ecosystems. *Deep Sea Research Part I: Oceanographic Research Papers*, 57(1):95–112.

Stock, C., Dunne, J., and John, J. (2014a). Drivers of trophic amplification of ocean productivity trends in a changing climate. *Biogeosciences*, 11(24):7125–7135.

Stock, C., Dunne, J. P., and John, J. G. (2014b). Global-scale carbon and energy flows through the marine planktonic food web: An analysis with a coupled physical–biological model. *Progress in Oceanography*, 120:1–28.

Stock, C., John, J. G., Rykaczewski, R. R., Asch, R. G., Cheung, W. W., Dunne, J. P., Friedland, K. D., Lam, V. W., Sarmiento, J. L., and Watson, R. A. (2017). Reconciling fisheries catch and ocean productivity. *Proceedings of the National Academy of Sciences*, 114(8):E1441–E1449.

Stramma, L., Johnson, G. C., Sprintall, J., and Mohrholz, V. (2008). Expanding oxygen-minimum zones in the tropical oceans. *Science*, 320(5876):655–658.

Stramma, L., Schmidtko, S., Levin, L. A., and Johnson, G. C. (2010). Ocean oxygen minima expansions and their biological impacts. *Deep Sea Research Part I: Oceanographic Research Papers*, 57(4):587–595.

Stukel, M. R., Ohman, M. D., Benitez-Nelson, C. R., and Landry, M. R. (2013). Contributions of mesozooplankton to vertical carbon export in a coastal upwelling system. *Marine Ecology Progress Series*, 491:47–65.

Sunda, W. G. and Huntsman, S. A. (1997). Interrelated influence of iron, light and cell size on marine phytoplankton growth. *Nature*, 390(6658):389–392.

Suttle, C. A. (2005). Viruses in the sea. *Nature*, 437(7057):356–361.

Sverdrup, H. (1953). On conditions for the vernal blooming of phytoplankton. *J. Cons. Int. Explor. Mer*, 18(3):287–295.

Sverdrup, H. U., Johnson, M. W., Fleming, R. H., and et al. (1942). *The Oceans: Their Physics, Chemistry, and General Biology*, volume 1087. Prentice-Hall New York.

Swart, N. C., Cole, J. N., Kharin, V. V., Lazare, M., Scinocca, J. F., Gillett, N. P., Anstey, J., Arora, V., Christian, J. R., Hanna, S., and et al. (2019). The Canadian earth system model version 5 (CanESM5. 0.3). *Geoscientific Model Development*, 12(11):4823–4873.

Tam, J., Taylor, M. H., Blaskovic, V., Espinoza, P., Ballón, R. M., Díaz, E., Wosnitza-Mendo, C., Argüelles, J., Purca, S., Ayón, P., and et al. (2008). Trophic modeling of the Northern Humboldt Current Ecosystem, Part I: Comparing trophic linkages under La Niña and El Niño conditions. *Progress in Oceanography*, 79(2-4):352–365.

Tang, W., Llort, J., Weis, J., Perron, M. M., Basart, S., Li, Z., Sathyendranath, S., Jackson, T., Sanz Rodriguez, E., Proemse, B. C., and et al. (2021). Widespread phytoplankton blooms triggered by 2019–2020 Australian wildfires. *Nature*, 597(7876):370–375.

Taucher, J. and Oschlies, A. (2011). Can we predict the direction of marine primary production change under global warming? *Geophysical Research Letters*, 38(2).

Taylor, A., Watson, A., Ainsworth, M., Robertson, J., and Turner, D. (1991). A modelling investigation of the role of phytoplankton in the balance of carbon at the surface of the North Atlantic. *Global Biogeochemical Cycles*, 5(2):151–171.

Tedesco, P., Gula, J., Ménesguen, C., Penven, P., and Krug, M. (2019). Generation of submesoscale frontal eddies in the Agulhas Current. *Journal of Geophysical Research: Oceans*, 124(11):7606–7625.

Terhaar, J., Frölicher, T. L., and Joos, F. (2021). Southern Ocean anthropogenic carbon sink constrained by sea surface salinity. *Science Advances*, 7(18):eabd5964.

Terhaar, J., Kwiatkowski, L., and Bopp, L. (2020). Emergent constraint on Arctic Ocean acidification in the twenty-first century. *Nature*, 582(7812):379–383.

Thomas, A., Carr, M.-E., and Strub, P. T. (2001). Chlorophyll variability in eastern boundary currents. *Geophysical Research Letters*, 28(18):3421–3424.

Thomas, M. K., Aranguren-Gassis, M., Kremer, C. T., Gould, M. R., Anderson, K., Klausmeier, C. A., and Litchman, E. (2017). Temperature–nutrient interactions exacerbate sensitivity to warming in phytoplankton. *Global Change Biology*, 23(8):3269–3280.

Thomsen, S., Kanzow, T., Krahmann, G., Greatbatch, R. J., Dengler, M., and Lavik, G. (2016). The formation of a subsurface anticyclonic eddy in the Peru-Chile Undercurrent and its impact on the near-coastal salinity, oxygen, and nutrient distributions. *Journal of Geophysical Research: Oceans*, 121(1):476–501.

Tittensor, D. P., Eddy, T. D., Lotze, H. K., Galbraith, E. D., Cheung, W., Barange, M., Blanchard, J. L., Bopp, L., Bryndum-Buchholz, A., Büchner, M., and et al. (2018). A protocol for the intercomparison of marine fishery and ecosystem models: Fish-MIP v1. 0. *Geoscientific Model Development*, 11(4):1421–1442.

Travers, M. (2009). *Couplage de modèles trophiques et effets combinés de la pêche et du climat, Coupling trophodynamic models for assessing the combined effects of fishing and climate*. Thesis, Université Pierre et Marie Curie.

Travers, M., Shin, Y.-J., Jennings, S., Machu, E., Huggett, J., Field, J., and Cury, P. (2009). Two-way coupling versus one-way forcing of plankton and fish models to predict ecosystem changes in the Benguela. *Ecological Modelling*, 220(21):3089–3099.

Travers, M., Shin, Y.-J., Shannon, L., and Cury, P. (2006). Simulating and testing the sensitivity of ecosystem-based indicators to fishing in the southern Benguela ecosystem. *Canadian Journal of Fisheries and Aquatic Sciences*, 63(4):943–956.

Travers-Trolet, M., Shin, Y., and Field, J. (2014a). An end-to-end coupled model ROMS-N2P2Z2D2-OSMOSE of the southern Benguela foodweb: parameterisation, calibration and pattern-oriented validation. *African Journal of Marine Science*, 36(1):11–29.

Travers-Trolet, M., Shin, Y.-J., and Field, J. (2014b). An end-to-end coupled model ROMS-N2P2Z2D2-OSMOSE of the southern Benguela foodweb: parameterisation, calibration and pattern-oriented validation. *African Journal of Marine Science*, 36(1):11–29.

Tsikliras, A. C. and Froese, R. (2019). Maximum Sustainable Yield. In Fath, B. D., editor, *Encyclopedia of Ecology*, volume 1, pages 108–115. Elsevier, 2 edition.

Tsujino, H., Nakano, H., Sakamoto, K., Urakawa, S., Hirabara, M., Ishizaki, H., and Yamanaka, G. (2017). Reference manual for the Meteorological Research Institute Community Ocean Model version 4 (MRI. COMv4). *Technical Reports of the Meteorological Research Institute*, 80:306.

Turner, J. T. (2015). Zooplankton fecal pellets, marine snow, phytodetritus and the ocean' s biological pump. *Progress in Oceanography*, 130:205–248.

Uchida, T., Balwada, D., Abernathey, R., Prend, C. J., Boss, E., and Gille, S. T. (2019). Southern Ocean phytoplankton blooms observed by biogeochemical floats. *Journal of Geophysical Research: Oceans*, 124(11):7328–7343.

Ulanowicz, R. E. (1995). Ecosystem trophic foundations: Lindeman exonerata. *Complex Ecology: the Part-Whole Relation in Ecosystems. Prentice Hall, Englewood Cliffs, NJ*, pages 549–550.

Vergnon, R., Shin, Y.-J., and Cury, P. (2008). Cultivation, Allee effect and resilience of large demersal fish populations. *Aquatic Living Resources*, 21(3):287–295.

Weaver, A. J., Eby, M., Wiebe, E. C., Bitz, C. M., Duffy, P. B., Ewen, T. L., Fanning, A. F., Holland, M. M., MacFadyen, A., Matthews, H. D., and Yoshimori, M. (2001). The UVic Earth System Climate Model: Model description, climatology, and applications to past, present and future climates. *Atmosphere-Ocean*, 39(4):361–428.

Williamson, M. S., Thackeray, C. W., Cox, P. M., Hall, A., Huntingford, C., and Nijsse, F. J. (2021). Emergent constraints on climate sensitivities. *Reviews of Modern Physics*, 93(2):025004.

Woodson, C. B. and Litvin, S. Y. (2015). Ocean fronts drive marine fishery production and biogeochemical cycling. *Proceedings of the National Academy of Sciences*, 112(6):1710–1715.

Worley, S. J., Woodruff, S. D., Reynolds, R. W., Lubker, S. J., and Lott, N. (2005). ICOADS release 2.1 data and products. *International Journal of Climatology: A Journal of the Royal Meteorological Society*, 25(7):823–842.

Xing, L., Chongliang, Z., Chen, Y., Shin, Y.-J., Verley, P., Yu, H., and Ren, Y. (2017). An individual-based model for simulating the ecosystem dynamics of Jiaozhou Bay, China. *Ecological Modelling*, 360:120–131.

Xue, T., Frenger, I., Oschlies, A., Stock, C. A., Koeve, W., John, J. G., and Prowe, A. E. (2022a). Mixed layer depth promotes trophic amplification on a seasonal scale. *Geophysical Research Letters*, 49(12):e2022GL098720.

Xue, T., Frenger, I., Prowe, A., José, Y. S., and Oschlies, A. (2022b). Mixed layer depth dominates over upwelling in regulating the seasonality of ecosystem functioning in the Peruvian Upwelling System. *Biogeosciences*, 19(2):455–475.

Yao, W., Kvale, K. F., Achterberg, E., Koeve, W., and Oschlies, A. (2019). Hierarchy of calibrated global models reveals improved distributions and fluxes of biogeochemical tracers in models with explicit representation of iron. *Environmental Research Letters*, 14(11):114009.

Yao, W., Kvale, K. F., Koeve, W., Landolfi, A., Achterberg, E., Bertrand, E. M., and Oschlies, A. (2022). Simulated future trends in marine nitrogen fixation are sensitive to model iron implementation. *Global Biogeochemical Cycles*, 36(3):e2020GB006851.

Ziehn, T., Chamberlain, M. A., Law, R. M., Lenton, A., Bodman, R. W., Dix, M., Stevens, L., Wang, Y.-P., and Srbinovsky, J. (2020). The Australian earth system model: ACCESS-ESM1. 5. *Journal of Southern Hemisphere Earth Systems Science*, 70(1):193–214.

List of Figures

List of Tables

Acknowledgments

I would love to express my most sincere thanks to many. This work would not have been possible without the support of them.

First, I would like to express my deepest gratitude to my supervisors: Andreas Oschlies, Ivy Frenger, and Friederike Prowe. Andreas, who gave me the opportunity for this PhD and always gives me full freedom and support on my project, makes me feel secure in doing whatever I am interested in. Ivy and Fi gave me constant support, guidance, and assistance throughout the whole time. Ivy constantly encourages me and makes it so easy to seek help. I always admire how passionate and optimistic she is about science and work. Fi always reminds me that it is important to balance work and life and that I should always follow my heart and do things that make me happy.

Second, I would like to thank Wolfgang Koeve for the inspiring research ideas and providing feedback on my work; Yonss José, for providing the initial help with the CROCO-BioEBUS model; Charles Stock and Jasmin John, for inspiring me with interesting research and providing the GFDL model data; and Wanxuan(Ben) Yao, for providing the UVic data for model comparing.

Then, I want to thank Andreas and Prof. Arne Körtzinger for taking the time to be my thesis examiners, and Prof. Sylvia Sander and Prof. Ulf Riebesell for being in my defence committee.

Furthermore, I would like to thank Ivy, Fi, Wolfgang, Vanessa, Michal, Giang, Chris, MarkusP and Niels for giving me feedback, helping translate the summary and proofreading this thesis.

I would like to thank the Biogeochemical Modelling group for the interesting science exchange. Special thanks to ChiaTe for being a great office mate and baring my constant "quick questions"; to Vanessa, Giang and Michal for the nice lunch & coffee breaks; and also my peers for being great companions, for the countless shares and occasional beers, for making the PhD time enjoyable despite the hard moments. Special thanks to Jiajun,

Mariana, Vanessa, Jaard, and Ben.

Other than that, I would like to thank my friends outside the group, namely Xin, Fangzhou, Qinqin, Li, Peixuan, and Te for the long phone calls, great travel time, and many many hotpots together.

Most importantly, I would like to express my appreciation and love to my parents. They always have my back unconditionally. And only because of this, I can pursue my dream without having any concerns (我要把我最诚挚的感谢和爱意献给我的爸爸妈妈，是他们对于我无条件的支持才给了我随心追梦的勇气). A special thanks to Niels for always being there for me and making life so sunny and "silly". I would also like to extend my thanks to my "German family", for warmly welcoming me in and making me feel at home despite being so far away from China.

Finally, I would like to acknowledge the financial support from the China Scholarship Council (TX, grant no.201808460055), the BMBF funded projects Coastal Upwelling System in a Changing Ocean (CUSCO, grant no. 03F0813A) and Humboldt Tipping (HTP, grant no. 01LC1823B).

Erklärung

Hiermit erkläre ich, dass ich diese Arbeit mit dem Titel: "Effects of Mixed Layer Depth on Productive Marine Ecosystems - from seasonality to climate change" selbstständig verfasst habe. Inhalt und Aufbau der Arbeit sind, abgesehen von der Betreuung durch den Betreuer der Arbeit, völlig selbstständig unter Verwendung der angegebenen Quellen erstellt worden. Diese Arbeit entspricht den Regeln guter wissenschaftlicher Praxis der Deutschen Forschungsgemeinschaft. Sie wurde weder einem anderen Begutachtungsverfahren unterzogen noch veröffentlicht. Es wurde kein akademischer Grad entzogen.

Kiel, June 2022

Tianfei Xue